

ELECTROMAGNETIC INTERACTIONS

Experimental 1

Chairman B. TOUSCHEK

Rapporteur B. RICHTER

Discussion Leaders P. LEHMANN
 E. LOHRMANN
 P. MARIN

Secretaries J. BAILEY
 J. LEMONNE

TWO-BODY PHOTOPRODUCTION

B. Richter

Stanford Linear Accelerator Center, Stanford University, Stanford, Calif.

As is usual at these conferences, too much material has been submitted to allow a complete summary of all new photoproduction data in this report. I have therefore restricted myself to summarizing those works which bear most immediately on the problems of strong interaction physics. This means that I will report almost exclusively on high-energy experiments, and will regretfully omit much very nice work in the region of the resonances.

* * *

1. CHARGED SINGLE-PION PHOTOPRODUCTION

1.1 π^+ production from the proton

New data are available from my group at SLAC¹⁾ which gives increased accuracy and extends the momentum transfer range of the results which have been previously reported²⁾. These new results, together with the old SLAC data and some of the DESY data³⁾, are shown in Fig. 1. The main characteristics of these data are the, by now well-known, spike in the forward differential cross-section for momentum transfers less than m_π^2 , a t -dependence of $e^{2.5t}$ out to momentum transfers of 0.6 GeV^2 , followed by a change in slope, and a t -dependence of e^{3t} out as far as the measurements extend. Figure 2 shows the data on an expanded scale where $(S - M^2)^2 d\sigma/dt$ is plotted versus $(|t|)^{1/2}$ (S is the square of the total centre-of-mass energy and M is the proton mass). The new data points are shown in black and the error bars are omitted from the old forward points to reduce confusion on the graph. (The error bars on the old points are larger than those on the new.) The previous data indicated what might have been a systematic trend toward a decrease in the forward differential cross-

section with increasing energy, although the errors made this conclusion quite uncertain. The new data show that this trend, if present at all, is very much smaller than had been allowed by the previous data. The upper curve shows the yield to be expected from the electric Born approximation with no absorption.

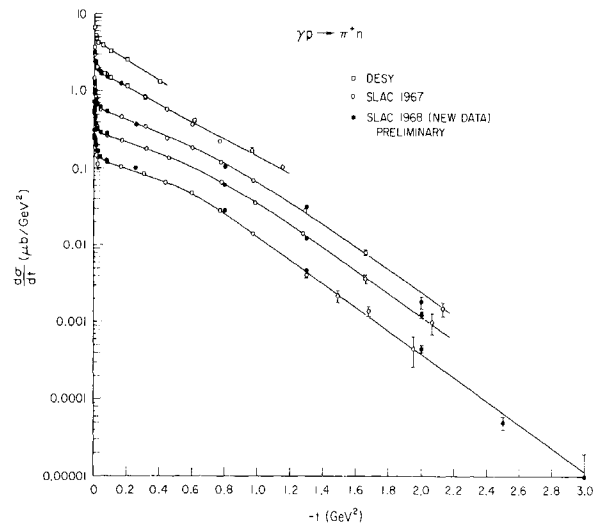


Fig. 1 π^+ photoproduction cross-section plotted versus momentum transfer. The data is from Refs. 1 to 3.

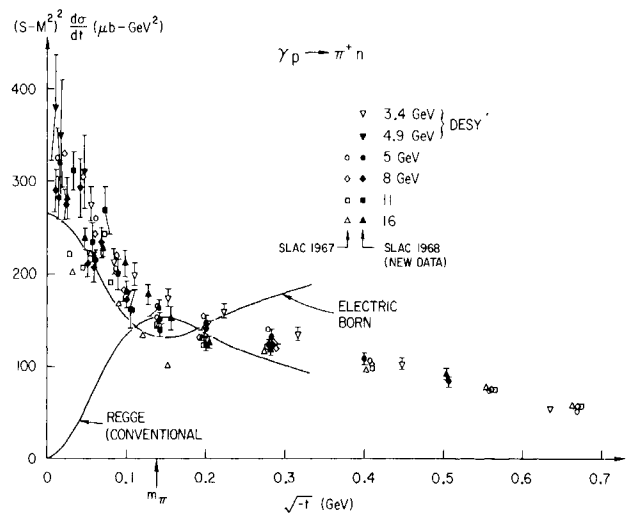


Fig. 2 Small momentum transfer π^+ photoproduction data plotted on an expanded scale. The data are from Refs. 1 and 2.

It is interesting to note how close the data come to the Born approximation cross-section at 0° . The lower curve indicates the momentum transfer dependence to be expected from models based solely on any combination of evasive Reggeized particle exchange⁴). The peaks in the forward π^+ photoproduction cross-section and in the np charge exchange cross-section constitute an insurmountable barrier for any such simple version of the Regge models.

The energy dependence of the differential cross-section at fixed momentum transfer was obtained by fitting the data to the form

$$\frac{d\sigma}{dt} = f(t)(S-M^2)^{2\alpha-2}, \quad (1)$$

where S is the square of the total energy in the centre-of-mass system and M is the proton mass. The quantity α in Eq. (1) should not be confused with the Regge trajectory for any given particle. α in Eq. (1) represents an effective energy dependence for the entire cross-section. The SLAC data at 8 GeV and above have been used in this fit. The lower energy data have been excluded because of the qualitative difference between the slope of the differential cross-section versus momentum transfers for $|t| < 0.6$ above and below 8 GeV. Inclusion of lower energy data would systematically decrease α . Figure 3 shows α versus t . The new points are shown as open circles. α remains at or near zero out to $-t \approx 1 \text{ GeV}^2$. α seems to

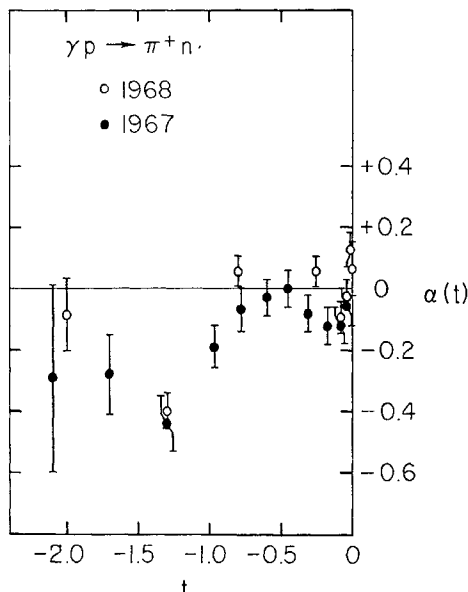


Fig. 3 Energy dependence of the π^+ photoproduction data. $\alpha(t)$ is defined in Eq. (1).

decrease at $-t = 1.3$ and to return to near zero at $-t = 2$.

1.2 π^- production from the neutron

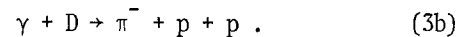
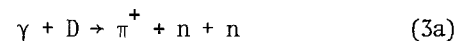
Since the electromagnetic current possesses both isotopic spin zero and one components, any photoproduction amplitude can be broken up into isotopic vector and isotopic scalar parts. Study of π^- photoproduction from the neutron and π^+ photoproduction from the proton allows us to learn something about the interference between the isovector and isoscalar parts of the amplitude. The cross-sections for π^+ production from the proton and π^- production from the neutron may be written as

$$\frac{d\sigma}{dt} (\gamma p \rightarrow \pi^+ n) = |A_v + A_s|^2 \quad (2a)$$

$$\frac{d\sigma}{dt} (\gamma n \rightarrow \pi^- p) = |A_v - A_s|^2, \quad (2b)$$

where the subscripts v and s refer to the isovector and isoscalar parts of the amplitude, respectively. Note that this does not refer to the isospin of any exchange particles. All exchange mesons in charged pion photoproduction have an isospin of 1. At high energies, an isovector-isoscalar interference term will occur only if there are at least two exchanges in the t -channel having opposite G -parity and both belonging to either natural parity ($P = -1^J$) or unnatural [$P = -(-1^J)$] sequences.

A group from DESY⁵) and my group at SLAC⁶) in contributions to this Conference have described experiments on photoproduction from deuterium in which only the charged pion was detected. The reactions studied were



The DESY experiment covered photon energies of 3.4 to 5 GeV, and momentum transfers from near 0 to 0.6 GeV^2 , whilst the SLAC experiment covered photon energies of 8 and 16 GeV and momentum transfers from 0 to roughly 1.5 GeV^2 . These experiments, together with the earlier work of Bar Yam et al.⁷) at CEA, give π^- differential cross-sections from deuterium which cover the entire range of energies over which π^+ production from the proton has been measured for momentum transfers $\lesssim 1.5 \text{ GeV}^2$.

We are interested in obtaining from this data the cross-section for π^- production from the free neutron. The cross-section for π^- production from deuterium differs from that of the free neutron because of three effects--the Pauli exclusion principle, Glauber corrections, and other nuclear physics problems. The effect of the exclusion principle has been calculated by many authors⁸⁾ and is given by

$$\frac{d\sigma}{dt}(D\pi^-) = \left[1 - \frac{1}{3} F(t)\right] \frac{d\sigma}{dt}(n\pi^-)_{\text{spin flip}} + \left[1 - F(t)\right] \frac{d\sigma}{dt}(n\pi^-)_{\text{non-spin flip}}, \quad (4)$$

where $F(t)$ is the deuteron form factor. Since the deuteron form factor falls very rapidly with momentum transfer, the Pauli principle correction also decreases rapidly with momentum transfer. The Glauber correction has been estimated to be of the order of 10%, and the miscellaneous nuclear physics has been estimated to be of the order of 5 to 10%⁸⁾. These effects are expected to be roughly the same for reactions (3a) and (3b).

Since the photoproduction cross-section is a pure spin flip transition at zero degrees, if we assume that the relative amounts of spin flip and non-spin flip do not change wildly in the small momentum transfer region where the deuteron form factor is significant, the cross-section for π^- production from the free neutron should be given to a good approximation by:

$$\frac{d\sigma}{dt}(n\pi^-) = \left[\frac{d\sigma}{dt}(D\pi^-) / \frac{d\sigma}{dt}(D\pi^+) \right] \frac{d\sigma}{dt}(p\pi^+) \equiv R \frac{d\sigma}{dt}(p\pi^+). \quad (5)$$

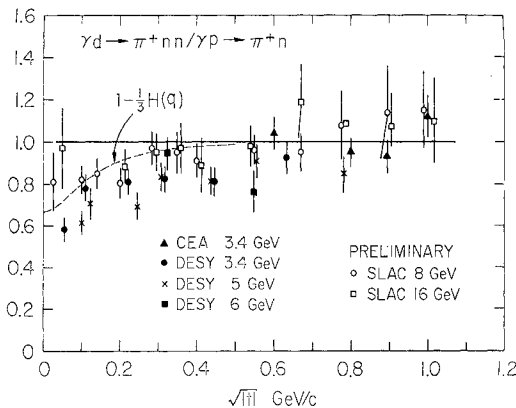


Fig. 4 Ratio of π^+ photoproduction cross-section from deuterium to the π^+ photoproduction cross-section from hydrogen. Data are from Refs. 5 to 7.

The assumption made about the behaviour of the relative amounts of spin flip and non-spin flip versus momentum transfer can itself be checked experimentally by studying the ratio of π^+ production from deuterium and π^+ production from hydrogen. Figure 4 summarizes all the data on this ratio. In general, the ratio of π^+ production from deuterium to the π^+ production from hydrogen behaves as we would expect the spin flip cross-section to behave. Note that this ratio is not expected to go to one because of the Glauber correction and the other nuclear physics corrections.

With these preliminaries out of the way, we can now go on to the π^- production cross-section from the neutron. Figure 5 shows all the data on the ratio of π^- production from deuterium to π^+ production from deuterium (R). The ratio R is about 1 in the forward direction, drops rapidly as $|t|$ increases, reaching 1/2 at $|t| \sim 0.1 \text{ GeV}^2$, and reaching 0.3 at a $|t| \sim 0.3 \text{ GeV}^2$. It then rises slowly as the momentum transfer increases. There appears to be a small systematic energy dependence of R --the high-energy data tending to lie below the low-energy data at small momentum transfers and above the low-energy data at large momentum transfers.

Figure 6a shows the proton cross-section measured from hydrogen and the neutron cross-section as determined from Eq. (5). The neutron π^- cross-section does not show the break slope at $|t| = m_\pi^2$ characteristic of π^+ data, but instead shows a smooth and very

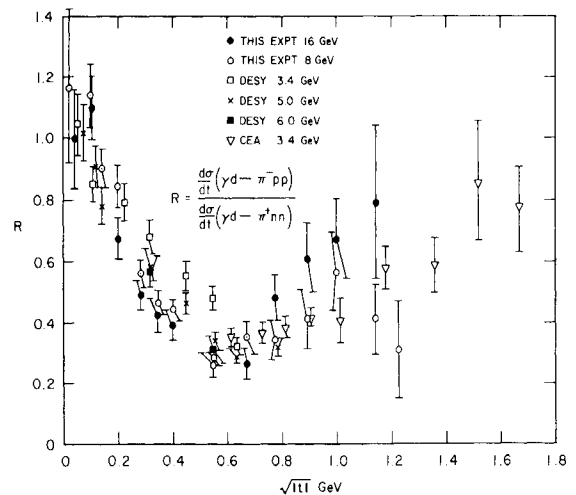


Fig. 5 Ratio of π^- photoproduction cross-section from deuterium to the π^+ photoproduction cross-section from deuterium. Data are from Refs. 5 to 7.

steep fall out to larger $|t|$. Figure 6b shows the cross-section for the vector amplitude squared plus the scalar amplitude squared $[(1 + R)(d\sigma/dt)(p\pi^+)]$ and the cross-section for the isovector-isoscalar interference $[(1 - R)(d\sigma/dt)(p\pi^+)]$. The square of the vector amplitude plus the square of the scalar amplitude shows the sharp forward spike, and the interference cross-section goes to zero in the forward direction.

The energy dependence of the data on R and $1 + R$ are shown in Figs. 7a and 7b. They were fit to

$$G(R) = f(t)(S - M^2)^{2\alpha} \quad (6)$$

$$\alpha_R = \alpha_n - \alpha_p$$

$$\alpha_{1+R} = \alpha_{v^2+s^2} - \alpha_p$$

The plots show both α_R and α_{1+R} to be near zero.

1.3 π^+ production by polarized photons

The results of the first high-energy experiment on π^+ photoproduction with polarized photons have been contributed to this Conference by a DESY group⁹. These experiments allow us to make further restrictions on the quantum numbers of the particles exchanged in the reaction. Only natural parity $[P = (-1)^J]$ exchange contributes to production when the γ -ray polarization is perpendicular to the production plane, and only unnatural parity $[P = -(-1)^J]$ exchange contributes when the polarization is parallel to the production plane.

A polarized photon beam was produced by coherent bremsstrahlung from a diamond crystal. Figure 8 shows the energy spectrum and polarization of the beam. The peak in photon yield shown in Fig. 8 is due to coherent bremsstrahlung from the crystal lattice and the background is due to incoherent bremsstrahlung. Only the coherent bremsstrahlung is strongly polarized. The high-energy edge of the coherent peak can be made extremely sharp by proper collimation of the incident electron beam. Both the height of the peak and its polarization increase when the energy of the peak is lowered with respect to the bremsstrahlung end-point. The bremsstrahlung polarization vector is changed by rotation of the crystal about the incident beam direction.

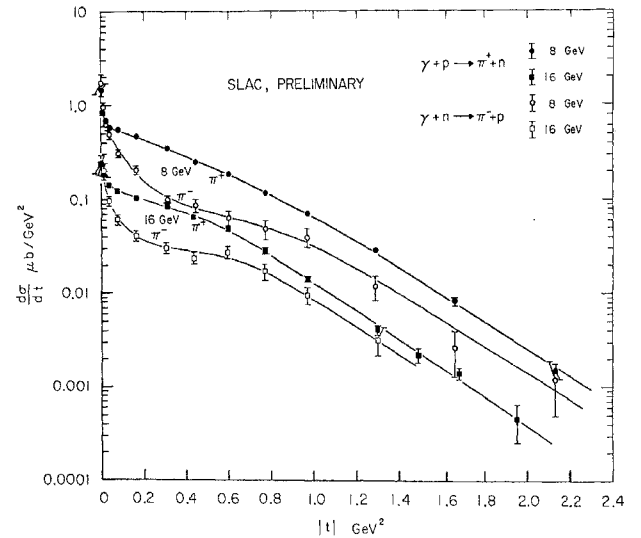


Fig. 6a The cross-section for π^+ production from the proton and π^- production from the neutron at 8 and 16 GeV. Data are from Ref. 6.

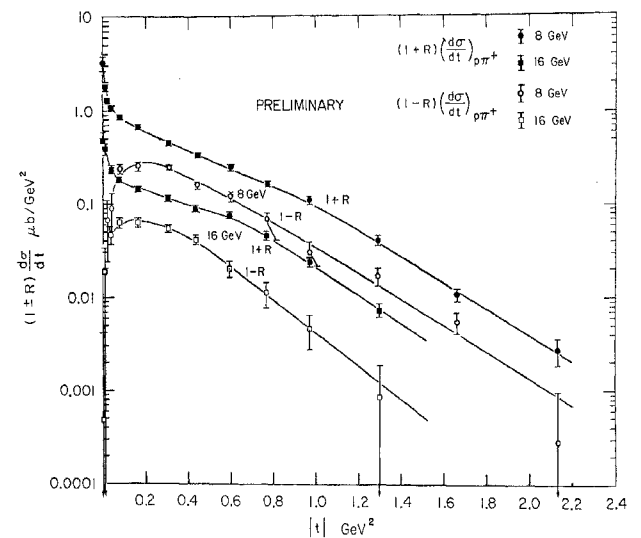


Fig. 6b Differential cross-sections for the sum and difference of π^+ production from the proton and π^- production from the neutron.

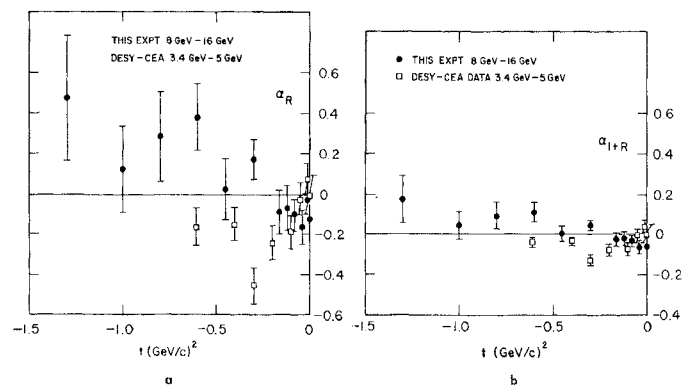


Fig. 7a Energy dependence of the π^-/π^+ cross-section ratio. $\alpha(R)$ is defined in Eq. (6).

Fig. 7b Energy dependence of the sum of π^+ and π^- cross-sections. α is defined in Eq. (6).

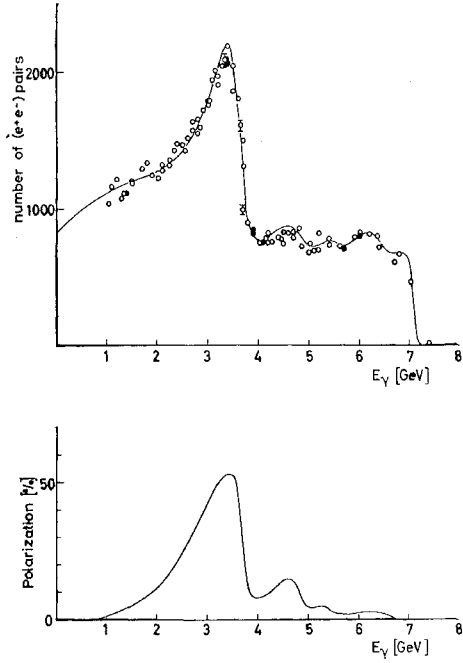


Fig. 8 Photon energy spectra and polarization for the DESY polarized photon beam from Ref. 9.

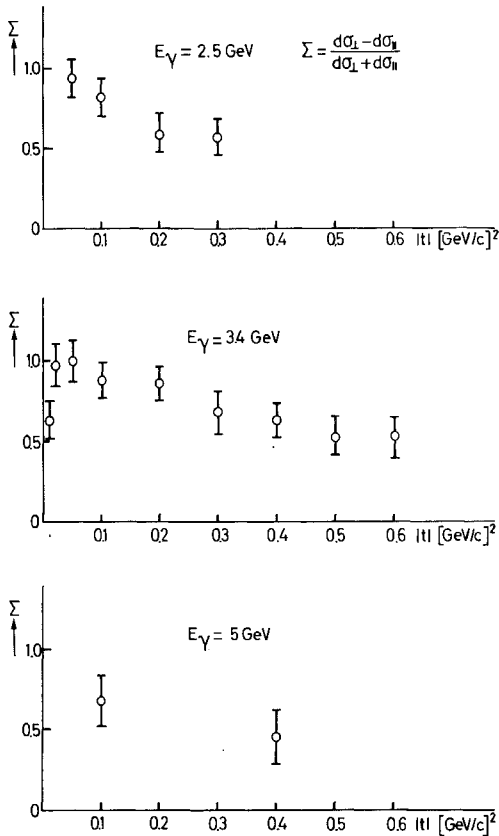


Fig. 9 The difference over the sum of cross-sections for photoproduction with the polarization perpendicular to and parallel to the production plane from Ref. 9.

The results of the DESY experiment are shown in Fig. 9. The difference over the sum of production perpendicular to and parallel to the production plane is plotted versus momentum transfer for various energies. The most extensive data have been obtained at 3.4 GeV. Since we have seen that the unpolarized differential cross-section and the π^-/π^+ ratio in pion photoproduction have the same general character at 3.4 GeV as at 16 GeV, we may reasonably hope that these polarization results are characteristic of the high-energy behaviour of the cross-section. The DESY results show that at $-t > m_\pi^2$, π^+ production goes almost entirely by natural parity exchange, i.e. π exchange contributes very little to the cross-section. At $|t| = 0.06$ $\sigma_{||}/\sigma_{\perp} \approx 5\%$, and at $|t| = 0.4$ $\sigma_{||}/\sigma_{\perp} = 0.25$. This result is surprising to me and will place severe restrictions on models used to explain pion photoproduction. [Bar-Yam, Dowd, De Paq A. Kern have just reported a polarized photoproduction measurement from the reaction $\gamma n \rightarrow \pi^- p$. They find $\Sigma = -0.08 \pm 0.2$ at $|t| = 0.6(\text{GeV})^2$, and $\Sigma = 0.15 \pm 0.2$ at $|t| = 1.2(\text{GeV})^2$.]

1.4 Comparison of the data with recent theoretical models

There has been a great deal of work published in the last year interpreting charged pion photoproduction in terms of various forms of the Regge model. I want to compare three of the calculations, which represent what one might call different classes of the Regge model, with experiments. To be successful, a model must account for the π^+ differential cross-section, the π^-/π^+ ratio from deuterium, and the cross-section for production with polarized photons. The π^-/π^+ ratio from deuterium implies that at very small momentum transfers there can be only one G-parity present in either the natural or unnatural spin parity sequence. The polarized photon data imply that at moderate momentum transfers the cross-section is dominated by natural spin parity exchange, and the π^-/π^+ ratio in this same region implies that both G-parities are present.

The first model is that of the recent work by Brower and Dash¹⁰). This is the most ambitious attempt that I have seen to use only conspiring and

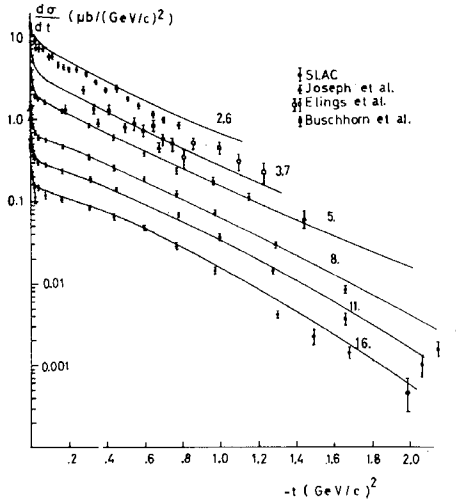


Fig. 10 The fit of Amati et al., to the π^+ photoproduction data.

conspiring Regge trajectories to fit the data. If no fixed poles are allowed. The authors use a background containing π trajectory and evasive ρ , A_2 , and B trajectories. The model gives reasonable agreement with the π^+ differential cross-section for momentum transfers $|t| = 0.5 \text{ GeV}^2$ and, if I put in the numbers, is in qualitative agreement with the data. This model, however, fails the π^-/π^+ ratio for deuterium, giving a ratio greater than that indicated by the data by a factor of 1.5. In addition, the energy dependence

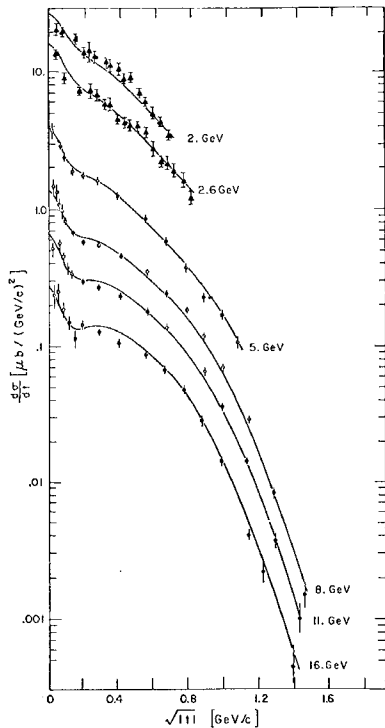


Fig. 11 The fit of Frøylund and Gordon to the π^+ photoproduction data.

of the differential cross-section will give increasing trouble beyond momentum transfers of 0.5 GeV^2 .

The second model is that of Amati et al.¹¹⁾ The authors use a phenomenological background containing both parities plus evasive π , B , and A_2 trajectories. The parameters of the background and the A_2 coupling were fit to the data, and a quite good fit to the π^+ differential cross-section was obtained as shown in Fig. 10. Unfortunately, the model predicts a π^-/π^+ ratio > 1 and is contradicted by the data. This is due to the sign chosen for the B coupling. At SLAC we have attempted to refit the data using the model of Amati et al., but with the opposite sign of the B coupling. However, we cannot get a decent fit to both the π^+ differential cross-section and the π^-/π^+ ratio.

The third model is that of Frøylund and Gordon¹²⁾, and this model uses π and ρ trajectories plus two cuts. The model agrees with the π^+ differential cross-section out to momentum transfers of 2 GeV^2 , with the π^-/π^+ ratio from deuterium, and with the polarization measured in the DESY experiment. Figure 11 shows the fit to the π^+ differential cross-section, Fig. 12 shows the π^-/π^+ ratio predicted, and Fig. 13 shows the polarization. The agreement is remarkable.

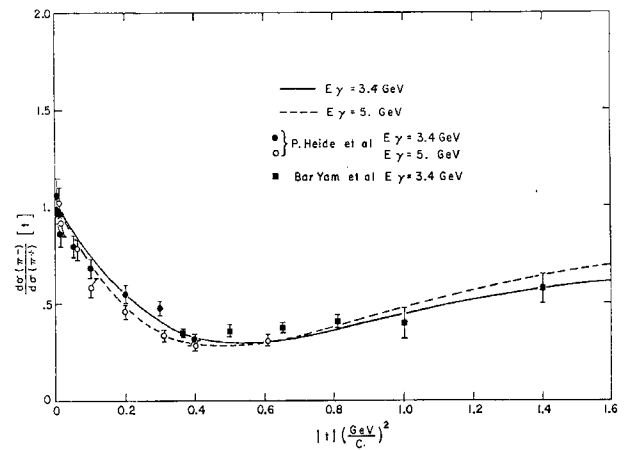
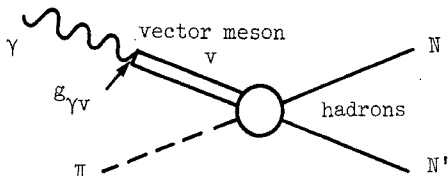


Fig. 12 The π^-/π^+ ratio in the model of Frøylund and Gordon.

1.5 Vector dominance and charged pion photoproduction

In the vector dominance model, the electromagnetic current is assumed to be identical to a linear superposition of vector-meson fields ($\rho\omega\phi$). The photon interacts with hadrons, as shown in the following sketch.



The photon turns into a vector meson with the appropriate coupling constant $g_{\gamma V}$, and then the vector meson interacts with hadrons. With this model and time reversal invariance, it is possible to relate the amplitude for π -meson photoproduction to the amplitude for the production of transversely polarized vector mesons by pions as shown in Eq. (7):

$$A(\gamma N \rightarrow \pi N') = \sum_{\rho \omega \phi} A(\pi N' \rightarrow V_{tr} N). \quad (7)$$

We can square both sides of Eq. (7) and write a relation between cross-sections as shown in Eq. (8):

$$\frac{d\sigma}{dt}(\gamma N \rightarrow \pi N') = g_{\gamma\rho}^2 \rho_{11} \frac{d\sigma}{dt}(\pi N' \rightarrow \rho^0 N) + g_{\omega\gamma}^2 \rho_{11} \frac{d\sigma}{dt}(\pi N' \rightarrow \omega^0 N) + (\rho\omega \text{ interference}) + \dots, \quad (8)$$

where g^2 is the appropriate coupling constant which can be determined from other experiments, ρ_{11} is an element of the appropriate density matrix in the helicity frame, and terms involving ϕ mesons have been

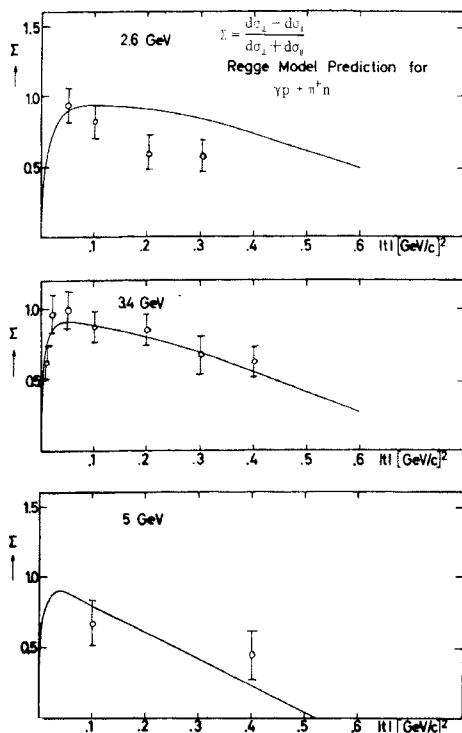


Fig. 13 The prediction of Frøylund and Gordon π^+ photoproduction by polarized photons.

dropped, since these can be shown experimentally to be small. One must be cautious in dealing with the $\rho\omega$ interference terms--strictly speaking, they can only be handled if the details of the amplitudes are known. Relations between cross-sections will be most reliable if the appropriate linear combination of cross-sections is chosen in which the interference terms cancel. Such a combination is

$$\frac{d\sigma}{dt}(\gamma p \rightarrow \pi^+ n) + \frac{d\sigma}{dt}(\gamma n \rightarrow \pi^- p) = 2g_{\gamma\rho}^2 \rho_{11} \frac{d\sigma}{dt}(\pi^- p \rightarrow \rho^0 n) + 2g_{\omega\gamma}^2 \rho_{11} \frac{d\sigma}{dt}(\pi^- p \rightarrow \omega^0 n). \quad (9)$$

Recently Dar, Weisskopf, Levinson and Lipkin¹³, Diebold and Poirier¹⁴, and Kramer and Schildknecht¹⁵ have published comparisons of the π -meson photoproduction cross-section with the predictions of the vector dominance model. Figure 14 shows a test of Eq. (9) from Dar et al., and Fig. 15 from Diebold and Poirier. Dar et al., and Kramer and Schildknecht used photon data from below 5 GeV, and determined the elements of helicity density matrix by rotation of published data which were given in the Jackson frame. Diebold and Poirier used 5 and 8 GeV photon data, and determined the helicity density matrix by refitting the raw data of Poirier et al.¹⁶). The vector dominance model passes this test with flying colours.

Kramer and Schildknecht have also used a quark model relation to determine the difference between the cross-sections for π^+ photoproduction from the proton, and π^- photoproduction from the neutron, in

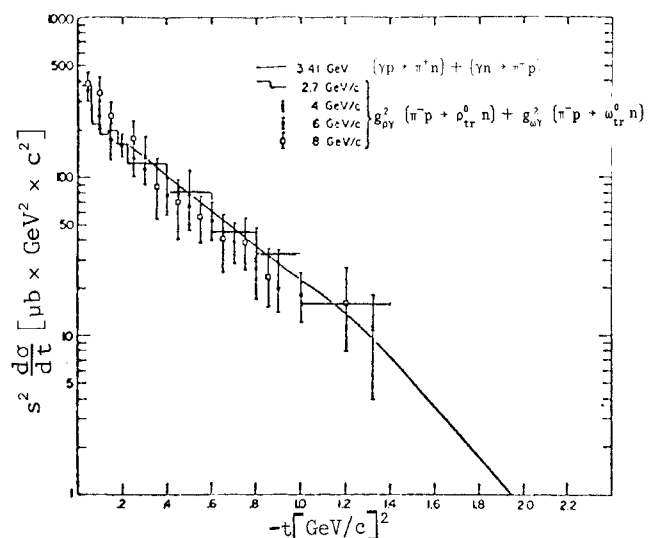


Fig. 14 Comparison of Ref. 13, using the vector dominance model, of ρ and ω production by pions to π^+ photoproduction.

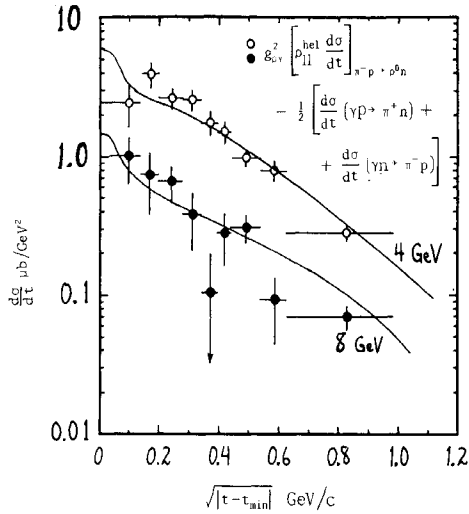


Fig. 15 Comparison of Ref. 14, using the vector dominance model, of ρ and ω production by pions to π^+ photoproduction.

terms of the cross-sections for $K^-\bar{p} \rightarrow \bar{K}^*n$ and $K^+n \rightarrow K^*p$. Figure 16 shows the results. The agreement is quite bad.

Dar and Weisskopf have predicted the ratio of π^-/π^+ photoproduction from deuterium by assuming a maximum interference between the ρ and ω amplitudes. Their results are shown in Fig. 17. In this case the agreement with the data is quite good.

Krammer and Schildknecht have also used the vector dominance model to predict the cross-section for π^+ photoproduction with polarized photons. Figure 18 shows the results, compared to the results of the DESY experiment. Again, the agreement is quite bad except at the $|t| < 0.1$ point in the 3.4 GeV data. This is not too surprising, since at all $|t| > 0.1$

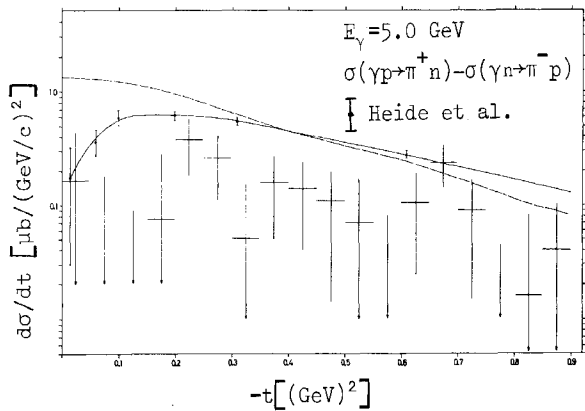


Fig. 16 Comparison of Ref. 15, using the vector dominance and quark models, of the production of K^* 's and K 's to the difference between π^+ production from the proton and π^- production from the neutron.

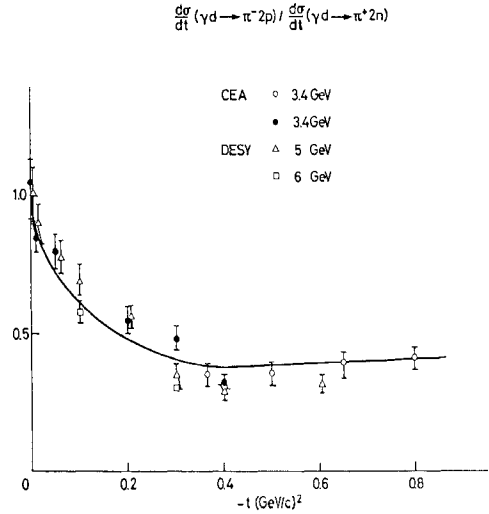


Fig. 17 Comparison of Ref. 13, using the vector dominance model, of ρ and ω production by pions to the ratio of π^-/π^+ photoproduction from deuterium.

(GeV)² the ρ - ω interference terms are important, and the same quark model relation is involved in predicting this cross-section as in determining the difference between π^- and π^+ photoproduction cross-sections. In view of the good agreement of the vector dominance model with ρ and ω data, the quark model relation should perhaps be re-examined.

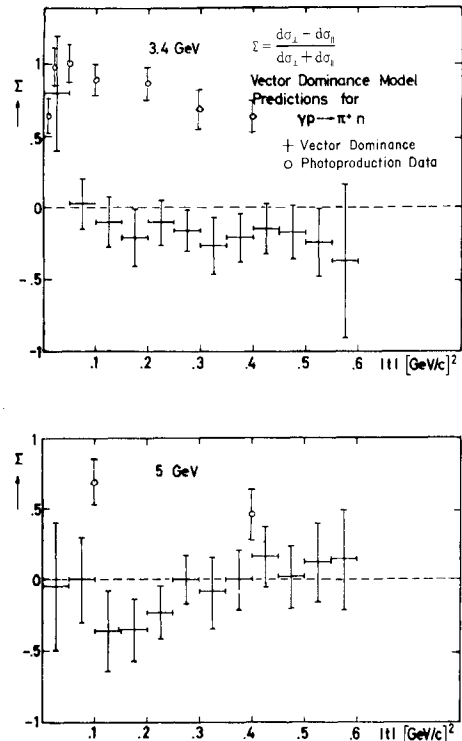


Fig. 18 Vector dominance and quark model prediction of the cross-section for π^+ photoproduction by polarized photons from Ref. 15.

2. π^0 PHOTOPRODUCTION

A considerable amount of data on forward photoproduction of π^0 mesons at energies up to 6 GeV has been obtained in the last three years by groups at DESY¹⁷⁾ and at CEA¹⁸⁾. An experiment has recently been completed by the Ritson group at SLAC¹⁹⁾, which extends the energy range over which the π^0 cross-section has been measured up to 16 GeV. This experiment covers a range of momentum transfers from 0.2 to roughly 1.4 GeV^2 . Only the lower energy experiments cover the region of very small momentum transfer.

The general characteristics of the data are a sharp spike in the cross-section in the forward direction from π^0 production in the Coulomb field of the nuclei (Primakoff effect), a moderately rapid fall with increasing momentum transfer (e^{5t}) out to a momentum transfer of about 0.5 GeV^2 , a dip or break slope at $|t| = 0.5$, a relatively flat cross-section out to a $|t|$ of 1.2, and again a fall-off with increasing $|t|$. Data from CEA, DESY, and SLAC are shown in Fig. 19a, where $(S - M_p^2)^2(d\sigma/dt)$ is plotted versus t . Only part of the existing data below 6 GeV are shown. Plotted in this way, the data show almost no energy dependence except in the region of $|t| = 0.5$. There the SLAC data, which have the highest statistical accuracy in this region, show a small dip in the cross-section at a photon energy of 6 GeV and no dip at all at a photon energy of 16 GeV.

The lowest mass particles which can be exchanged in the π^0 photoproduction reaction are ρ and ω . If exchanged as elementary particles, without absorption, $d\sigma/dt$ at fixed momentum transfer should be independent of photon energy. Since the data are clearly not independent of photon energy, the π^0 photoproduction reaction has been interpreted in terms of a model involving Reggeized ω and B-meson exchange. The ω exchange accounts for most of the cross-sections, but ω exchange alone would give a zero in the cross-section at $|t| = 0.5$, where the ω trajectory goes through 0. B-meson exchange fills in this dip. The specific model of Ader, Capdeville and Salin²⁰⁾ which has been used to fit the DESY data predicts that the dip in the cross-section at $|t| = 0.5$ should become deeper as the energy increases, since the B trajectory lies below the ω trajectory.

The data of Fig. 19a near $|t| = 0.5$ show that the dip seems to be filling in as the energy increases. In addition, the energy dependence of the cross-section outside the region of the dip seems incompatible with the simple picture of Reggeized ω exchange. Using a straight-line Regge trajectory, the 16 GeV data of the SLAC group should be a factor of about 2 above the 4 GeV data of DESY at $-t = 0.2$, and should be a

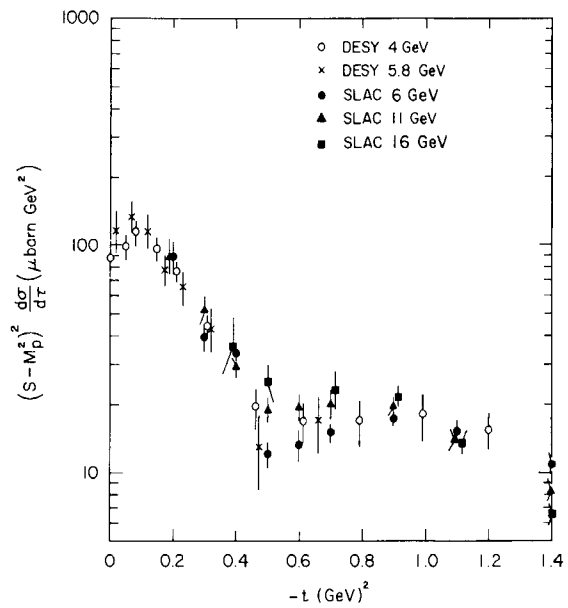


Fig. 19a π^0 photoproduction cross-sections from Refs. 17 to 19.

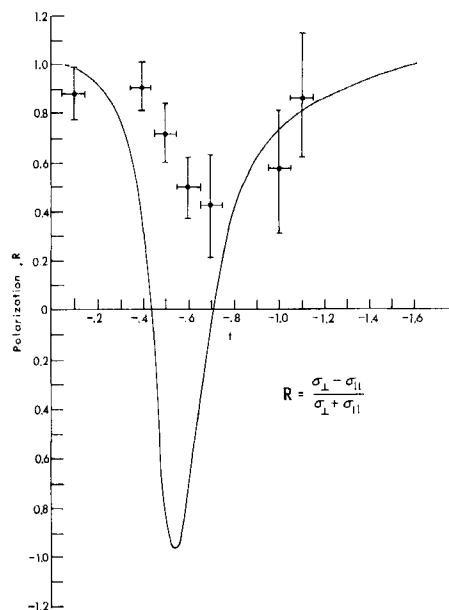


Fig. 19b π^0 photoproduction cross-sections with polarized photons from Ref. 20.

factor of $\sqrt{2}$ below the 4 GeV data at $-t = 0.8$. Since this is clearly not the case, we must conclude that this simple model does not work sufficiently well to account for the high-energy data.

The Osborne group²¹⁾ at CEA has reported at this Conference on measurements of the cross-section for $\gamma p \rightarrow \pi^0 p$ with polarized photons which also contradict the model using ω and B exchange. The polarized photon beam was produced by coherent bremsstrahlung from a crystal, as described previously in the discussion of the DESY experiment on π^+ production with polarized photons. The results of this experiment are shown in Fig. 19b, where $(\sigma_{\perp} - \sigma_{\parallel})/(\sigma_{\perp} + \sigma_{\parallel})$ is plotted versus t . The results show that at the point where the ω trajectory goes through zero, $R \approx 0.5$, which implies that $\sigma_{\perp}/\sigma_{\parallel} \approx 3$, i.e. the cross-section is dominated by natural spin-parity exchange.

Harari²²⁾ has assumed the validity of the vector dominance model and uses this assumption to test the hypothesis that π^0 photoproduction goes through Reggeized ω and B exchange. In this model, at the point where the ω trajectory passes through 0, the π^0 photoproduction proceeds via isoscalar photons, and the π^0 cross-section is given in the vector dominance model by

$$\frac{d\sigma}{dt}(\gamma p \rightarrow \pi^0 p) = \frac{g_{\omega\gamma}^2}{4} \frac{d\sigma}{dt}(\pi^- p \rightarrow \omega_{tr} N). \quad (10)$$

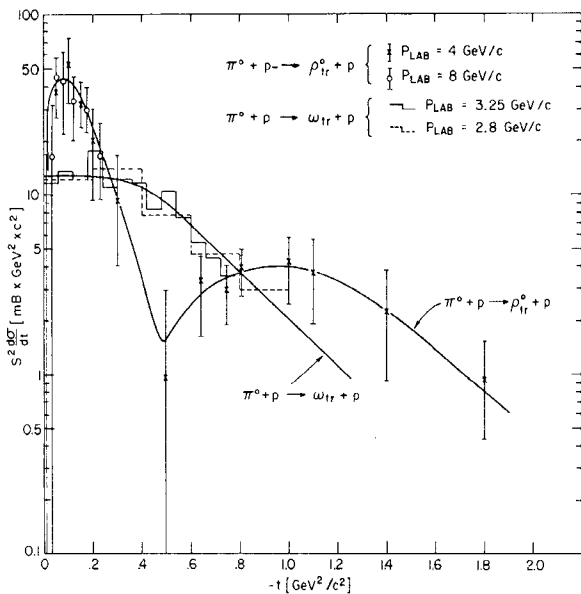


Fig. 20a Transversely polarized vector meson production (calculated) from Ref. 13.

Harari finds that the π - ω cross-section is too small by a factor of 10 to account for π^0 photoproduction at this momentum transfer. By pushing all errors to their limits, he can reduce the discrepancy to a factor of 4. Since the π - ω cross-section determines the sum of all isovector exchanges, the Regge model is in serious difficulty.

The implications of the π^0 photoproduction experiments for the Regge theory can be summarized as follows. In the region of the "dip":

- a) isoscalar exchange is required (Harari: vector dominance)
- b) natural spin parity exchange is required (Osborne: polarized photon experiments)
- c) $\alpha(t) \geq 0$ for $|t| \lesssim 1 \text{ GeV}^2$ (Ritson: π^0 cross-section measurements)
- d) charge conjugation = (-1) (conservation of C).

There is no established or conjectured particle in the latest edition of the Rosenfeld table that fulfills requirements 1, 2, and 4 except the ϕ and the ω (the ϕ is usually ignored in these discussions, but since we are grasping at straws, we will keep it). Either the ω and or ϕ have very strange trajectories, or something equivalent to poles or cuts is required, or the Regge model must be abandoned. I am sure the theorists will find a way around this problem with dispatch.

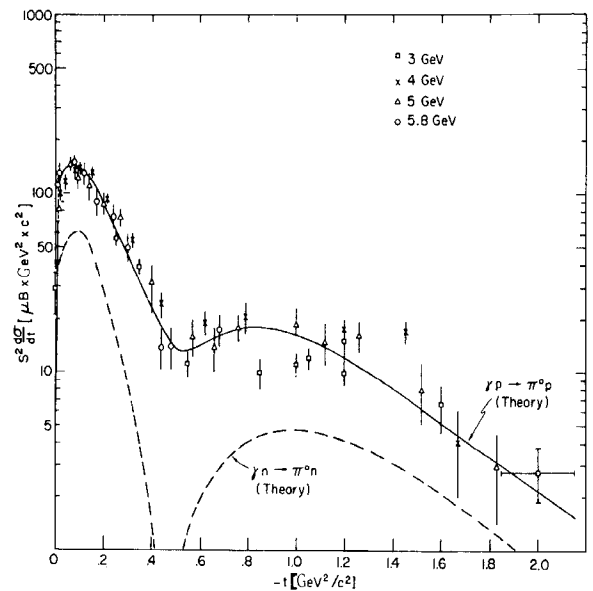


Fig. 20b Vector dominance prediction of the π^0 photoproduction cross-section from Ref. 13.

Dar, Weisskopf, Levinson, and Lipkin¹³⁾ have compared the vector dominance prediction of π^0 photoproduction with the experimental data. They write the π^0 cross-section as

$$\frac{d\sigma}{dt} \left(\gamma_n^p \rightarrow \pi_n^0 p \right) = \frac{1}{2} \left\{ g_{\rho\gamma} \left[\frac{d\sigma}{dt} (\pi^0 p \rightarrow \rho_{tr}^0 p) \right]^{\frac{1}{2}} \pm g_{\omega\gamma} \left[\frac{d\sigma}{dt} (\pi^0 p \rightarrow \omega_{tr} p) \right]^{\frac{1}{2}} \right\}^2, \quad (11)$$

where the + and - signs on the right-hand side of Eq. (11) refer to π^0 photoproduction from the proton and neutron, respectively, ρ_{tr} and ω_{tr} indicate the cross-section for production of ρ and ω mesons transversely polarized in the helicity frame, and the relative phase of the ρ and ω contributions comes from SU(6). The cross-sections on the right-hand side of Eq. (11) are of course unmeasurable, but they can be obtained by using isospin relations from measurable quantities as follows:

$$\frac{d\sigma}{dt} (\pi^0 p \rightarrow \rho^0 p) = \frac{1}{2} \left[\frac{d\sigma}{dt} (\pi^- p \rightarrow \rho^- p) + \frac{d\sigma}{dt} (\pi^+ p \rightarrow \rho^+ p) - \frac{d\sigma}{dt} (\pi^- p \rightarrow \rho^0 n) \right] \quad (12)$$

$$\frac{d\sigma}{dt} (\pi^0 p \rightarrow \omega^0 p) = \frac{1}{2} \frac{d\sigma}{dt} (\pi^- p \rightarrow \omega n). \quad (13)$$

The results of applying these relations are shown in Fig. 20a. In the figure, the curve labelled ω gives the square of the amplitude for all isoscalar exchanges and the curve labelled ρ gives the square of the amplitude for all isovector exchanges. The curves are fitted to the data by eye, and the ρ curve is very badly determined in the region $0.2 < -t < 0.6$. Figure 20b shows the comparison to the π^0 photoproduction data. The theoretical curve agrees fairly well with the data, but in view of the large uncertainty in the $\pi\rho$ data near the dip in the π^0 cross-section, agreement between the curve and experiment in this region should be regarded as fortuitous.

A report on a new measurement of the π^0 lifetime has been contributed to this Conference by the group of Braunschweig, Braunschweig, Husmann, Lübelmeyer, and Schmitz, working at DESY¹⁷⁾. They have measured the π^0 photoproduction cross-section in the Coulomb

field of a proton. Their data are shown in Fig. 21. The sharp rise in the cross-section at 0° is presumably due to the Primakoff effect. The curves show a fit to the data using the Primakoff effect plus Reggeized ω exchange, the solid curves being for constructive interference and the dashed curves for destructive interference. The π^0 lifetime obtained is strongly sensitive only to the assumption that the background under the Primakoff peak goes to 0 at 0° and is not too sensitive to the detailed shape of the background. The value of the π^0 lifetime obtained is

$$\tau_{\pi^0} = \left(0.6_{-0.08}^{+0.2} \right) \times 10^{-16} \text{ sec}, \quad (14)$$

which gives

$$\Gamma(\pi^0 \rightarrow \gamma\gamma) = 11_{-2.8}^{+1.6} \text{ V}. \quad (15)$$

This new lifetime still does not remove the discrepancy between the SU(3) prediction without $\eta - \chi^0$ mixing of the ratio of the partial width of $\pi^0 \rightarrow 2\gamma$ and $\eta \rightarrow 2\gamma$. Using the measurements of Bemporad et al.^{2,3)} on the Primakoff effect in η production from complex nuclei, and the measurements of Baltay et

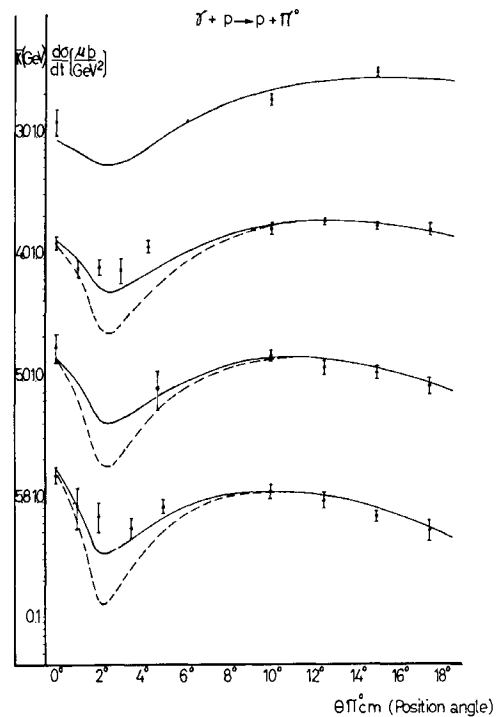


Fig. 21 Forward π^0 photoproduction cross-section from Ref. 17.

a1.²⁴) on the branching ratio of $\eta \rightarrow 2\gamma$, we find

$$\Gamma(\eta \rightarrow \gamma\gamma) \approx 1 \pm 0.15 \text{ keV} . \quad (16)$$

The SU(3) prediction is

$$\left[\frac{\Gamma(\eta \rightarrow \gamma\gamma)}{\Gamma(\pi^0 \rightarrow \gamma\gamma)} \right]_{\text{SU}(3)} \times \Gamma(\pi^0)_{\text{exp}} = 235_{-60}^{+35} \text{ eV} . \quad (17)$$

3. PHOTOPRODUCTION OF $N^*(1238)$

My group at SLAC has reported at this Conference²⁵) on the results of cross-section measurements of the reaction

$$\gamma + p \rightarrow \pi^- + N^{*++}(1238) . \quad (18)$$

The experiment was done by detecting only the π^- and fitting the excitation function with the N^* and various combinations of background terms. The results are shown in Fig. 22, where the errors on the points include our estimate of the variation of the cross-section with different background models. The dashed lines on the graph are the differential cross-sections for the reaction $\gamma p \rightarrow \pi^+ n$. The results of this experiment are somewhat surprising. At momentum transfers $\geq 0.2 \text{ GeV}^2$, the N^* cross-section is quite close to the cross-section for single π^+ production. As the momentum transfer decreases, the differential cross-section rises sharply ($d\sigma/dt \approx e^{12t}$), reaching a maximum of roughly six times the π^+ cross-section at small momentum transfer. The N^* cross-section then dips down as the momentum transfer

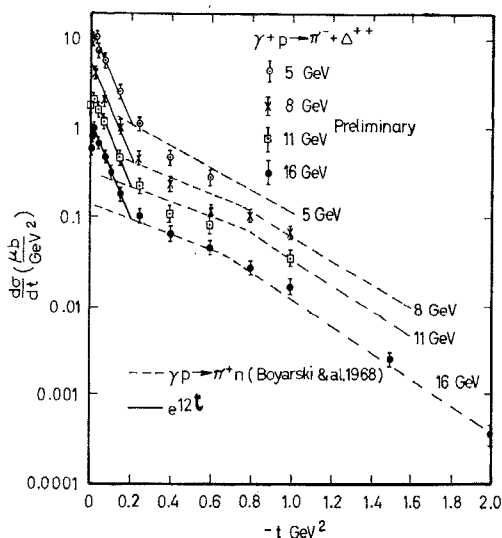


Fig. 22 Cross-section for photoproduction for $\pi^- N^{*++}(1238)$ from Ref. 24.

goes toward the minimum momentum transfer. The small momentum transfer data are shown on an expanded scale in Fig. 23, where $(S - M^2)^2 (d\sigma/dt)$ is plotted versus $\sqrt{-t}$. Plotted in this way, the data seem to be independent of photon energy. The dip in the forward differential cross-section is clear, but it is not clear whether the cross-section extrapolates to zero or a finite value at $|t| = 0$. We do not think that these data can be much improved, since uncertainties in the background subtraction under the N^* contribute an error comparable to the statistical error at the small momentum transfer points. Figure 24a shows the parameter α of Eq. (1) for the N^* reaction. α remains near 0 for the entire range of momentum transfers covered.

We have seen in the case of $\gamma p \rightarrow \pi^+ n$ and $\gamma n \rightarrow \pi^- p$ that the $(S - M^2)^2 d\sigma/dt$ is nearly independent of energy over the range of roughly 2-16 GeV. It should then be no surprise that the same thing seems to happen in $\gamma p \rightarrow \pi^- N^{*++}$. When scaled in this way, the DESY bubble chamber²⁶) data are consistent for $|t| < 0.3$ with the SLAC data for all energies above 1.4 GeV. At $|t| > 0.3$ there is insufficient bubble chamber data to allow a comparison.

The N^* photoproduction data can be compared to the cross-sections for $\pi^+ p \rightarrow \rho^0 N^{*++}$ and $\omega^0 N^{*++}$ using the vector dominance model and S-U crossing. Dar and Weisskopf, and Iso and Yoshii²⁷) have made such comparisons using the DESY bubble chamber data for the γ cross-sections, and data from several bubble chamber experiments for the π cross-sections. I have added

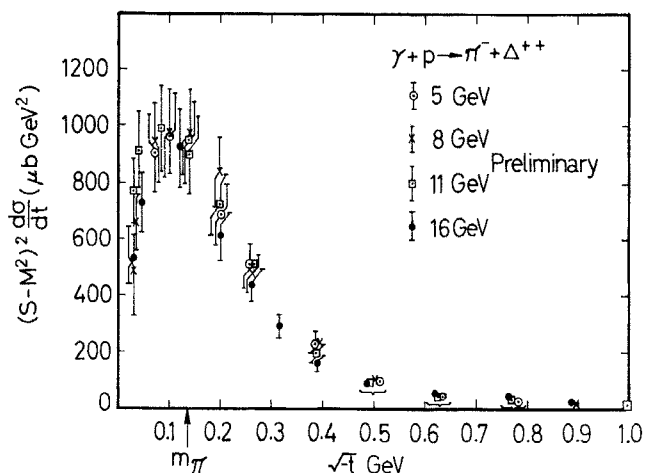


Fig. 23 N^* photoproduction cross-section at small momentum transfers on an expanded scale.

points from the high-energy photoproduction experiment to the Dar and Weisskopf graph, and the results are shown in Fig. 24b. The shape is approximately correct, but the normalization is off. The principal

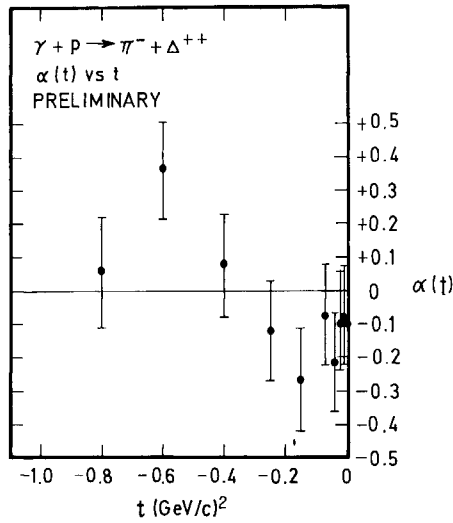


Fig. 24a Energy dependence of the N^* photoproduction cross-section at fixed momentum transfer.

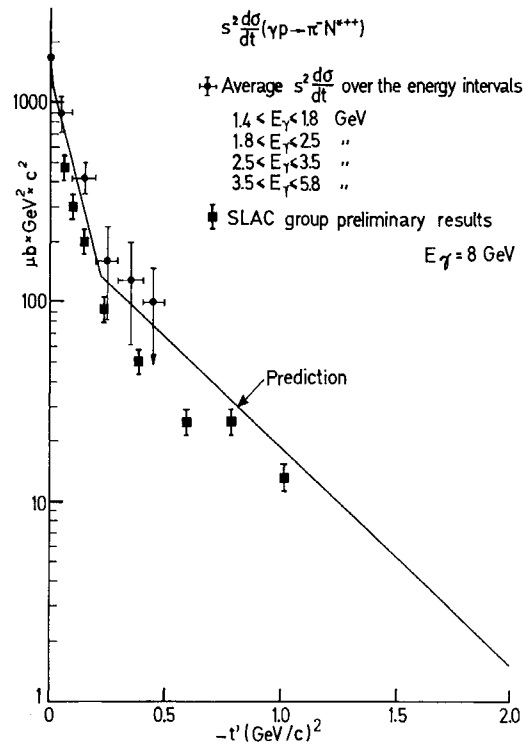


Fig. 24b Vector dominance comparison of $\gamma p \rightarrow \pi N^*$ and $\pi^+ p \rightarrow \rho^0 N^*$ and $\omega^0 N^*$ from Refs. 27a and 25.

contributors of the bubble chamber data, the ABC Collaboration (private communication from D.R.O. Morrison) have urged great caution in using the $N^{*++} \rho^0$ cross-section, since they consider that there is no satisfactory method for determining this cross-section. With this in mind, we can only conclude that the agreement may be better or worse than indicated in Fig. 24b, but that whatever causes the steep rise for $|t| < 0.2 \text{ (GeV)}^2$ in the photoproduction reaction, also causes such a rise in the $N^* \rho$ reaction.

4. CHARGED K-MESON PHOTOPRODUCTION

The only new data on charged K-meson photoproduction come from my group at SLAC²⁸⁾ where we have extended our measurement on the reactions

$$\gamma + p \rightarrow K^+ + \Lambda^0 \quad (19a)$$

$$\gamma + p \rightarrow K^+ + \Sigma^0. \quad (19b)$$

The statistics at small momentum transfers have been improved, and the measurements extended to cover larger momentum transfers. The differential cross-section for the reaction $\gamma + p \rightarrow K^+ + \Lambda^0$ is shown in

Fig. 25. The data show a sharp dip at small momentum transfer in contrast to the π^+ data which show a sharp rise. At large momentum transfer, the data show the same slope as is shown in π^+ production and the K- Λ differential cross-section is about 1/3 of the π^+ differential cross-section. The energy dependence of the cross-section at fixed momentum transfer was determined by fitting the data to the

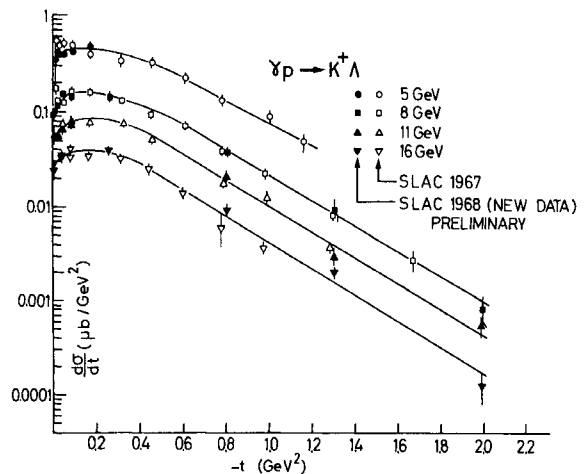


Fig. 25 Differential cross-section for the photoproduction of $K^+ \Lambda^0$ from Ref. 28.

form of Eq. (1). The parameter α is plotted versus t in Fig. 26. The figure shows that α is quite small to momentum transfers of -2 GeV^2 . Figure 27 shows the ratio of $K^+\Sigma^0/K^+\Lambda^0$ production as a function of momentum transfer. This ratio is consistent with one at all photon energies except in the region of very small momentum transfers. The low-energy data show the Σ/Λ ratio decreasing as $-t \rightarrow 0$. The higher energy data do not show this trend, but they do not go down to as small a momentum transfer.

The π , $K\Lambda$, and $K\Sigma$ data can be used to test the SU(3) prediction of the following relations between the amplitudes for these three processes:

$$\sqrt{2} A(\pi^+n) = -\sqrt{3} A(K^+\Lambda^0) - A(K^+\Sigma^0). \quad (20)$$

This relation between amplitudes can be turned into relation between cross-sections as follows:

$$2\sigma(\pi n) = \left| [3\sigma(K\Lambda)]^{\frac{1}{2}} + [\sigma(K\Sigma)]^{\frac{1}{2}} e^{i\phi} \right|^2, \quad (21)$$

where ϕ is the relative phase of the amplitudes. We have used the new SLAC data to test these relations. In Fig. 28 $\cos \phi$ is plotted versus momentum transfer for energies from 5 to 16 GeV. The SU(3) relation is good if $\cos \phi$ lies between ± 1 . The data show that SU(3) is indeed satisfied for all momentum transfers $> 0.1 \text{ GeV}^2$ but is badly broken for momentum transfers smaller than this value. This is a consequence of

the sharp rise in the π^+ cross-section and the sharp fall in the K cross-section at small momentum transfers.

There has not been a great deal of theoretical activity on K photoproduction in the past year. Two sets of authors [Ball, Frazer, and Jacob²⁹), and Henyey³⁰)] have tried to analyse both the forward π photoproduction and K photoproduction data in terms of a Regge conspiracy model, and both have reached what I would call qualitatively similar conclusions. Ball, Frazer and Jacob find that the very forward momentum transfer K data are consistent with a conspiracy model, although with a weaker conspiracy than occurs in the case of the pion. Henyey finds that the small momentum transfer K data are consistent with no conspiracy at all. Both find that, except at the very most forward points, K exchange must in fact contribute little to the cross-section, and the cross-section must be dominated by something like K^* exchange. The reason for this conclusion is that, using the $K\Lambda$ and $K\Sigma$ coupling constants derived recently by Kim³¹), one should find very small Σ production relative to Λ production. Since the data indicate comparable Λ and Σ production, K exchange must be excluded as the dominant mechanism in Λ and Σ photoproduction.

Meshkov and Ponzini³²) have used SU(6)_W to predict the ratio of forward $K\Lambda/K\Sigma$ photoproduction.

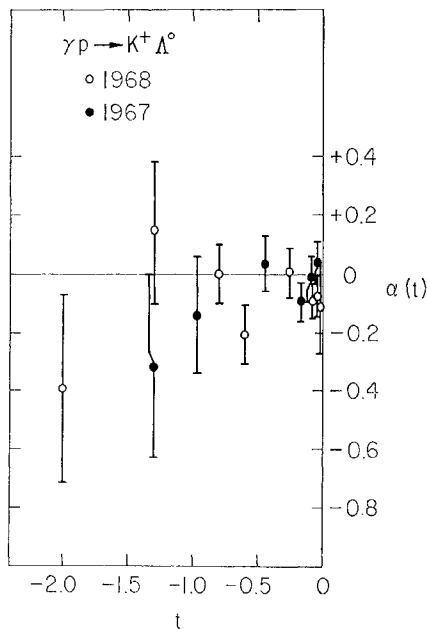


Fig. 26 Energy dependence of the $K^+\Lambda^0$ photoproduction cross-section from Ref. 28.

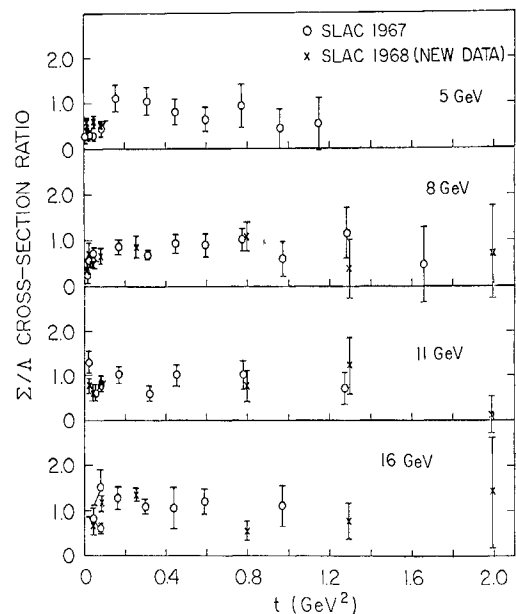


Fig. 27 Ratio of $K^+\Sigma^0/K^+\Lambda^0$ photoproduction cross-section from Ref. 28.

They find that this ratio should be between 0.5 and 1 in a photon energy range of 5 to 16 GeV, which is in quite good agreement with the data, and represents an improvement over the prediction of Lipkin and Scheck³³), based on the quark model, that these cross-sections should be in a ratio of 1/27. However, $SU(6)_W$ is based on $SU(3)$, and we have seen that $SU(3)$ is violated at small momentum transfer based on the breakdown of the triangle inequality of Eq. (21). Meshkov and Ponzini blame the $SU(3)$ violation on the π , and assume that $SU(3)$ and hence $SU(6)_W$ is good for predicting relative $K\Lambda$ and $K\Sigma$ cross-sections.

5. MISCELLANEOUS

Diebold³⁴) at SLAC has been making a compilation of integrated cross-sections as a function of energy for various photoproduction reactions. At low energies, complete angular distributions are available and the integration is easy. At high energies, the forward cross-section is known and some measurements have been made in the backward direction. These backward cross-sections give limits on the intermediate $|t|$ region, and Diebold estimates that the integrated cross-sections should be accurate to 5-10%. Figures 29 and 30 show $k^2\sigma_{\text{total}}$ [$k^2 \propto (S - M^2)^2$] versus k for various reactions. All of these reactions show an astonishing similarity -- $k^2\sigma_T$ tends toward a constant at energies between 1.5 and 4 GeV.

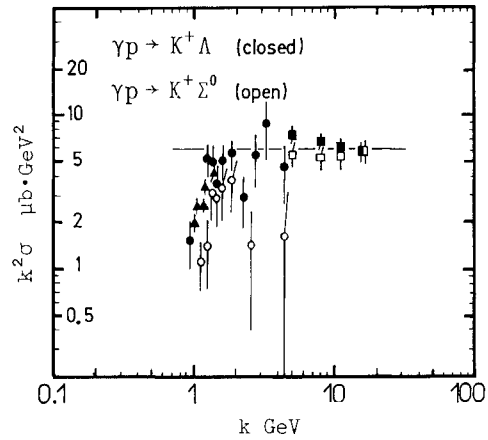


Fig. 29 Total cross-section for various π photoproduction reactions versus photon energy from Ref. 34.

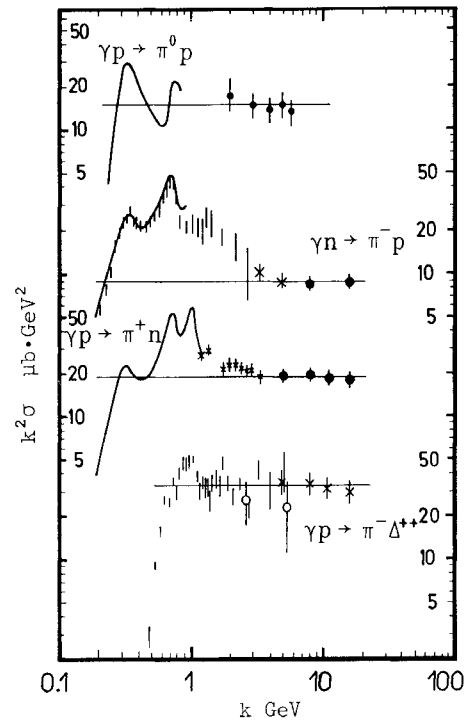


Fig. 30 Total cross-section for various K photoproduction reactions versus photon energy from Ref. 34.

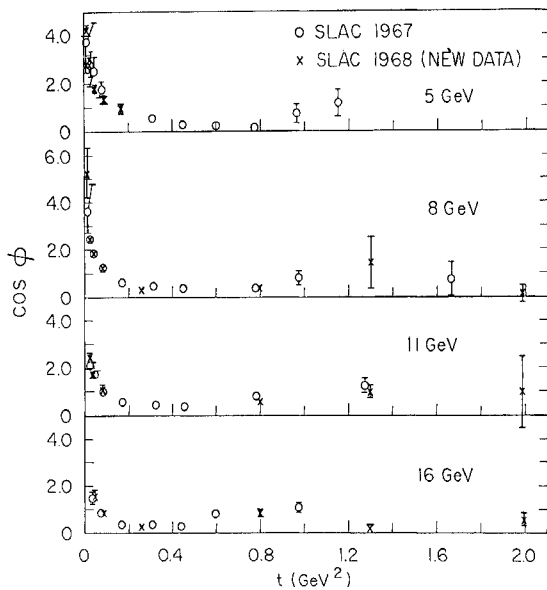


Fig. 28 Test of the $SU(3)$ triangle inequality using the data of Ref. 28.

6. SUMMARY AND CONCLUSIONS

Recent photoproduction experiments at CEA, DESY, and SLAC have given a wealth of information on the photoproduction of pseudoscalar mesons. We now have available differential cross-sections for production from the proton and the neutron with polarized and unpolarized photon beams. These experiments impose several restrictions on theoretical models, and will hopefully clear up some of the existing theoretical ambiguities. I would summarize what we have learned

from photoproduction studies in the past year as follows.

1. The vector dominance model works well when combinations of cross-sections can be used in which ρ - ω interference terms cancel out. When the ρ - ω interference term is important, reasonable assumptions on the relative phase of the ρ and ω amplitudes yield good agreement between reactions involving photons and reactions involving vector mesons.

2. The photon is not a special object which gives rise to features in various cross-sections which are not seen in hadron-induced reactions. This is, of course, implied by the success of vector dominance. However, the photon could be special if the vector mesons were also.

3. Charged pion photoproduction implies that theories using only linear Regge trajectories are untenable, and that theories using linear conspiring trajectories will probably not work.

4. π^0 photoproduction leads to stronger conclusions. Linear trajectories will not work.

5. The N^* production cross-section measurements have shown some peculiar features which need to be explained. Among these are the rough equality with π^+ cross-sections seen at $|t| > 0.2(\text{GeV})^2$, the e^{12t} behaviour seen for $m_\pi^2 < |t| < 0.2$, and the decrease in the cross-section for $|t| < m_\pi^2$.

6. SU(3) fails to predict properly the relation between the cross-section for production of members of the pseudoscalar octet. However, the failure occurs in a region of t where mass-difference effects may be important.

7. All the well-measured pseudoscalar meson production cross-sections exhibit a k^{-2} behaviour. The differential cross-sections also exhibit roughly the same k^{-2} dependence out to $|t| > 1(\text{GeV})^2$, with the exception of a limited t region near $|t| = 0.5$ in π^0 production. This regularity seems to begin at photon energies of around 2 GeV.

There are still other features of the data which might be mentioned, but I think these are sufficient to generate a great deal of thought. Hopefully, they will all be explained by the next conference.

REFERENCES AND FOOTNOTES

1. A.M. Boyarski et al., paper 430.
2. A.M. Boyarski, F. Bulos, W. Busza, R. Diebold, S.D. Ecklund, G.E. Fischer, J. Rees and B. Richter, Phys. Rev. Letters 20, 300 (1968).
3. G. Buschnorn, J. Carroll, R.D. Eandi, P. Heide, R. Hübner, W. Kern, U. Kötz, P. Schmüser and H.J. Skronn, Phys. Rev. Letters 17, 1027 (1966); Phys. Rev. Letters 18, 511 (1967).
4. See, for example, S.D. Drell and J.D. Sullivan, Phys. Rev. Letters 19, 268 (1967).
5. P. Heide, U. Kötz, R.A. Lewis, P. Schmüser, H.J. Skronn and H. Wahl, Phys. Rev. Letters 21, 248 (1968).
6. A.M. Boyarski et al., paper 431.
7. Z. Bar-Yam, J. de Pagter, M.M. Hoenig, W. Kern, D. Luckey and L.S. Osborne, Phys. Rev. Letters 19, 40 (1967).
8. A. Dar and A. Gal, MIT preprint CTP 28 (1968), and K. Schilling, DESY preprint 68/35 (1968).
9. Chr. Geweniger et al., abstract 336.
10. R. Brower and J.W. Dash, UCRL 18199 (1968).
11. D. Amati, G. Cohen-Tannoudji, R. Jengo and Ph. Salin, Physics Letters 26 B, 510 (1968).
12. J. Frøyland and D. Gordon, MIT preprint CTP 38 (1968).
13. A. Dar, V.F. Weisskopf, C.A. Levinson and H.J. Lipkin, Phys. Rev. Letters 20, 1261 (1968).
14. R. Diebold and J.A. Poirier, Phys. Rev. Letters 20, 1532 (1968).
15. M. Kramer and D. Schildknecht, DESY Report 68/33 (1968).

16. Notre Dame-Purdue-SLAC-LRL Collaboration, to be published in Phys. Rev.
17. M. Braunschweig, W. Braunschweig, D. Husmann, K. Lübelmeyer and D. Schmitz, Phys. Letters 26 B, 405 (1968), and paper 297.
18. G.C. Bolon, D. Garelick, S. Homma, R. Lewis, W. Lobar, D. Luckey, L.S. Osborne, R. Schwitters and J. Uglum, Phys. Rev. Letters 18, 926 (1967).
19. R. Anderson, D. Gustavson, J. Johnson, D. Ritson, R. Weinstein, W.G. Jones and D. Kreinick, Phys. Rev. Letters 21, 384 (1968), and paper 681.
20. J.P. Ader, M. Capdeville and Ph. Salin, Nucl. Phys. 33, 407 (1967).
21. D. Bellenger et al., paper 531.
22. H. Harari, SLAC preprint PUB-477 (1968); Phys. Rev. Letters 21, 835 (1968).
23. C. Bemporad, P. Braccini, L. Foa, K. Lübelmeyer and D. Schmitz, Phys. Letters 25 B, 380 (1967).
24. C. Baltay, P. Franzini, J. Kim, L. Kirsch, R. Newman, N. Yeh, J. Cole, J. Lee-Franzini and H. Yarger, Phys. Rev. Letters 19, 1498 (1967).
25. A.M. Boyarski et al., paper 429.
26. Aachen-Berlin-Bonn-Hamburg-Heidelberg-Munich Collaboration, DESY report 68/8.
- 27a. A. Dar and V.F. Weisskopf, CERN preprint 68/917/5 (1968).
- 27b. C. Iso and H. Yoshii, Ann. Phys. 47, 424 (1968); 48, 237 (1968).
28. A.M. Boyarski et al., paper 432.
29. J. Ball, W. Frazer and M. Jacob, Phys. Rev. Letters 20, 518 (1968).
30. F. Henyey, Phys. Rev. 170, 1619 (1968).
31. J.K. Kim, Phys. Rev. Letters 19, 1074 (1967).
32. S. Meshkov and R. Ponzini, NBS preprint (1968).
33. H.J. Lipkin and F. Scheck, Phys. Rev. Letters 18, 347 (1967).
34. R. Diebold, private communication.

DISCUSSION

SAKURAI: You emphasized essentially two points
 i) For a large class of photoproduction reactions, $s^2 d\sigma/dt$ is constant; ii) vector meson dominance works. A naive conclusion we can draw from these two points is that the dominant mechanism for a large class of purely hadronic reaction amplitudes is due to a flat trajectory with $\alpha_{\text{eff}} \approx 0$. Now this statement is unconnected with the electromagnetic interactions. I would therefore like to ask: can we infer the existence of a flat $J = 0$ trajectory (or fixed pole) just by studying hadronic processes? Can Dar or Weisskopf say?

DAR: The answer is "yes". The production of transverse vector mesons in π -nucleon collisions exhibits constant $s^2 d\sigma/dt$.

RITSON: Is the good agreement with vector dominance based on the old value of $\gamma_\rho^2/4\pi \approx 0.45$ or on the possible new value 1.1?

RICHTER: All the curves I have shown used values around 0.45 to 0.6, depending on the author.

MESHKOV: Two comments. i) I think that you would expect SU(3) to hold much better at high E and large $|t|$ than at high E and zero $|t|$. At zero $|t|$, I think that the effect of the mass differences becomes very important. ii) As far as the SU(6)_W calculations go, the breaking of SU(3) certainly pops out because you get a $\pi^+ n$ prediction (which is part of the triangular inequality) that is wrong. We have said that the $K^+ \Lambda$ and $K^+ \Sigma^0$ cross-sections should be reasonably good because the mass difference between

Λ and Σ is relatively unimportant compared to the mass difference between, say, the $K^+\Lambda$ and π^+n final states.

BERTOCCHI: A good fit to the forward spike in π^+ photoproduction has been obtained by di Vecchia, Drago, Ferro Fontán, Paciello, and Odorico, using π and π -conspirator exchange, and finite-energy sum rules, without any free parameter. They have not yet analysed the π^+ polarization, but the zero of the π residue at $t \approx -0.027 (\text{GeV}/c)^2$ (which also occurs in the Ball-Frazer-Jacob high-energy fit) shows that the forward spike is dominated by the natural parity π -conspirator.

TER MARTIROSYAN: What is the energy dependence of $d\sigma/dt$ for π^+ and π^0 photoproduction? Do the cross-sections always go as k^{-2} ?

RICHTER: For π^+ , the cross-section goes as k^{-2} out to $t \approx 1 \text{ GeV}^2$; for π^0 , the same thing happens with the exception of the region around $t \approx 0.5 \text{ GeV}^2$, where the cross-section decreases less rapidly than k^{-2} .

DI LELLA: Could the forward dip in the $\gamma p \rightarrow \pi^- \Delta^{++}$ cross-section be due to the Δ^{++} width, since t_{\min} depends on the mass?

RICHTER: For the high-energy data, t_{\min} is very much smaller than m_π^2 , where the cross-section starts to decrease, and the variation of t_{\min} with Δ mass is also small compared to m_π^2 . So I believe that the dip is not just an effect due to t_{\min} .

ELECTROMAGNETIC INTERACTIONS

Experimental 2

Chairman B. TOUSCHEK

Rapporteur W.K.H. PANOFSKY

Discussion Leaders P. LEHMANN
 E. LOHRMANN
 P. MARIN

Secretaries J. ALLABY
 J. BARLOW

LOW q^2 ELECTRODYNAMICS, ELASTIC AND INELASTIC ELECTRON (AND MUON) SCATTERING

W.K.H. Panofsky

Stanford Linear Accelerator Center, Stanford University, Stanford, Calif.

1. ELECTRODYNAMICS AT LOW MOMENTUM TRANSFER

In discussing electromagnetic processes at high energies, it is customary to start examining the validity of electrodynamics at high momentum transfers.

We will depart from tradition by dividing the subject into a discussion of quantum electrodynamics at low momentum transfers with high precision, and high momentum transfers at low precision. I will deal with the first subject, whilst other speakers will deal with the second. The justification for this otherwise illogical procedure is that high momentum transfer QED from the experimental point of view happens to overlap with experiments on the photo-production of vector mesons and their leptonic decays, and also that storage-ring work on high momentum transfer electrodynamics coincides with those experiments which again relate primarily to vector meson production processes; both of these subjects fall into the province of other rapporteurs. Another reason that permits the splitting of a discussion of the validity of QED into these two regions is the fact that the relation between low- and high-energy momentum transfer processes is highly model-dependent, should a meaningful deviation be found. At this time there is no reason for confidence in a particular model of a deviation, nor is there any persuasive evidence for the existence of any deviation, either from high q^2 or low q^2 experiments.

Low momentum transfer quantum electrodynamics is in a somewhat confusing state. On the one hand, one problem which has plagued physicists for the last years, namely the problem relating to consistency among different methods of determining the fine structure constant, has probably gone away. On the other hand, the discrepancy of the value of the Lamb shift

with theory has persisted, and new discrepancies in the values of the g-factor of the muon and electron seem to have appeared. I believe, however, it is also fair to say that none of these discrepancies are such that they may not be either experimental in nature, or may be the result of subtle points having been missed in analysis.

To discuss these questions let me first make reference to the spectrum of the hydrogen atom (Fig. 1). In past years the hydrogen fine structure

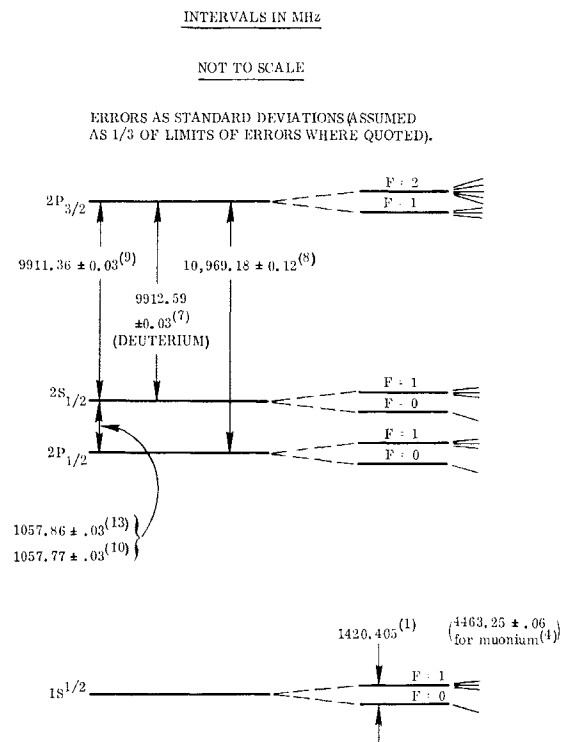


Fig. 1 The hydrogen spectrum (not to scale).

discrepancy has been identified by plotting values of

$$\alpha^{-1} - 137$$

which appeared to cluster near two values, one being 0.036, and the other 0.039. Although only few experiments have been reported to this Conference which

bear on this question, I would like to discuss the complete picture in order to provide some context.

The hyperfine structure of the ground state of hydrogen gives the experimental value¹⁾

$$\gamma_{\text{HFS}}^{\text{H}} = 1420.405 \dots \text{ MHz}$$

as measured by the hydrogen maser. The precision is beyond anything of interest here. The problem is mainly a theoretical one, namely how to take the nucleon structure into account. If one makes a purely static calculation²⁾ of nucleon structure, the value of the fine structure constant becomes

$$\alpha^{-1} = 137.0359$$

accurate to about one part per million. Although I am plotting this particular value on the summary sheet (Fig. 2) of values of the fine structure constant,

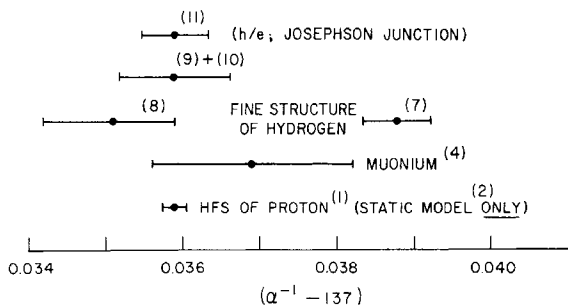


Fig. 2 Values of the fine structure constant.

there is little question that a static calculation will probably over-estimate the effect of finite nucleon size. The reason is that as the electron moves around the nucleon, the polarization of the nucleon will vary correspondingly, and therefore the effective finite size effect might be smaller. This effect has been estimated by Drell and Sullivan³⁾ and might give an additional correction in α of the order of five parts per million. It is this uncertain theoretical picture which in the past has led people not to take the HFS value of alpha too seriously, although no rational reason has been presented why the error should be larger than that estimated.

A shift has occurred during the last year in the measurement of the hyperfine structure of muonium. Amato et al.⁴⁾ have reported measurements of the hyperfine structure of muonium at very low magnetic field (10^{-2} gauss) in which the Zeeman splitting has

not been resolved. In a paper submitted to this conference they quote:

$$\gamma_{\text{HFS}}^{\mu} = 4463.25 \pm 0.06 \text{ MHz}$$

which is slightly higher than the values quoted earlier⁵⁾ at higher magnetic fields. To go from these measurements to a value of the fine structure constant, we need the measurement of the ratio of the muon moment to the proton moment as measured by the ratio of precession rates; this ratio is known to about 12 parts per million, and the correction due to Ruderman⁶⁾ which corrects for the fact that the proton and the muon find themselves in different chemical fields when undergoing such precession. Applying these auxiliary considerations one obtains

$$\alpha^{-1} = 137.0369 \pm 0.0013.$$

Although the use of muonium and also positronium is attractive to avoid the complications of finite nucleon structure in hyperfine structure, the muonium measurements are marred by such auxiliary considerations, while the positronium measurements and also the calculation of positronium fine structure have as yet not reached sufficient accuracy.

Let us now return to the proton. The most direct measurement of the fine structure constant should presumably derive from measurement of the fine structure interval ($2p^{3/2} - 2p^{1/2}$) as shown in Fig. 1. Historically the most accurate measurement was that of Lamb and collaborators [Dayhoff et al.⁷⁾] which measured the $2p^{3/2} - 2s^{1/2}$ interval and added to this the value of the Lamb-shift interval ($2s^{1/2} - 2p^{1/2}$). This combination gave a value of $\alpha^{-1} - 137$ slightly lower than 0.039 which had been extensively quoted in the literature and which is plotted in Fig. 2. However, two recent measurements have changed the situation: a direct measurement⁸⁾ of the fine structure separation has been made by determining precisely the magnetic field required to lead to crossing of the $2p^{3/2}$ and the $2p^{1/2}$ levels. This measurement has given a value of

$$\alpha^{-1} = 137.0353 \pm 0.0008 .$$

Although this may appear to be a more straightforward approach than that of Dayhoff et al.⁷⁾, one still should note that the error quoted requires confidence

in locating the line to one part in 2,000 of its width; for this one has to rely on complete theoretical understanding of line shape. Recently another measurement⁹⁾ has been made of the $2p^{3/2} - 2s^{1/2}$ interval, which when combined with the experimental Lamb-shift interval gives a value of

$$\alpha^{-1} = 137.0359 \pm 0.0007$$

for the inverse fine structure constant.

Finally, we have the new result obtained with cryogenic techniques which gives new precision to the ratio of Planck's constant to the electronic charge. This work by Parker et al.¹⁰⁾ used the precision determination of the voltage generated in a Josephson junction when irradiated at a fixed microwave frequency. This voltage appears to be related to the frequency in the cavity by the equation

$$2eV = h\nu,$$

from which the fine structure constant can be determined by the equation

$$\alpha^{-1} = \left(\frac{mc}{2Ry_{\infty} \hbar} \right)^{\frac{1}{2}} \left[\frac{c}{4Ry_p} \left(\frac{\mu_p}{\mu_0} \right) \left(\frac{1}{\gamma_p} \right) \left(\frac{2e}{h} \right) \right]^{\frac{1}{2}},$$

where Ry_{∞} is the value of the Rydberg constant at infinite mass measured in inverse centimetres, and where γ_p is the gyromagnetic ratio of the proton, while (μ_p/μ_0) is the value of the proton magnetic moment measured in Bohr magnetons. These auxiliary constants are known to such a sufficient precision that Parker et al. could quote a value of

$$\alpha^{-1} = 137.0359 \pm 0.0004.$$

The question of whether the theory of the Josephson junction is really sufficiently clean to permit confidence in this measurement has recently been answered experimentally to almost complete satisfaction by a series of remarkable measurements by John Clarke¹¹⁾. He demonstrated that the Josephson voltage steps are independent of the nature of the materials used to about one part in 10^8 .

All these experimental values, when plotted on Fig. 2, suggest strongly that now all measurements of $\alpha^{-1} - 137$, other than the early ones of Dayhoff et al.⁷⁾, cluster about 0.036, and that the new muonium measurements reported to this Conference appear to join the crowd.

Thus all appears to be well, except for the fact that the measurements of the Lamb shift itself (which affect the determination of α only in a minor way through addition to the partial fine structure interval $2p^{3/2} - 2s^{1/2}$) continue to fail to agree with theory. The two independent measurements, one the direct measurement of the separation due to Lamb and co-workers¹²⁾, and the other by the level crossing method of Robiscoe et al.¹³⁾, are now in agreement with one another to within about two standard deviations but are in disagreement with theory by more than four standard deviations; most of the estimate of probable error rests on uncertainty of theory rather than experiment.

Let me now go on to the g-factors. During the preceding conferences (Stanford and Heidelberg) the CERN group of Bailey et al. announced progress of their measurements on the g-2 value of the muon using their 1.5 GeV weak-focusing muon ring. I assume that the disposition of the experiment is well-known and will not repeat it here. Out of these measurements a discrepancy between theory and experiment had apparently emerged. At this Conference, Bailey et al.¹⁴⁾ announce a value of

$$(g-2)/2 = (116614 \pm 31) \times 10^{-8}$$

for the muon anomaly which compares to a quoted theoretical value of

$$(g-2)/2 = (116560) \times 10^{-8}$$

if QED is assumed to be valid to smallest distances, and where estimates of strong interaction loops and the effect of a possible intermediate boson have been included. The deviation is thus reduced to $(54 \pm 31) \times 10^{-8}$ in $(g-2)/2$ which may no longer deserve to be called a discrepancy.

There are both theoretical and experimental sources of the uncertainty in the gyromagnetic anomaly of the muon. Even the contribution from pure quantum electrodynamics to the anomaly (for which no uncertainty is discussed by the authors) still has an outstanding contribution to the α^3 term which has not been calculated as yet. The hadronic contribution to the anomaly has been calculated¹⁵⁾ using the ρ -meson width and height from the earlier Novosibirsk experiments¹⁶⁾ and inferring the ω and ϕ contribu-

tions from SU(3). More recent data on the ρ vector meson are now available from Novosibirsk, and directly measured widths and amplitudes of the ρ and other vector mesons from the Orsay colliding beam experiments are reported at this Conference. For this reason the theoretical correction to the anomaly due to hadronic contributions might well shift by a few parts in 10^8 , but this point can be cleared up with the new data. The weak interaction correction is very small and therefore its uncertainty appears not to be significant. However, it should be noted that this calculation assumes an intermediate boson without an anomalous magnetic moment to moderate the Fermi interaction. The correction would increase linearly with a possible anomalous moment of the W; moreover the calculation requires cut-off procedures. Considering all the circumstances one might conclude that a presumed theoretical uncertainty of $\pm 10 \times 10^{-8}$ is not overly generous.

The group of Bailey et al. has carried out diligent searches for sources of error in their experiment which might account for the deviation. The mean life of muons trapped in the ring appears to lengthen with trapping time and approaches the theoretical value at large times, thus indicating some continued muon loss; this loss is probably caused by imperfections in the magnetic field. This, combined with the fact that the measurement of mean magnetic field as seen by the trapped muons rests on observation of the cyclotron frequency of the initially trapped bunches, gives rise to speculations that possibly the mean field seen during the entire muon history and that seen by the early bunches may not be the same. This effect has been studied experimentally by using different time intervals for observation of the bunch rotation frequency, and consistent results were obtained; however, there is an unexplained loss of particles between the time intervals chosen. In addition, many checks using variable aperture stops have given consistent results with the orbit population calculated by Monte Carlo methods. The shift in mean orbit radius required to remove the deviation is in excess of permissible limits. The reason for the reduction of the deviation relative to the result reported earlier is attributed to the fact that the data interval used

in the fitting of the precession for the preliminary result started at a time t_1 , which was unfortunately atypical. In the measurement reported here, a variety of starting times were used; a systematic dependence on the starting time t_1 was discovered and has been corrected for.

Discussions of a new version of this experiment are under way at CERN and in the United States, since a possible deviation in the measurement of this important quantity clearly needs confirmation.

The situation concerning the electron g-factor is no better. Rich¹⁷⁾ has recently recalculated the old measurements of Crane and collaborators, and has uncovered corrections originally overlooked. The measurement can be quoted by stating that the α^3/π^3 term appears to have a coefficient

$$-(6.5 \pm 2.5)$$

as compared to the theoretical estimate of 0.15. Note that this discrepancy^{*)}, if any, is in the opposite direction to that of the g-factor of the muon. As an experimentalist one has, of course, not the greatest confidence in such recently resurrected corrections to an old measurement and one hopes for a new determination. Experiments using cryogenic and other techniques are under way towards that end in several laboratories.

This is the situation on low momentum transfer electrostatics. Some clarity has been added in one corner but possible problems have emerged in others. I will now proceed in the rest of the talk to sweep all these problems under the rug and assume that quantum electrostatics is an exact science.

2. ELASTIC ELECTRON-NUCLEON AND MUON-NUCLEON SCATTERING

In addition to assuming the validity of quantum-electrostatics over the full range of parameters covered, all analyses of elastic and inelastic scattering experiments continue to assume single-photon absorption only. This assumption can be tested by comparing electron and positron scattering cross-sections, by observing the polarization of the recoil

*) $[(g-2)/2]_{\text{electron;exp.}} = (115955.7 \pm 3.0) \times 10^{-8}$
 $[(g-2)/2]_{\text{th.; } 137-\alpha^{-1}=0.036} = (115964.1 \pm 0.3) \times 10^{-8}$

nucleon, and by observing deviations from a linear "Rosenbluth" plot. The recent work of Mar et al.¹⁸⁾ has extended the positron-electron comparison to $q^2 = 5 \text{ (GeV/c)}^2$ without any evidence for a deviation from equality of the cross-sections for elastic and some inelastic scattering from the proton.

The measurements give limits on the real part of the two-photon exchange amplitude relative to the one-photon amplitude of the order of one per cent. No further new evidence on the two-photon amplitudes has been developed recently; none of the numerous "Rosenbluth" plots involved in the elastic and inelastic scattering experiments reported below exhibit deviation from the straight-line relationship of the cross-section with $\tan^2(\theta/2)$, where θ is the scattering angle.

Relatively little new experimental information has been submitted to this Conference on elastic electron-nucleon scattering. You may recall from an earlier conference that at SLAC¹⁹⁾, spectrometer experiments have extended measurements on electron-proton scattering to four-momentum transfers of $q^2 = 25 \text{ (GeV/c)}^2$, and that these data continued to fit reasonably well the so-called "dipole" formula for the form factor, although this fit exhibits some deviations when viewed in detail. Earlier data from DESY showed agreement with the so-called "scaling law"

$$G_{Ep}(q^2) = \frac{G_{Mp}(q^2)}{\mu_p} = \frac{G_{Mn}(q^2)}{\mu_n} \approx \frac{1}{(1 + q^2/0.71)^2} .$$

Recent precision measurements²⁰⁾ using the external beam of the Bonn 2.5 GeV Electron Synchrotron have given the first possibly statistically significant indication that the scaling law may be violated. The Bonn data cover a range to 2 (GeV/c)^2 as shown in Fig. 3, and can be fitted by an equation of the form

$$G_{Ep}(q^2) = G_{Mp}(q^2) [1 - (0.063 \pm 0.018) q^2] / \mu_p .$$

Considering the difficulties of these measurements, the authors do not claim that this deviation is necessarily significant.

The data on the electric form factors of the neutron remain in an extremely unsatisfactory state

but are compatible with being close to zero everywhere; however, the interaction between electrons and thermal neutrons leads to a non-vanishing derivative of the electric form factor of the neutron at $q^2 = 0$.

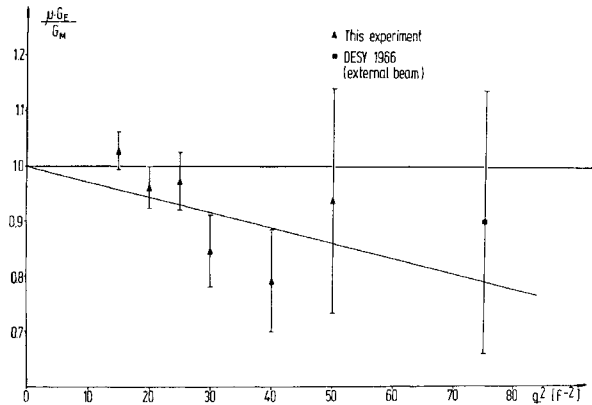


Fig. 3 Plot of $\mu_p G_{Ep}(q^2)/G_{Mp}(q^2)$ (from Ref. 20).

The slope of the variation of $G_{En}(q^2)$ with q^2 is no longer in disagreement with the low [$q^2 < 0.2 \text{ (GeV/c)}^2$] measurements²¹⁾. This is partially due to an upward shift of these measurements of $G_{En}(q^2)$ originating from elastic scattering on the deuteron at low q^2 and from improved dispersion calculations presented at this Conference²²⁾. The situation is shown in Fig. 4. There is some new experimental material at higher values of q^2 . Recent measurements are reported at this Conference by Galster et al.²³⁾ on deuteron elastic scattering using an electron-deuteron coincidence technique. The result places a new upper limit on the value of G_{En} ; the results are $G_{En} = 0.02 \pm 0.05$ at $q^2 = 0.27 \text{ (GeV/c)}^2$ and $G_{En} = 0.06 \pm 0.06$ at $q^2 = 0.4 \text{ (GeV/c)}^2$. The limit

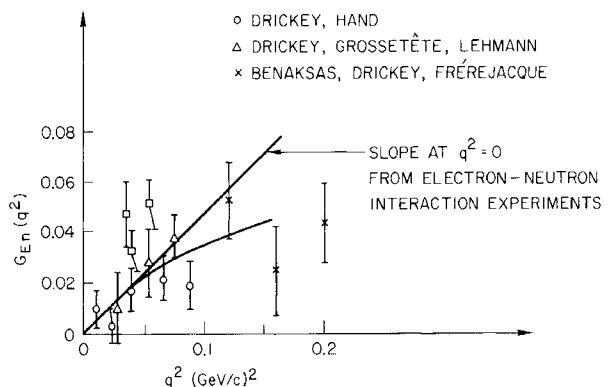


Fig. 4 Plot of $G_{En}(q^2)$ for $0 < q^2 < 0.2 \text{ (GeV/c)}^2$. Solid curve: Theory of Höhler et al.²²⁾.

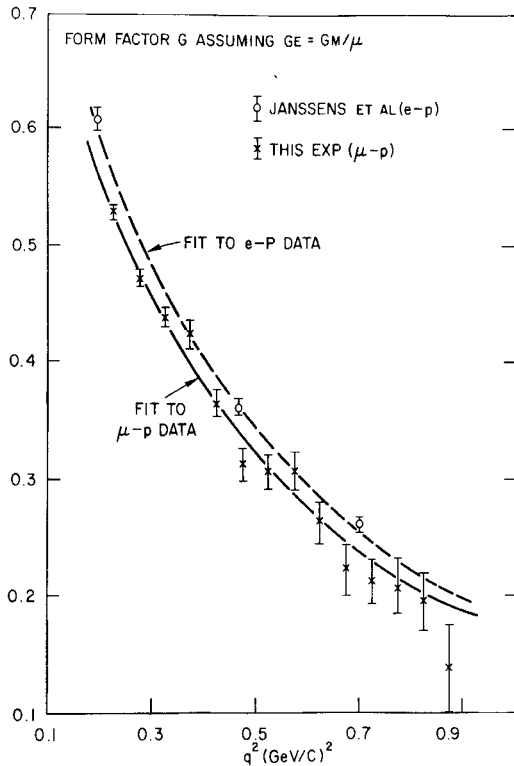


Fig. 6 Comparison of muon and electron form factors of the proton.

is sensitive to the statistics obeyed by the muon. Although the reaction was clearly observed for the first time, the experiment was not sufficiently sensitive to differentiate between Fermi and Bose statistics. To summarize, we find that all evidence currently available relating to the electromagnetic interactions of leptons does not reveal any deviation from muon-electron equality.

3. INELASTIC ELECTRON SCATTERING ON THE NUCLEON

Possibly the most important experiments in the field of high-energy electrodynamics reported in this Conference are in the field of inelastic electron scattering. Part of this field is just beginning to be exploited and therefore the results reported here are frequently only indicative and their full power will have to be demonstrated later.

Inelastic electron scattering gives results in the following areas:

- a) tests of T violation;
- b) examination of the pion electromagnetic form factor;
- c) the form factors of specific resonant states and extrapolation of inelastic electron scattering

to zero momentum transfer, yielding the total photon absorption cross-sections;

- d) examination of the excitation of the nucleon into the continuum.

Let me discuss the relevant information on these four topics in the order given, although information on each topic frequently results from the same experiments.

3.1 Tests of T violation

After the discovery of CP violation in neutral kaon decay, speculations by T.D. Lee and collaborators indicated the possibility that electromagnetic interactions involving hadrons might also exhibit T violations. The likelihood of such predictions corresponding to reality has undergone several fluctuations as further information has become available on such questions as the η -decay asymmetry, the electric dipole moment of the neutron, and other relevant parameters.

It was suggested specifically by Christ and Lee²⁹⁾ that a T-violating asymmetry predicted in interactions of the kind

$$(\vec{p} \times \vec{p}') \cdot \vec{\sigma}_p$$

might be detectable by inelastic electron scattering of electrons of initial momentum \vec{p} , final momentum \vec{p}' , scattering on protons of spin orientation $\vec{\sigma}_p$. It can be shown that such a term cannot be present in elastic scattering. However it can also be shown that should the data exhibit the asymmetry implied by such an interaction, this can be taken as a proof of violation of T invariance only if the process can be described purely by one-photon exchange. Therefore, should an asymmetry be found, the result should be checked with inelastic positron scattering. The choice of the specific excited state offers an additional complication: the most prominent state available to be studied by inelastic electron scattering is the $N^*(1238)$. However, since the isotopic spin of $N^*(1238)$ is $3/2$, no asymmetry would be expected in inelastic scattering should the T-violating interaction be an isotopic scalar. Therefore the most conclusive test on this question would be study of the asymmetry of inelastic scattering from $N^*(1512)$ which has isotopic spin $1/2$. Experimental results

on this question have been reported to this Conference by Appel et al.³⁰⁾ using the CEA external electron beam. The polarized target used was a "doped" mixture of ethanol and water in which typical proton polarizations of about 24% were attained. Radiation damage to the target by the electron beam required frequent changes of target. This experiment is a very difficult one since statistics of observation of the asymmetry are diluted by scattering from the carbon component of the target, by the partial polarization of the protons, and by the fact that the state under study is superimposed on a background of unknown character. The asymmetry in inelastic scattering is caused by interference between scattering of longitudinal and transverse virtual photons. The ratio between the effective longitudinal and transverse photon content involved in the scattering process is given by the well-known polarization factor $\epsilon = 1/\{1+2[1+(E-E')^2/q^2]\} \operatorname{tg}^2(\theta/2)$ which is a purely kinematic quantity; here E and E' are the primary and secondary electron energies, respectively; and $q^2 = 4EE' \sin^2(\theta/2)$ is the square of the four-momentum transfer; note that $q^2 = 0$ and thus $\epsilon = 0$ for real (transverse) photons.

In general the differential cross-section for inelastic scattering can be written as

$$\frac{d^2\sigma}{d\Omega dE'} = \Gamma_t \left\{ \sigma_T + \epsilon\sigma_s + [2\epsilon(1+\epsilon)]^{\frac{1}{2}} \frac{\vec{\sigma}_p \cdot (\vec{p} \times \vec{p}')}{|\vec{p} \times \vec{p}'|} \sigma_{TS} \right\},$$

where $\Gamma_t(q^2, E'-E)$ is a purely kinematic factor given by

$$\Gamma_t = \frac{\alpha}{2\pi^2} \frac{K}{q^2} \frac{E'}{E} \frac{1}{1-\epsilon}$$

with $K = E-E'-q^2/2M = (M^{*2}-M^2)/2M$. Here K is the energy of the photon giving the same excitation M^* to the nucleon system as inelastic scattering of the electron. The quantities σ_T and σ_s are the cross-sections per equivalent transverse and longitudinal photon, respectively. The quantity σ_{TS} is the effective cross-section due to interference between transverse and longitudinal photon amplitudes. The degree of T violation can then be measured by a phase difference δ between these two amplitudes. The asymmetry can then be shown to be

$$a = A \sin \delta = \frac{[2\epsilon(1+\epsilon)]^{\frac{1}{2}}}{\sigma_T + \epsilon\sigma_s} \sigma_{TS} \sin \delta.$$

The relation of σ_{TS} to σ_s and σ_T depends on the multipolarity of the transition which is well established for the 1238 and 1512 MeV resonances.

The authors give the following table for these results (Table 1). Clearly no evidence for T violation has been demonstrated, and therefore there exists no incentive for the matching positron experiment. A similar experiment at higher energies and higher sensitivity is in preparation.

A second experiment examining T violation in electromagnetic scattering has been reported by Prepost et al.³¹⁾. The experiment, following the suggestion of Kobsarev et al.³²⁾ examines the polarization of recoil deuterons from elastic electron scattering; in contrast to the situation in the case of elastic (but not inelastic) scattering from spin 1/2 particles, elastic electron scattering from particles of spin 1 or greater can retain T-violating terms which do not vanish identically due to current conservation. The term in elastic electron-deuteron scattering corresponding to scattering by the quadrupole moment of the deuteron can interfere with a T-violating amplitude to give polarization to the deuteron; at the same time the square of the T-violating amplitude contributes to the elastic cross-section itself. An upper limit on the maximum polarization can then be estimated by ascribing the difference between the most recent measurements³³⁾ of the elastic e-D scattering and the Born approximation calculation entirely to a T-violating term; this limit corresponds to a value of 0.34 for the polarization.

The experiment was carried out by analysing deuterons recoiling from scattering by 1 GeV electrons using a magnetic spectrometer combined with time-of-flight identification. The identified deuterons were analysed for right-left asymmetry by a carbon scatterer. The observed polarization was 0.070 ± 0.083 which is well below the maximum value quoted above. Unfortunately it is difficult to relate this null result to the T-violation experiment using inelastic electron-proton scattering referred to above, since the estimate of the maximum possible polarization in

itself may be too large, quite apart from the question whether T-invariance violation may occur.

3.2 The pion form factor

Two methods for direct measurement of the pion form factor by electromagnetic means have been applied previously. One of the methods involves inelastic electron scattering; somewhat more sensitive measurements have been reported at this Conference³⁴⁾ Inelastic electron scattering is observed under kinematic conditions where the pion pole diagram of low-energy photoproduction plays a dominant role in the cross-section. This diagram involves the direct absorption of the virtual photon by the emitted pion, and therefore the resultant cross-section should be sensitive to the pion form factor. Since this diagram cannot be separated from the other production amplitudes in a gauge invariant manner, isolation of the pion form factor demands the study of the sensitivity of a complete production model to the value of this form factor. Earlier experiments of this type have been carried out by Akerlof et al.³⁵⁾ The new data of Mistretta et al.³⁴⁾ are shown in Fig. 7. This figure shows the measurements compared to a simple ρ dominance calculation as well as to the more complete dispersion calculations of Zagury³⁶⁾ in which the pion form factor is introduced as a free parameter. Both experiments can be fitted with a pion form fac-

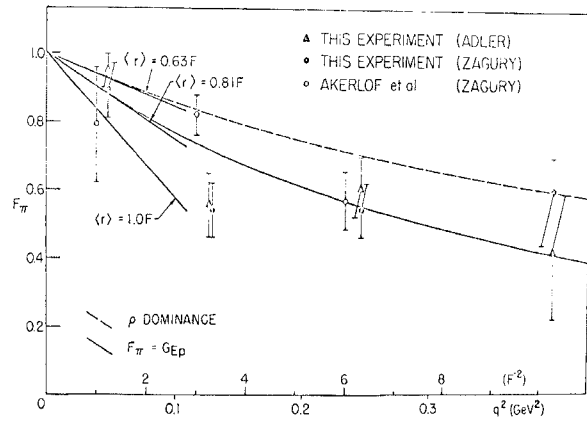


Fig. 7 The data of Mistretta et al.³⁴⁾ and Akerlof et al.³⁵⁾ relating to the pion form factor $F_\pi(q^2)$.

tor equal to that of the proton, but the data are also compatible with a simple ρ -vector dominance model. Considering that the r.m.s. proton radius is 0.8 f, whilst a ρ -vector dominance propagator as a form factor would give a radius of $\sqrt{6}/m_\rho = 0.63$ f, these measurements leave considerable uncertainty in the pion electromagnetic radius. The second approach to obtaining the electromagnetic pion form factor by observation of the interference term between Coulomb and nuclear scattering in pion-helium scattering has thus far failed to give results which are quantitatively useful. Earlier work on this subject by M.M. Block and collaborators has yielded limits of error too wide to be significant; current work now in progress at LRL by Crowe³⁷⁾ and collaborators ap-

TABLE I

Limits on the T non-invariance phase δ at $W = 1238, 1512, 1470, \text{ and } 1688$ MeV.

| Resonance (MeV) | q^2 (GeV/c) ² | Θ (Degrees) | A (%) | (A)×(Correc-tion factor) (%) | a/P (%) | $\pm\Delta\epsilon/P$ (%) | δ (Degrees) | $\pm\Delta\delta$ (Degrees) |
|-----------------|----------------------------|--------------------|-------|------------------------------|---------|---------------------------|--------------------|-----------------------------|
| 1238 | 0.23 | 7.34 | 34 a) | 31 | 3.5 | ± 3.9 | 6.5 | ± 7.2 |
| 1512 | 0.52 | 7.59 | 39 b) | 36.5 | -2.4 | ± 7.7 | -3.8 | ± 12.2 |
| 1512 | 0.72 | 9.05 | 39 b) | 36.9 | 3.4 | ± 4.4 | 5.3 | ± 6.9 |
| 1470 | 0.52 | 7.59 | 78 c) | 73 | -2.6 | ± 11.2 | -2.0 | ± 8.8 |
| 1470 | 0.72 | 9.05 | 78 c) | 74 | 5.1 | ± 6.5 | 4.0 | ± 5.0 |
| 1688 | 0.49 | 7.59 | 50 d) | 47 | 4.1 | ± 8.5 | 5.0 | ± 10.4 |
| 1688 | 0.68 | 9.05 | 50 d) | 47 | -0.5 | ± 4.2 | -0.6 | ± 5.1 |

- a) from experimental data
- b) theoretical
- c) theoretical, if resonance exists
- d) estimate

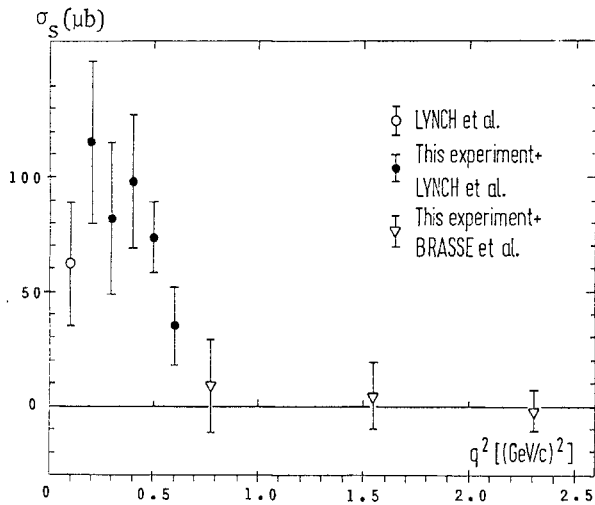


Fig. 8 The longitudinal cross-section σ_S of the $N^*(1238)$ resonance according to the measurements of Bartel et al.³⁹⁾.

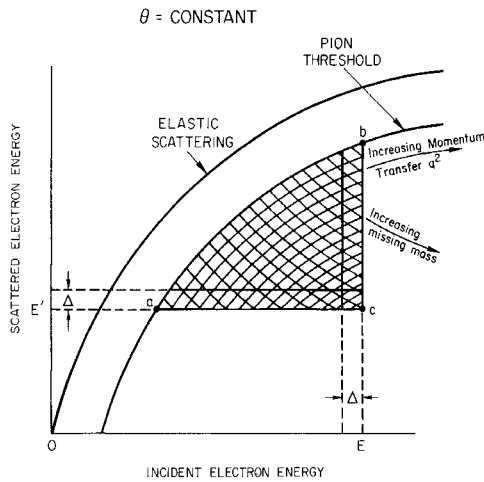


Fig. 9 The radiative correction triangle.

curves were run as a function of the polarization parameter ϵ defined previously. Transverse cross-sections are in agreement with earlier work. The longitudinal cross-sections are shown in Fig. 8, combined with the work of Brasse et al. carried out using the internal beam at DESY, and with the earlier work at Stanford. It is noted that the lower q^2 cross-sections are in agreement with the earlier Stanford work of Lynch et al.⁴⁰⁾, whilst the longitudinal cross-sections at values of q^2 larger than $0.7 \text{ GeV}/c^2$ are compatible with being zero. It is interesting to note that oscillatory behaviour of the longitudinal element has been predicted by the model of Walecka which is reported at a different session. However, experimental data bearing on the longitudinal-transverse separation, resulting from a

combination of work from different laboratories, should be viewed with caution.

New high-energy data have been presented to this Conference from SLAC by Bloom et al.⁴¹⁾ and from the internal DESY beam by Albrecht et al.⁴²⁾; the new measurements have not as yet been extended over a sufficient range of parameters to permit separation of longitudinal and transverse elements.

In order to obtain meaningful cross-sections, considerable effort has to be devoted to carrying out radiative corrections in an exact quantitative manner. This can only be done consistently by a numerical method applied to the cross-sections themselves, since the measurements at each value of incident electron energy E and scattered energy E' contain radiative contributions from the entire kinematically accessible region which can feed E' from E at a given scattering angle. Specifically, if we consider the situation at a given scattering angle θ as shown in Fig. 9, then the cross-section from the entire shaded triangular region contained between the kinematic point E, E' of interest and the kinematic line corresponding to elastic scattering can contribute to the observed cross-section. Complete unfolding of the radiative corrections therefore demand, in principle, a complete set of measurements in the shaded triangular region in Fig. 9. An approximation to such a program has been carried out by the SLAC group using the methods of Mo and Tsai⁴³⁾ at a production angle of 6° by interpolating among measurements made at four primary energy values between 7 and 16 GeV, as shown in Fig. 10.

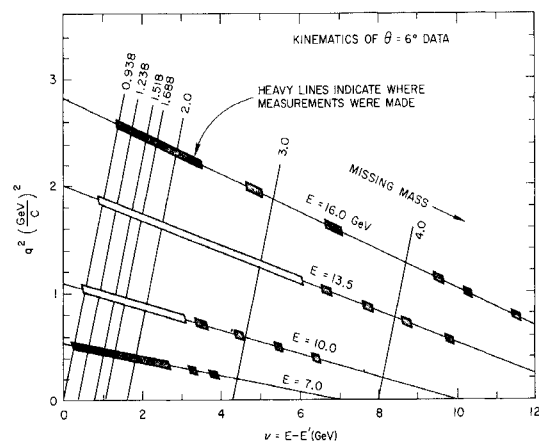


Fig. 10 Kinematic region covered by the SLAC inelastic scattering measurements at 6° .

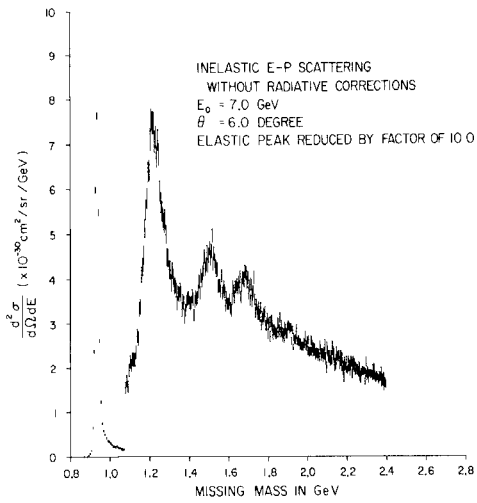


Fig. 11 Uncorrected inelastic spectrum taken at SLAC at 6° and primary energy of 7 GeV.

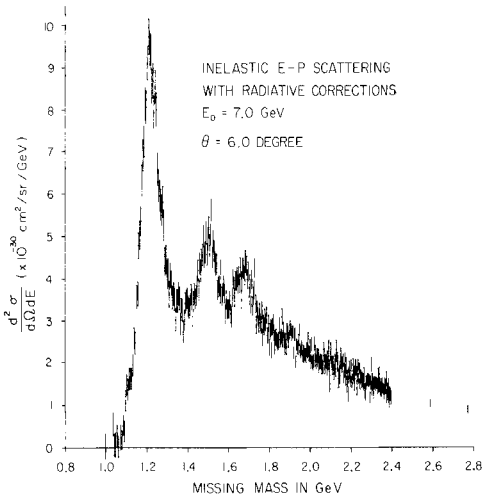


Fig. 12 Figure 11, after radiative correction.

Figure 11 shows an inelastic spectrum taken at a primary energy of 7 GeV obtained before radiative correction, and Fig. 12 shows the resultant spectrum after such a radiative correction has been applied. Figure 13 shows similar data taken at 16 GeV before correction, and Fig. 14 shows the corrected data. The following features are evident from these measurements:

- a) Three and possibly four resonant states are clearly distinguishable, and their cross-sections can be isolated using a fitting programme which demonstrates that the amplitude of the excited states is quite insensitive to the polynomial order of the background assumed; the result is shown in Fig. 15.

- b) The continuum excitation falls off much more slowly with momentum transfer than does the excitation of specific excited states. At higher angles, data not presented here show that the spectra are almost totally dominated by the continuum.

Analysis of the amplitudes and widths of the states must be approached with caution, since in particular the background subtraction program may be sensitive to the assumption as to spectral shape. With this caveat, the cross-sections for three of the states

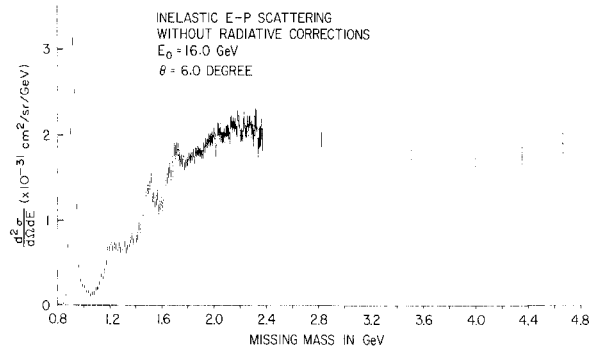


Fig. 13 Uncorrected inelastic spectrum taken at SLAC at 6° and primary energy of 16 GeV.

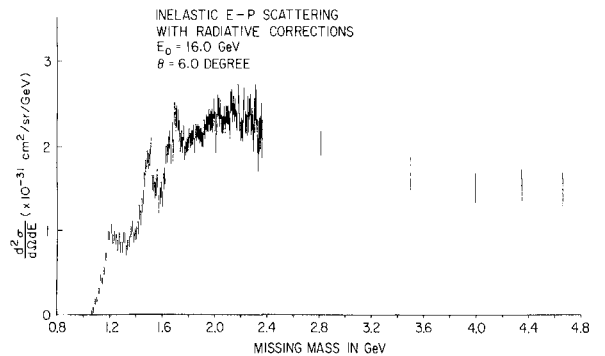


Fig. 14 Figure 13, after radiative correction.

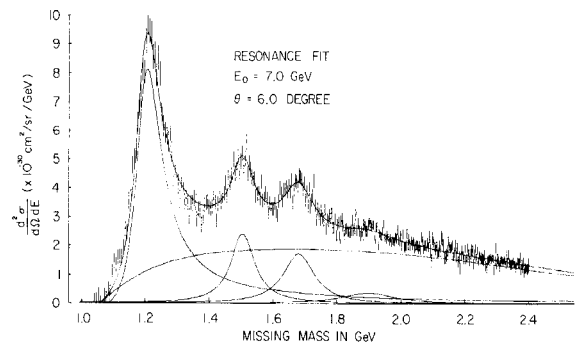


Fig. 15 The inelastic spectrum at 7 GeV, 6°, resolved into Breit-Wigner peaks by a fitting procedure.

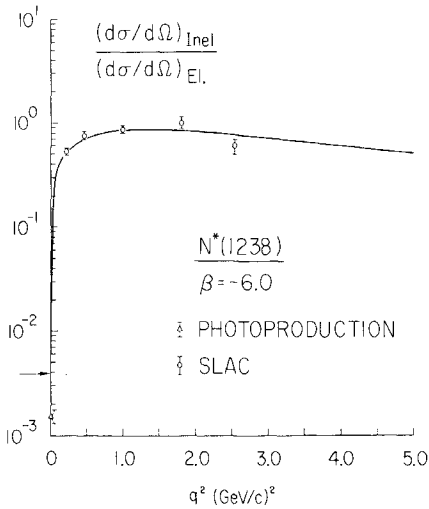


Fig. 16 The cross-section ratio $\sigma_{\text{resonance}}/\sigma_{\text{elastic}}$ for $N^*(1238)$.

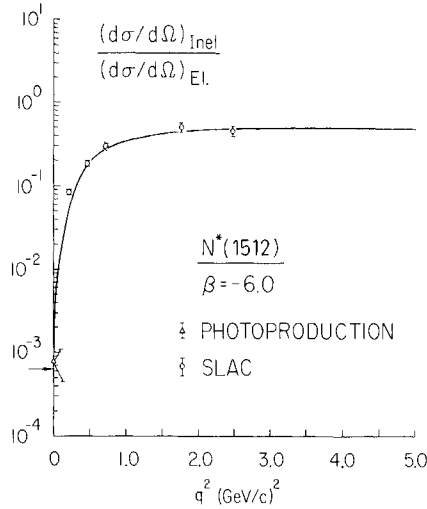


Fig. 17 The cross-section ratio $\sigma_{\text{resonance}}/\sigma_{\text{elastic}}$ for $N^*(1512)$.

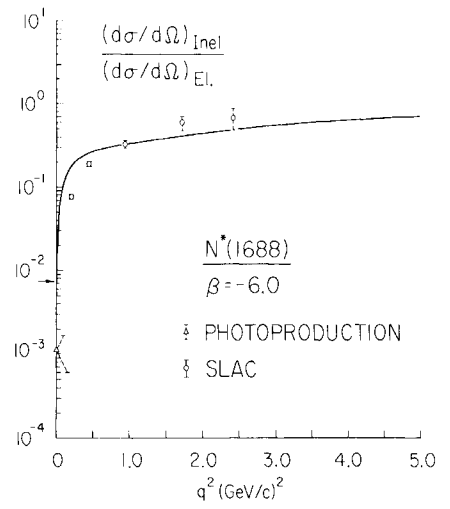


Fig. 18 The cross-section ratio $\sigma_{\text{resonance}}/\sigma_{\text{elastic}}$ for $N^*(1688)$.

are shown in Table 2. Similar data at lower primary energy but much larger scattering angle (about 48°) are derived from the recent DESY work⁴²⁾.

Some simple connections can be drawn:

- It appears from the work at DESY⁴²⁾ that the inelastic cross-section near the $N^*(1238)$ resonance falls off more rapidly with q^2 than near the higher resonances; considering the uncertainties in background subtraction, this interesting result is in need of confirmation when applied to the form factors themselves.
- From the SLAC data⁴¹⁾, it appears that for large q^2 the fall-off of the cross-section matches that observed in elastic scattering; Figs. 16, 17 and 18 show this clearly for $N^*(1238)$, $N^*(1512)$, and $N^*(1688)$; theoretical curves are those discussed by Walecka at a different ses-

sion. At low q^2 , the "threshold behaviour" depends on the angular momentum of the state; e.g. for a magnetic dipole transition we should have simply

$$\sigma_T(q^2, K) = \sigma_T(K) |q|^2 \left| \frac{G_{MV}(q)}{G_{MV}(0)} \right|^2,$$

where $G_{MV}(q^2) = G_{Mp}(q^2) + G_{Mn}(q^2)$ is the isotopic vector form factor of the nucleon. Figure 19 shows a plot from the recent DESY work qualitatively verifying a relation of this type; agreement is fair. However, comparison of the excitation of the $N^*(1238)$ as observed at SLAC with the complete dispersion calculations of Adler⁴⁴⁾ shows that the experimental cross-sections are well above the theory. Figure 20 shows the data from the DESY external beam experiment³⁹⁾ for the cross-section of $N^*(1238)$ as a function of

TABLE 2

Cross-sections for production of three nucleon isobars by inelastic scattering⁴¹⁾.

| E_0 (GeV) | θ_0 (Degrees) | $d\sigma/d\Omega$ (cm ² /sr) | | |
|----------------|-------------------------|--|--|--|
| | | N_1^* $M = 1.219 \pm 0.010$ GeV $\Gamma = 0.130$ GeV | N_2^* $M = 1.503 \pm 0.010$ GeV $\Gamma = 0.077$ GeV | N_3^* $M = 1.691 \pm 0.010$ GeV $\Gamma = 0.102$ GeV |
| 7.00 | 6.000 | $(2.15 \pm 0.17) \times 10^{-30}$ | $(5.21 \pm 0.37) \times 10^{-31}$ | $(5.30 \pm 0.29) \times 10^{-31}$ |
| 10.00 | 6.000 | $(3.95 \pm 0.25) \times 10^{-31}$ | $(1.36 \pm 0.12) \times 10^{-31}$ | $(1.48 \pm 0.16) \times 10^{-31}$ |
| 13.50 | 6.000 | $(7.02 \pm 0.84) \times 10^{-32}$ | $(3.62 \pm 0.40) \times 10^{-32}$ | $(4.17 \pm 0.83) \times 10^{-32}$ |
| 16.02 | 6.000 | $(1.24 \pm 0.19) \times 10^{-32}$ | $(9.81 \pm 1.41) \times 10^{-33}$ | $(1.43 \pm 0.42) \times 10^{-32}$ |

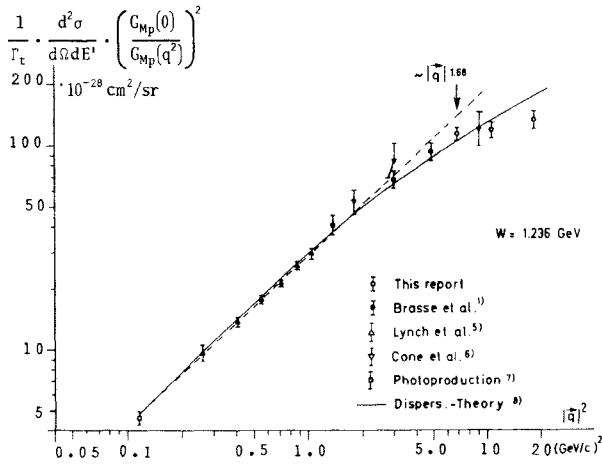


Fig. 19 Plot of $\sigma_T [G_{Mp}(0)/G_{Mp}(q^2)]^2$ in $|q^2|$. The exponent of the observed power law is a measure of the transition multipolarity.

q^2 . The authors express the q^2 -dependence as a product of $|q^2|$ times an "effective" form factor $G^*(q^2)$ which is plotted in comparison with the dipole formula. Some deviation is observed, but the fit to the dispersion calculations of Gutbrod and Simon⁴⁵⁾ is good.

All old and newly available data from the various laboratories relating to the four resonances have been collected and are plotted in Fig. 21. The quantity shown as a function of q^2 is $\Gamma_T^{-1} d^2\sigma/d\Omega dE'$ which should approach the photoproduction σ_γ as $q^2 \rightarrow 0$; this limit is also shown.

It has been speculated that the "Roper" resonance $N^*(1470)$, whose existence has been inferred from phase-shift analysis of π -p scattering, should be prominently excited by inelastic electron scattering. Neither the SLAC⁴¹⁾ nor the DESY⁴²⁾ work has

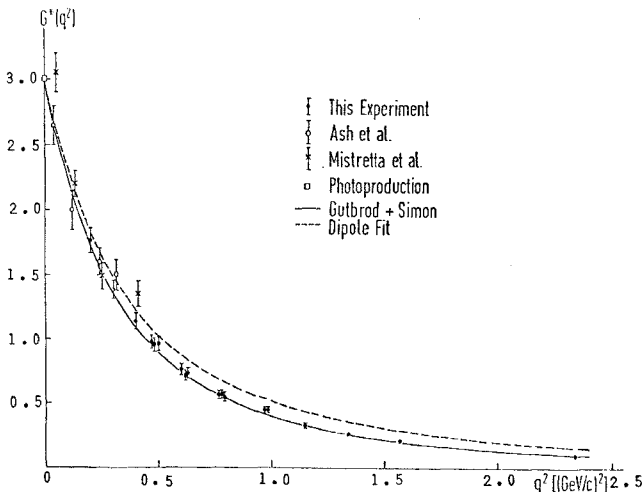


Fig. 20 Plot of the "effective" form factor $G^*(q^2)$ for $N^*(1238)$ production.

revealed its existence. A special search on a neutron (i.e. deuteron) target at CEA by Alberi et al.⁴⁶⁾ has likewise given negative results; the photo cross-section obtained by extrapolating the data to $q^2 = 0$ is estimated to be less than 120 μb .

3.4 Continuum excitation

Possibly the most important implication of inelastic scattering which, however, rests on very incomplete data, relates to excitation of the continuum. Here detailed interpretation will have to await further data, but some general remarks can be made in terms of the W_1 and W_2 formalism discussed above.

For small-angle θ , the ratio of the contribution to the differential scattering cross-section of the W_1 term to that of the W_2 is given by

$$\frac{\sigma_T}{\sigma_T + \sigma_S} \frac{(E-E')^2}{2EE'}$$

where σ_T and σ_S are the cross-sections per transverse and longitudinal photon as defined previously. (For moderate inelasticity and high primary energies this term is small for the entire region $0 < \sigma_T/\sigma_S < \infty$.) From SLAC data, the function $W_2(q^2, \nu)$ is plotted numerically against ν for various values of q^2 in Fig. 22, assuming W_1 to vanish. Note that the continuum cross-sections appear to converge to a ν^{-1} behaviour for large inelasticity. This same data can be plotted in different parametrization: Fig. 23 shows the function

$$F(\omega) = [\nu W_2(q^2, \nu)]$$

plotted against the variable ν/q^2 . Since, as mentioned above, the experimenters have as yet not been able to gather the necessary data for separating the transverse and longitudinal elements, the curve is plotted under the alternate assumptions of vanishing of either the transverse or the longitudinal cross-sections. Two striking facts emerge from this parametrization:

1. At least qualitatively, using the variable ν/q^2 leads to a fairly universal representation of the "deep" inelastic continuum covered so far.
2. The function plotted appears to approach a constant for large ν/q^2 .

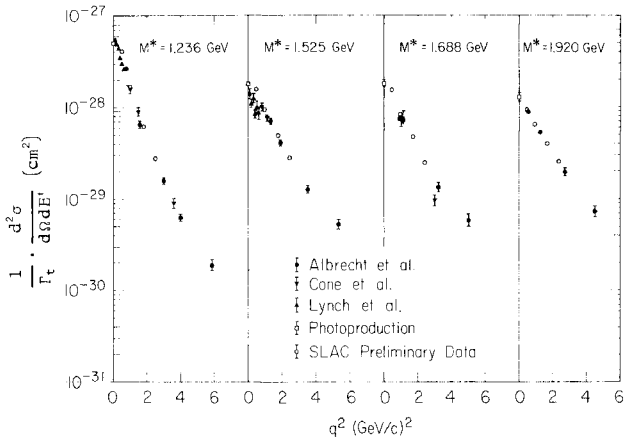


Fig. 21 Plots of $(d^2\sigma/d\Omega dE')/\Gamma_T$ for the first four resonances, compiling data reports from various laboratories.

The inelastic muon data reported by Zipf et al.²⁷⁾ cover inelasticities up to an equivalent photon energy of 7 GeV and a range of $q^2 < 0.9$ (GeV/c)². An optical spark chamber technique is used; the statistical accuracy is, of course, well below that of the electron data. Within this limited accuracy, there is fair agreement in the region of overlap between the electrons and muons.

The qualitatively striking fact is that these cross-sections for inelastic electron and muon scattering leading to the continuum are very large and decrease much more slowly with momentum transfer

than the elastic scattering cross-sections and the cross-sections of the specific resonant states; in fact, indications are that they probably decrease even more slowly than would be predicted from a simple ρ -vector dominance propagator. Therefore theoretical speculations are focused on the possibility that these data might give evidence on the behaviour of point-like, charged structures within the nucleon.

Treating the proton by a non-relativistic point quark model, Godfrey has derived a sum rule for the integral $\int W_2(q^2, \nu) d\nu$. Evaluation of the integral over the SLAC data gives about 60% of the required amount. There is no visible quasi-elastic peak at a defined inelasticity $\nu = q^2/2m$, where m is some characteristic mass, but the apparent success of the parametrization of the cross-sections in the variable ν/q^2 in addition to the large cross-section itself is at least indicative that point-like interactions are becoming involved. Numerical evaluation of the sum rules is difficult since the integrals will converge only if the curves shown in Fig. 23 eventually decrease more rapidly with (ν/q^2) than over the region covered by present data.

I have only attempted to point out the qualitative features of the data; specific comparisons with models and sum-rules are discussed in the theoretical sessions. However, a great deal more fundamental experimental material must be developed in this field before a clear picture can emerge.

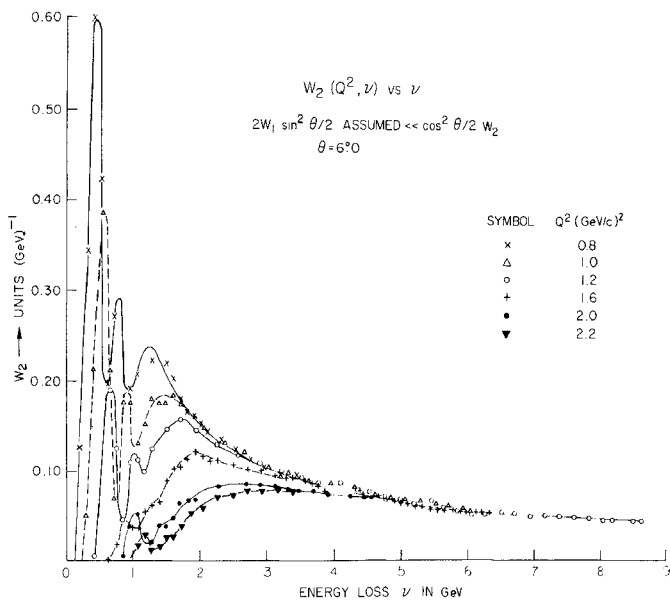


Fig. 22 Plot of $W_2(q^2, \nu)$ versus q^2 for various values of $\nu = E - E'$.

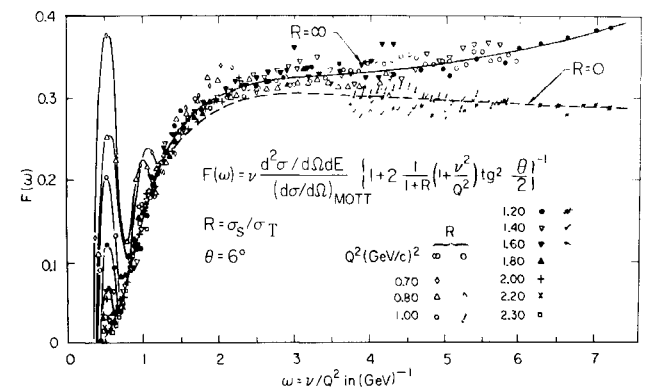


Fig. 23 Plot of $F(\omega) = \nu W_2(q^2, \nu)$, as a function of $\omega = \nu/q^2$.

REFERENCES AND FOOTNOTES

1. S.B. Crampton, D. Kleppner and N.F. Ramsey, *Phys. Rev. Letters* 11, 338 (1963); R. Beehler, D. Halford, R. Harrach, D. Allan, D. Glaze, C. Snider, J. Barnes, R. Vessot, H. Peters, J. Vanier, L. Cutler and L. Bodily, *Proc. IEEE* 54, 301 (1966).
2. C.K. Iddings, *Phys. Rev.* 138 B, 446 (1965).
3. S.D. Drell and J.D. Sullivan, *Phys. Rev.* 154, 1477 (1967).
4. J.J. Amato et al., paper 214.
5. W.E. Cleland, J.M. Bailey, M. Eckhouse, V.W. Hughes, R.M. Mobley, R. Prepost and J.E. Rothberg, *Phys. Rev. Letters* 13, 202 (1964).
6. M.A. Ruderman, *Phys. Rev. Letters* 17, 794 (1966).
7. E.S. Dayhoff, S. Triebwasser and W.E. Lamb, Jr., *Phys. Rev.* 89, 106 (1957).
8. H. Metcalf, J.R. Brandenberger and J.C. Baird, *Phys. Rev. Letters* 21, 169 (1968).
9. Kaufman, Leventhal and Lea, to be published.
10. W.H. Parker, B.N. Taylor and D.N. Langenberg, *Phys. Rev. Letters* 18, 287 (1967).
11. J.C. Clarke, to be published. The accuracy claimed has been reduced from 10^{-11} to 10^{-8} in a private communication.
12. S. Triebwasser, E.S. Dayhoff and W.E. Lamb, Jr., *Phys. Rev.* 89, 98 (1953).
13. R.T. Robiscoe, *Phys. Rev.* 168, 4 (1968), and subsequent communications.
14. J. Bailey et al., paper 405.
15. B.E. Lautrup and E. de Rafael, BNL 12567 (May 1968).
16. V.L. Auslender, G.I. Budker, Yu.N. Pestov, V.A. Sidorov, A.N. Skrinsky and A.G. Khabakhpashev, *Proc. Int. Symp. on Electron and Photon Interactions at High Energies, SLAC, Stanford (1967)*, p. 385.
17. A. Rich, *Proc. Conf. on Atomic Masses, University of Manitoba, Winnipeg (1967)*, p. 383; *Phys. Rev. Letters* 20, 967 (1968) and Erratum; *Phys. Rev. Letters* 21, 1221 (1968).
18. J. Mar, B. Barish, J. Pine, D.H. Coward, H. de Staebler, Jr., J. Litt, A. Minten, R.E. Taylor and M. Breidenbach, *Phys. Rev. Letters* 21, 482 (1968).
19. D.H. Coward, H. de Staebler, Jr., R.A. Early, J. Litt, A. Minten, L.W. Mo, W.K.H. Panofsky, R.E. Taylor, M. Breidenbach, J.I. Friedman, H.W. Kendall, P.N. Kirk, B.C. Barish, J. Mar and J. Pine, *Phys. Rev. Letters* 20, 292 (1968).
20. Chr. Berger et al., paper 516.
21. For a review of the experimental material, see: G. Weber, "Nuclear form factors below 6 GeV", *Proc. Int. Symp. on Electron and Photon Interactions at High Energies, SLAC, Stanford (1967)*; see pp. 70-71.
22. G. Höhler et al., paper 233.
23. S. Galster et al., paper 492.
24. T.T. Wu and C.N. Yang, *Phys. Rev.* 137 B, 708 (1965).
25. H.D.I. Abarbanel, S.D. Drell and F.J. Gilman, *Phys. Rev. Letters* 20, 280 (1968).
26. L.M. Ledermann et al., paper 264.
27. T.F. Zipf et al., paper 370.
28. J.J. Russell et al., paper 221.
29. N. Christ and T.D. Lee, *Phys. Rev. Letters* 139 B, 1650 (1965).
30. J.A. Appel et al., paper 483; also J. Chen, Thesis, Harvard University (1968).

31. R. Prepost, R.M. Simonds and B.H. Wiik, Report No. HEPL 566, Stanford University, Stanford (June 1968), paper 786.
32. I. Kobsarev, L.B. Olson and M.V. Terentyev, JETP Letters 2, 289 (1965).
See also V.M. Dubovik and A.A. Cheshkov, Soviet Phys. JETP 24, 111 (1967); D. Schildknecht, DESY 66/30 (1966);
V.M. Dubovik, E.P. Likhtman and A.A. Cheshkov, Soviet Phys. JETP 25, 464 (1967).
33. R.E. Rand, R.F. Frosh, C.E. Littig and M.R. Yearian, Phys. Rev. Letters 18, 469 (1967).
34. C. Mistretta et al., paper 489.
35. C.W. Akerlof, W.W. Ash, K. Berkelman, A.C. Liechtenstein, A. Romananskas and R.H. Siemon, Phys. Rev. 163, 1482 (1967).
36. N. Zagury, Phys. Rev. 150, 1406 (1966).
37. K.M. Crowe, Conference on Intermediate Energy Physics, Los Alamos (June 19, 1968).
38. S. Devons et al., paper 338.
39. W. Bartel et al., paper 821.
40. H.L. Lynch, J.V. Allaby and D.M. Ritson, Phys. Rev. 164, 1635 (1967).
41. E. Bloom et al., abstract 563.
42. W. Albrecht et al., abstract 313.
43. L.W. Mo and Y.S. Tsai, Report No. SLAC-PUB-380 (to be published in Rev. Mod. Phys.).
44. S.L. Adler, unpublished calculation.
45. F. Gutbrod and D. Simon, Nuovo Cimento 51 A, 602 (1967).
46. J.L. Alberi et al., paper 484.

DISCUSSION

ZICHICHI: I would like to make two comments:

1. Two new features come from electron-proton scattering. i) The lack of validity of the so-called dipole formula in the high q^2 region (the non-validity in the low q^2 region was already known). ii) The lack of validity of the scaling law at the highest values of q^2 which can be reached for G_{Ep} ; in particular, the new Bonn data point to $G_{Ep} \approx 0$ at $q^2 \approx 4 \text{ (GeV/c)}^2$.

Both these features are in agreement with the form factor model proposed by Massam and myself about two years ago.

Let me point out that if the dipole formula did

work, we should ask: "Why does it work?" On the contrary, if our model works the answer is very simple: because it is an intuitive model which incorporates all known facts such as pole dominance, SU(3), and the new gauge invariant way of describing the coupling of the electromagnetic field to the hadrons, due to T.D. Lee, and to Kroll, Lee and Zumino.

2. The variation of the muon $g-2$ anomaly with the starting time t , could be attributed to the variation of the range of initial phases with t . This is why it would be desirable to perform other measurements with the same apparatus, but at different incident proton energies.

ELECTROMAGNETIC INTERACTIONS

Experimental 3

Chairman B. TOUSCHEK

Rapporteur S.C.C. TING

Discussion Leaders P. LEHMANN
 E. LOHRMANN
 P. MARIN

Secretaries P. DALPIAZ
 T. MASSAM

ELECTRODYNAMICS AT SMALL DISTANCES, LEPTONIC DECAYS OF VECTOR MESONS AND PHOTOPRODUCTION OF VECTOR MESONS

S.C.C. Ting

Department of Physics and Laboratory for Nuclear Science, Massachusetts Institute of Technology, Cambridge, Mass.
and Deutsches Elektronen-Synchrotron, DESY, Hamburg

My report to this conference consists of three closely related subjects: experiments to test quantum electrodynamics at small distances; leptonic decays of vector mesons; and photoproduction of vector mesons.

As most of what I have to say is based on the validity of quantum electrodynamics at small distances, I will present my report in the order outlined above.

The important works on electron scattering, muon scattering, high-precision quantum electrodynamics at small momentum transfers, photoproduction of bosons, etc., will be conveyed in the talks given by Professor Panofsky and Professor Richter, and will not be referred to here.

1. QUANTUM ELECTRODYNAMICS AT SMALL DISTANCES

A beautiful experiment from the Stanford-Princeton colliding beam group was reported to this Conference¹. In this experiment, two beams of electrons with 70 mA current each at 550 MeV collided in an interaction region surrounded by a large solid-angle counter and spark-chamber system (Fig. 1). Veto counters were used around the detector such that the cosmic-ray background was about 3%. Radiative corrections were kept small ($\approx 10\%$) by including events with radiated real photons up to more than 0.1 E for radiation along the initial direction, and to ≈ 0.6 E for radiation along the final direction.

The lowest-order diagram for Møller scattering contains space-like virtual photons; this experiment can therefore be regarded as a test of space-like photon propagators and of the electron vertex function. The Møller cross-section modified by the Feynman regulator and by a radiative correction is

$$\frac{d\sigma}{d\Omega}(\theta, K) = \frac{r_0^2}{8} \left(\frac{m}{E}\right)^2 \left[\frac{s^4 + q_0^4}{q^4} G_K^2(q^2) + \frac{2s^4}{q^2 q_0^2} G_K(q^2) G_K(q_0^2) + \frac{s^4 + q^4}{q_0^2} G_K^2(q_0^2) \right] (1 + \delta), \quad (1)$$

where

$$G_K(q^2) = \left(1 - \frac{q^2}{K^2}\right)^{-1}, \quad q^2 = -4E^2 \sin^2(\theta/2),$$

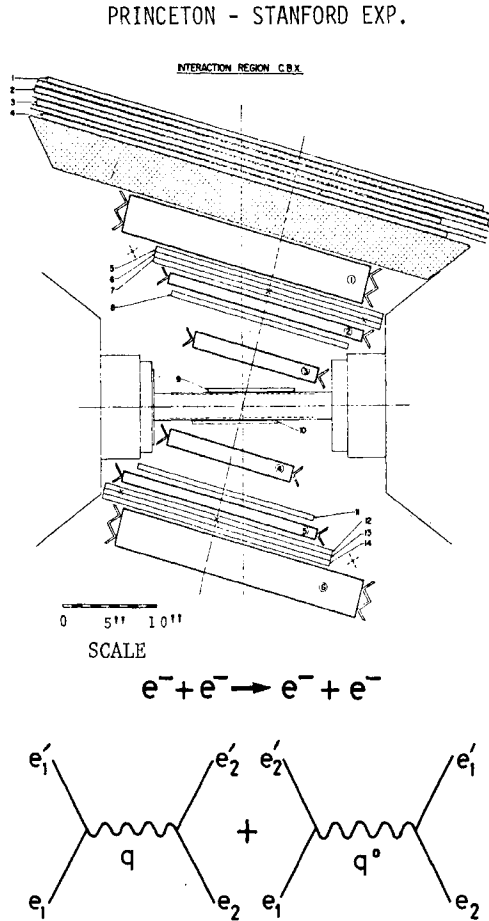
$$s^2 = 4E^2, \quad q_0^2 = -4E^2 \cos^2(\theta/2).$$

A value of zero for K^{-2} would be equivalent to $G_K(q^2) = 1$ consistent with a point-like electron and no cut-off on the photon propagator.

The result, based on 7000 events, is $K^{-2} = -(0.06 \pm 0.06) (\text{GeV}/c)^{-2}$ which is consistent with $K^{-2} = 0$.

A series of large momentum transfer e^+e^- pair production experiments and wide-angle bremsstrahlung experiments were also reported to this Conference.

To first order, three diagrams contribute to pair production (Fig. 2). The first two, the BH diagrams, can be calculated by QED. The last, the Compton diagram, cannot be calculated exactly, but experimental conditions can be chosen such that its contribution is small; in particular, since the e^+e^- pairs in the BH diagrams behave under charge conjugation as two photons ($C = +1$) and the BH cross-section varies rapidly with angle ($\sim \theta^{-6}$ to θ^{-8}), whereas the Compton term behaves under C like one photon ($C = -1$) and the Compton cross-section decreases smoothly with θ ($\sim \theta^{-3}$). By choosing a symmetrical detector with small opening angles, one eliminates the interference between the BH and Compton terms, and at the same time suppresses the Compton term to a few per cent level.



$$\frac{d\sigma}{d\Omega}(\theta, K) = \frac{r_0^2}{8} \left(\frac{m}{E}\right)^2 \left[\frac{s^4 + q_0^4}{q^4} G_K^2(q^2) + \frac{2s^4}{q^2 q_0^2} G_K(q^2) G_K(q_0^2) + \frac{s^4 + q^4}{q_0^4} G_K^2(q_0^2) \right] (1 + \delta)$$

$$s^2 = 4E^2, G_K(q^2) = \left(1 - \frac{q^2}{K^2}\right)^{-1}$$

$\frac{1}{K^2} = 0 \Rightarrow G_K(q^2) = 1 \Rightarrow$ point-like electron \Rightarrow no cut-off for photon propag.

Results: Based on 7000 events:

$$\frac{1}{K^2} = (-0.06 \pm 0.06)(\text{GeV}/c)^2$$

consistent with $\frac{1}{K^2} = 0$

Fig. 1 Apparatus and brief review of the Princeton-Stanford e^+e^- scattering experiment.

For symmetrical pairs with $\theta_- = \theta_+ \leq 10^\circ$ the momentum transfer to the recoil nucleus $q \approx E\theta^2 \leq 100$ MeV/c, whilst the mass of the virtual electron propagator $t \approx \sqrt{2}E\theta \leq 1000$ MeV/c. Thus under these conditions, a heavy nuclear target may be used with rela-

tively small form factor corrections. The yield goes up as Z^2 , and thus enables one to compare the measured e^+e^- rate with predictions of quantum electrodynamics to a momentum transfer of 1 GeV/c.

The DESY-MIT group has reported a new result on pair production with a precision of $\pm 5\%$ and up to a pair invariant mass of 1 GeV/c². Using the 7.5 GeV synchrotron and restricting the pair production angle to $\leq 7.7^\circ$, with a carbon target and with four high-precision Čerenkov counters to reject pions (using fast electronics for handling accidentals) this experiment yields results, based on 400-1000 events at each point, which are in good agreement with the predictions of quantum electrodynamics. The result of their measurement, together with their first result on pair production with the same apparatus, is shown in Fig. 2.

Following the analysis of Kroll, who shows that correct application of the Ward identities of higher

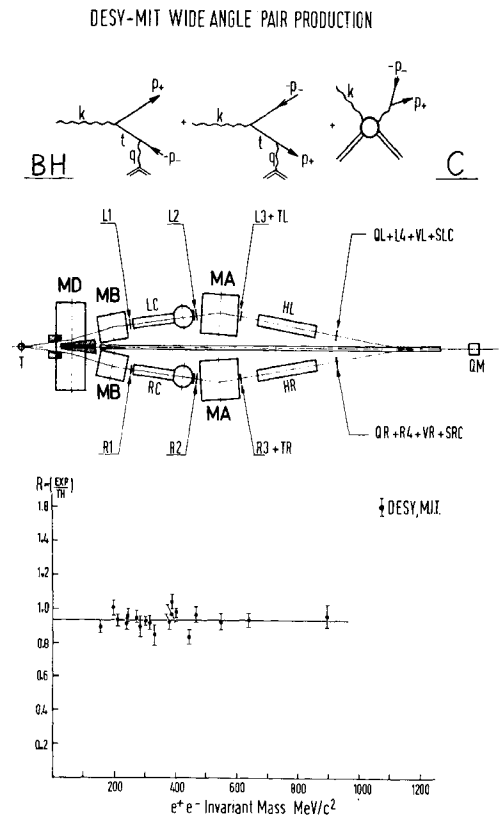


Fig. 2 The Feynman diagrams, the apparatus, and the results of the DESY-MIT wide-angle electron pair production experiment.

orders requires that modification of BH cross-section must be of the form $\sigma_{\text{exp}}/\sigma_{\text{BH}} = 1 \pm (m/\Lambda)^n$, $n \geq 4$, where Λ is a cut-off parameter used as a standard of comparison between various experiments on QED, the DESY-MIT group experiment yields a $\Lambda > 2$ GeV with 68% confidence level ($n = 4$).

Two beautiful experiments on wide-angle bremsstrahlung were also reported. The diagrams of bremsstrahlung and pair production are identical if one interchanges $p_- \rightarrow -p_-$ in Fig. 2. Thus the bremsstrahlung experiments enable one to probe time-like virtual electron propagators, whereas the pair production experiments test QED with space-like virtual leptons.

The experiment by the Berkelman, Littauer group³⁾ used the internal beam of the Cornell 10 GeV electron synchrotron, a carbon target, and counters to detect the scattered electron and photon in coincidence. Their set-up is shown in Fig. 3. The scattered electrons were detected at 6.4° by a single focusing spectrometer, and the photon aperture was defined by a collimator at 6.2° . The photons were detected by lead-glass counters. Time-of-flight and pulse-height information were used to select the $e\text{-}\gamma$ events from background. One hundred events were collected at each point, and their result as a function of final-state mass M is shown in Fig. 3. The best straight line fit to these points is $R = 0.94 \pm 0.14 + (0.9 \pm 1.9) \times 10^{-4} M$; the results are consistent with QED which predicts a straight line at 1.0 with zero slope.

The experiment of C. Bernardini et al.⁴⁾ at Frascati used a hydrogen target and counter techniques to detect the final proton, electron, and γ in triple coincidence up to an (e,γ) invariant mass of 100 MeV/c^2 . Their results also agree with QED.

The summary of the three latest experiments on QED is shown in Fig. 4, which clearly gives us confidence that first-order quantum electrodynamics of electrons and photons is valid, to at least 5% level, in both the space-like and the time-like region, and up to a momentum transfer of 1 GeV/c with a corresponding cut-off $\Lambda > 2$ GeV at a 68% confidence level.

2. LEPTONIC DECAYS OF VECTOR MESONS

Having obtained some experimental evidence on the validity of quantum electrodynamics at momentum trans-

Berkelman et al.

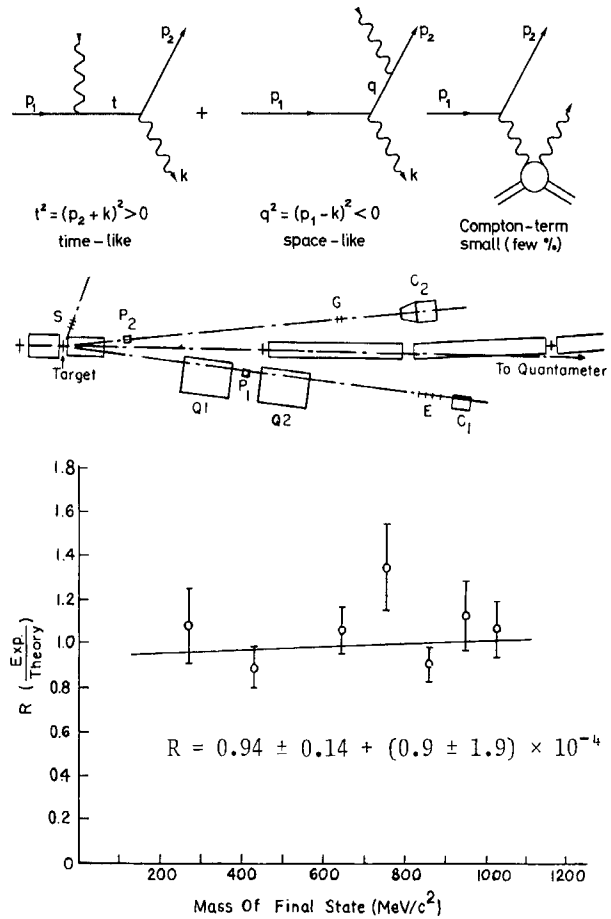


Fig. 3 The Feynman diagrams, the apparatus, and the results of the experiment on wide-angle bremsstrahlung by Ash, Berkelman et al.

fers up to 1 GeV/c , we turn to experiments on the detailed understanding of the nature of light.

The rest of the talk will be on experiments designed to measure the coupling between photons and

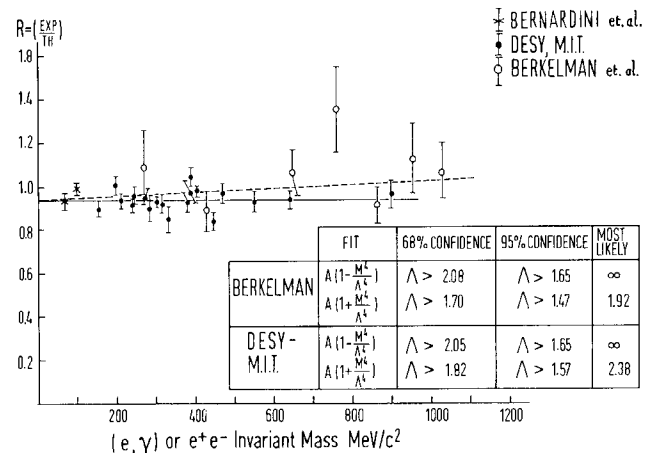


Fig. 4 Summary of the results of the pair production and wide-angle bremsstrahlung experiments.

vector mesons (massive photons, which have the same quantum numbers as the photon $J = 1, C = -1, P = -1$, but with non-zero rest mass) and the photoproduction of vector mesons.

2.1 Motivation

The purposes of studying leptonic decays of vector mesons are fourfold (A, B, C, D)⁵⁾:

A. Measuring the branching ratio $BR = (V^0 \rightarrow \ell^+ + \ell^-) / (V^0 \rightarrow \text{all modes})$ is the only direct way to determine the coupling constant between the vector mesons ρ , ω , ϕ , and the γ ray.

The coupling constant γ_V is related to the partial decay width $\Gamma(V^0 \rightarrow \ell^+ + \ell^-)$ via:

$$\frac{\gamma_V^2}{4\pi} = \frac{\alpha^2}{12} \frac{m_V}{BR \cdot \Gamma_{\text{tot}}} = \frac{\alpha^2}{12} \cdot \frac{m_V}{\Gamma(V^0 \rightarrow \ell^+ + \ell^-)}. \quad (2)$$

The precise knowledge of γ_V or $\Gamma(V^0 \rightarrow \ell^+ \ell^-)$ enables us to determine the ω - ϕ mixing angles directly via

$$\begin{aligned} \text{tg } \theta &= \frac{m_\omega}{m_\phi} \quad \text{tg } \Theta_\gamma = \frac{m_\phi}{m_\omega} \text{tg } \Theta_B \\ \frac{\Gamma(\omega \rightarrow \ell^+ \ell^-)}{\Gamma(\phi \rightarrow \ell^+ \ell^-)} &= \frac{m_\omega}{m_\phi} \text{tg}^2 \Theta_\gamma = \frac{m_\phi}{m_\omega} \text{tg}^2 \Theta = \frac{\gamma_\phi^2}{\gamma_\omega^2}, \end{aligned} \quad (3)$$

to check Weinberg's first sum rule which is based on the current mixing model and predicts

$$\frac{1}{3} \frac{m_\rho^2}{\gamma_\rho^2} = \frac{m_\omega^2}{\gamma_\omega^2} + \frac{m_\phi^2}{\gamma_\phi^2}, \quad (4)$$

and to compare it with quark model calculations of Dar and Weisskopf⁶⁾:

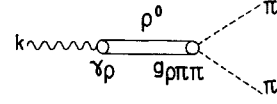
$$\Gamma(\rho \rightarrow ee) = 5.8 \text{ keV}, \quad \Gamma(\phi \rightarrow ee) = 0.95 \text{ keV}, \text{ etc.}$$

In particular, the quantity γ_V appears directly in the vector dominance model approximation, which relates the electromagnetic current $J_\mu(x)$ of the hadrons to the phenomenological fields $\rho_\mu(x)$, $\omega_\mu(x)$, $\phi_\mu(x)$ of the vector mesons via:

$$J_\mu(x) = - \left[\frac{m_\rho^2}{2\gamma_\rho} \rho_\mu(x) + \frac{m_\omega^2}{2\gamma_\omega} \omega_\mu(x) + \frac{m_\phi^2}{2\gamma_\phi} \phi_\mu(x) \right]. \quad (5)$$

Thus in the vector dominance model, the knowledge of γ_V is essential to our understanding of the electromagnetic form factors of nucleons and of pseudoscalar mesons, and to our understanding of the electromagnetic decays of mesons.

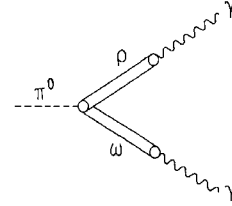
For example⁷⁾, the simple vector dominance model calculates the pion form factor from the graph



giving the result

$$F(k^2) = \frac{g_{\rho\pi\pi}}{2\gamma_\rho} \cdot \frac{m_\rho^2}{m_\rho^2 - k^2}, \quad (6)$$

where $g_{\rho\pi\pi}$ can be calculated from the width of $\rho \rightarrow \pi\pi$, and the normalization condition $F_\pi(0) = 1$ gives $g_{\rho\pi\pi} = 2\gamma_\rho$ and the decay of $\pi^0 \rightarrow 2\gamma$ according to



which gives

$$\Gamma(\pi^0 \rightarrow 2\gamma) = \frac{\alpha^2}{192} \left(\frac{\gamma_\rho^2}{4\pi} \right)^{-1} \left(\frac{\gamma_\omega^2}{4\pi} \right)^{-1} \frac{f_{\rho\pi\omega}^2}{4\pi} \frac{m_\pi^3}{3}. \quad (7)$$

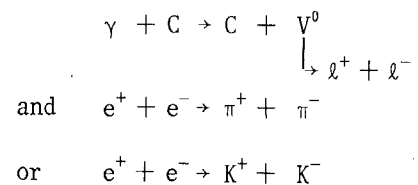
Thus

$$\frac{\Gamma(\omega \rightarrow \pi^0 + \gamma)}{\Gamma(\pi^0 \rightarrow 2\gamma)}$$

depends only on $\gamma_\omega^2/4\pi$.

B. Comparing the rates of $V^0 \rightarrow e^+ + e^-$ versus $V^0 \rightarrow \mu^+ + \mu^-$ gives us a direct check of μ, e universality in the time-like region and at the high momentum transfers of $q^2 = m_V^2 > 0$. This probes any possible differences in the form factors $F_e(q^2)$ and $F_\mu(q^2)$ between electrons and muons in a domain which cannot be covered by either elastic scattering experiments ($\mu + p \rightarrow \mu + p$ versus $e + p \rightarrow e + p$ with $q^2 < 0$) or low momentum transfer experiments like the $(g-2)_e$ versus $(g-2)_\mu$.

C. In principle, studying the $e^+ e^-$ mass spectrum from reactions such as



gives us the best way to determine the mass m_V and

the width Γ_V of the vector mesons. This is because the background contribution to the mass peak $V^0 \rightarrow \ell^+ + \ell^-$ can be calculated exactly.

D. It follows from Eq. (5) that the photoproduction cross-section of vector mesons can be related directly to the vector meson nucleon cross-sections via⁸⁾

$$\sigma(\gamma + A \rightarrow B + C) = \sum_V \frac{\alpha\pi}{\Gamma_V^2} \sigma(V + A \rightarrow B + C). \quad (8)$$

This part of the physics I will discuss in detail later on.

2.2 Experimental considerations

There are two ways in which to study the leptonic decays of vector mesons: (A) from measuring the relative rates of production of vector mesons (via strong interactions) and the rate of vector meson decay into $\ell^+\ell^-$ pairs; and (B) from measuring the rates of vector meson decays in storage rings.

For both cases the best way to measure the branching ratio $BR = (V \rightarrow \ell^+\ell^-)/(V \rightarrow \text{all})$ is to detect all final-state decay particles $V_0 \rightarrow x + y \dots$ with a 4π detector. In such a case the branching ratio follows without any phase-space and acceptance corrections.

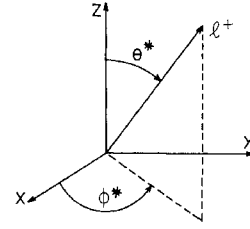
In practice, however, since one can only detect the final-state particles within a rather limited solid angle, the angular distribution of all final-state particles must be measured in order that the yields of $V_0 \rightarrow \ell^+\ell^-$ pairs and $V_0 \rightarrow \text{all}$ modes be corrected for different acceptances.

2.2.1 For production experiments

It follows from a general analysis by Oakes⁹⁾, based on invariance arguments, that the $\ell^+\ell^-$ pair production from any unpolarized initial state of strongly interacting particles is completely described by five real form factors, that are simply related to the density matrix elements for the production of a virtual photon, which then decays into the pair. By measuring the angular distribution and polarizations of the pair, one can determine all five form factors (or their density matrix equivalents) and thereby also investigate the structure of the production process.

In the centre of momentum of the $\ell^+\ell^-$ pair (taking the incident beam direction along the z-axis and the

normal to the production plane along the y-axis)



the angular distribution of the decay of a vector meson into two spinless particles x^+, x^- is:

$$W_{x^+x^-}(\theta^*, \phi^*) = N^1(\rho^{11} \sin^2 \theta^* + \rho^{00} \cos^2 \theta^* - \rho^{1-1} \times \sin^2 \theta^* \cos 2\phi^* - \sqrt{2} \operatorname{Re} \rho^{10} \times \sin 2\theta^* \cos \phi^*) \quad (9)$$

(where N^1 is a normalization constant), and the angular distribution of the $V^0 \rightarrow \ell^+\ell^-$ is

$$W(\theta^*, \phi^*) = \left[1 - \frac{W_{x^+x^-}(\theta^*, \phi^*)}{N^1} \right] / \frac{8\pi}{3}. \quad (10)$$

The following cases of formulas (9) and (10) are of special interest:

1. If V^0 mesons are produced by an incident beam of high-energy π mesons, in the one-meson exchange approximation either G-even or G-odd states can be exchanged. For the G-odd exchange (the case of ρ^0 production via one-pion exchange mechanism) we have $\rho^{00} = 1$ and $\rho^{i,j} = 0$, where i or $j \neq 0$.

Thus we have:

$$W_{(\rho \rightarrow \pi^+\pi^-)}(\theta^*, \phi^*) = \frac{3}{4\pi} \cos^2 \theta^* \quad (11)$$

(independent of ϕ^*)

$$W_{(\rho \rightarrow \ell^+\ell^-)}(\theta^*, \phi^*) = \sin^2 \theta^* \times \frac{3}{8\pi}. \quad (12)$$

For the G-even exchange (the case of ω^0 production via ρ^0 exchange) we have $\rho^{11} = \rho^{-1-1}$, $\rho^{1-1} \neq 0$, all other $\rho^{i,j} = 0$. Thus for $\omega \rightarrow \ell^+\ell^-$ we have:

$$W_{(\omega \rightarrow \ell^+\ell^-)}(\theta^*, \phi^*) = \frac{1 - \frac{1}{2} \sin^2 \theta^* (1 - 2\rho^{1-1} \cos 2\phi^*)}{8\pi/3} \quad (13)$$

(depends on ϕ^*),

and on averaging over the azimuthal angle ϕ^* one obtains

$$W_{(\omega \rightarrow \ell^+\ell^-)}(\theta^*, \phi^*) = \frac{3}{16\pi} (1 + \cos^2 \theta^*). \quad (14)$$

Thus measuring the decay angular spectrum of $\rho \rightarrow \ell^+ \ell^-$ (the θ, ϕ dependence) and the value of the density matrix, as a function of momentum transfer, yields us information on the production mechanism of ρ^0 , as well as determining the $\omega \rightarrow \ell^+ \ell^-$ contamination in the $\rho^0 \rightarrow \ell^+ \ell^-$ spectrum.

2. For a beam of high-energy photons incident on complex nuclei, coherent production of ϕ in the forward region requires that ϕ and the incident photon carry the same spin orientation, and thus we have

$$W_{\phi \rightarrow \text{KK}}(\theta^*, \phi^*) = \frac{3}{8\pi} \sin^2 \theta^* \quad (15)$$

and (P-wave decay)

$$W_{\phi \rightarrow \ell\ell}(\theta^*, \phi^*) = \frac{3}{16\pi} (1 + \cos^2 \theta^*) \quad (16)$$

(S- and D-wave decay).

2.2.2 For colliding beam experiments

The annihilation of $e^+ e^-$ into n spinless bosons through the one-photon channel leads¹⁰⁾ to a final state with $P = -1$, $C = -1$, $J = 1$, $T = 1$ for n even, $T = 0$ for n odd.

If $\vec{\mathcal{F}}$ is the most general vector (pseudovector for n odd) formed out of independent final momenta for even (odd) number of bosons, the final distribution can be shown to have the general form

$$\frac{1}{2} |\vec{\mathcal{F}}|^2 \sin^2 \theta \quad (17)$$

where θ is the angle formed between $\vec{\mathcal{F}}$ and the initial line of collision. Thus for

$$\begin{aligned} e^+ + e^- \rightarrow \rho \rightarrow \pi_1^+ \pi_2^- \\ \rightarrow \phi \rightarrow K_1^+ K_2^- \end{aligned}$$

the only vector is $\vec{p}_1 - \vec{p}_2$ and we get a $\sin^2 \theta^*$ distribution.

For $e^+ e^- \rightarrow \omega \rightarrow 3\pi$ the only pseudovector is the normal to the production plane, and we have the normal with a $\sin^2 \theta$ distribution around the initial line of collision.

Assuming a Breit-Wigner description for the resonance cross-section near its maximum, we have then

$$\sigma(E^2) \simeq \frac{2J+1}{4} \frac{\Gamma_i \Gamma_f}{(2E-m)^2 + \Gamma^2/4},$$

where Γ_i, Γ_f are the rates into initial $e^+ e^-$ and final state, respectively.

If the energy resolution in c.m. is $2\Delta E$, and if $\Gamma \gg 2\Delta E$, we then have

$$\overline{\sigma}_R = \frac{1}{\Delta E} \int_{\frac{1}{2}(m-\Delta E)}^{\frac{1}{2}(m+\Delta E)} \sigma(E) dE$$

or

$$\sigma_R = \sigma(2m) = \pi \kappa^2 (2J+1) B_i B_f,$$

where B_i, B_f are the branching ratios for decay into initial and final state, respectively. For our case $J = 1$, $\kappa = 2/m$:

$$\sigma_{R(\text{Breit-Wigner})} = \frac{12\pi}{m_0^2} \cdot \frac{\Gamma_{ee}}{\Gamma_\rho}. \quad (18)$$

Thus the cross-section [Eq. (18)] at the peak determines the branching ratio of leptonic decays of vector mesons.

For case of $\rho \rightarrow \pi^+ \pi^-$ and $\phi \rightarrow K^+ K^-$ pairs, the differential cross-section in the c.m. system is

$$\frac{d\sigma}{d\Omega}(\theta) = \frac{\pi\alpha^2}{16} \cdot \frac{1}{E^2} \left| F(E^2) \right|^2 \sin^2 \theta, \quad (19)$$

where $F(E^2)$ is the e.m. form factor of π or K . Thus measuring this cross-section also enables one to determine the e.m. form factors of π and K mesons in the time-like region.

The cross-section as a function of energy:

$$\sigma = C \frac{m_\rho^4}{(4E^2 - m_\rho^2)^2 + m_\rho^2 \Gamma_\rho^2} \quad (20)$$

allows us to make a unique determination of the mass and width of the vector mesons.

2.3 Experimental results

2.3.1 The branching ratio of $\rho \rightarrow \ell^+ \ell^-$

Many experiments have been done on the branching ratio of $\rho \rightarrow \ell^+ \ell^-$, such as the experiment done by the Northeastern-MIT group at CEA¹¹⁾, etc. All these experiments yield results consistent with each other. But the resolutions of these experiments are not precise enough to make a definite statement on the width of ρ^0 .

The results of the DESY-MIT group¹²⁾ on the $\rho \rightarrow e^+e^-$ is shown in Fig. 5. This experiment is done with a precision spectrometer with a mass resolution of $\pm 15 \text{ MeV}/c^2$. To reduce systematic errors, both the production of ρ^0 and the subsequent $\rho^0 \rightarrow e^+e^-$ decay

were measured with the same apparatus. The experiment was done at a low photon energy of 2.7 GeV on a carbon ($T = 0$) target, such that the $\omega \rightarrow e^+e^-$ contamination is small.

At low energy, the bubble chamber data show that photoproduction of ω on protons is consistent with OPE. No ω contamination was observed and the measured $\rho \rightarrow e^+e^-$ width is $120 \pm 20 \text{ MeV}/c^2$. The branching ratio is obtained by dividing the area under the two curves, and it yields

$$\text{BR} = (6.4 \pm 1.5) \times 10^{-5}$$

The result of the beautiful experiment done by Wilson's group¹³⁾ at the AGS is also shown in the same figure. This experiment yields a $\text{BR} = (5.8 \pm 1.2) \times 10^{-5}$ and a width of $97 \pm 20 \text{ MeV}$.

Two beautiful experiments on the branching ratio and width of the ρ^0 were done by the Novosibirsk¹⁴⁾ and the Orsay¹⁵⁾ colliding beam groups. Figure 6 shows some of the important characteristics of the storage rings used by these groups, together with the ring used to test QED by the Stanford group.

Both groups measured the e^+e^- annihilation into $\pi^+\pi^-$. The two experimental set-ups are very similar. Figure 7 shows the Orsay one. They used thin-plate spark chambers to measure the angles of the particles, range and shower spark chambers to distinguish pions from electrons and muons, and coincidence counter arrangements triggered in phase with the beam bunches and additional veto counters to reduce cosmic-ray background.

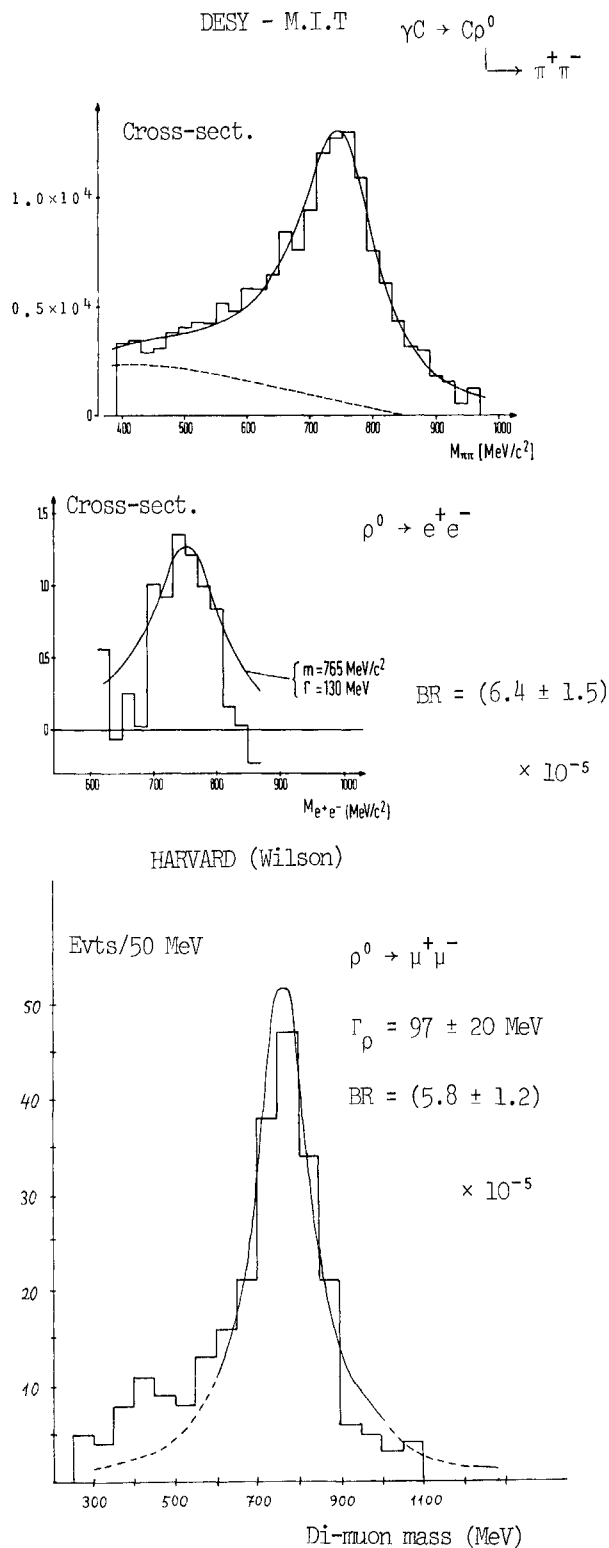


Fig. 5 Invariant mass spectra in $\rho \rightarrow \ell^+\ell^-$ from DESY-MIT and from Harvard. The $\rho \rightarrow \pi^+\pi^-$ spectra measured by the DESY-MIT group under the same kinematical conditions are also shown.

| | Stanford | Novosibirsk | Orsay |
|--|--|--|--|
| Type of Machine | Weak Focusing | Weak Focusing | Strong Focusing |
| Number of Interacting Regions | | | |
| Bunch Length Length of Exp. Section | 90 cm at 550 MeV 70 cm | 90 cm at 385 MeV 70 cm | 18 cm at 385 MeV 180 cm |
| Type of Collision | Angle Crossing | Head On | Head On |
| Currents $I_1 \times I_2$ | 70 mA \times 70 mA (at 550 MeV) | 20 mA \times 50 mA (at 385 MeV) | 5 mA \times 5 mA (at 385 MeV) |
| Beam Lifetime | 1/2 hour | 1 hour | 25 hours |
| Effective Luminosity | $5 \cdot 10^{31} \text{ cm}^{-2} \text{ h}^{-1}$ | $3 \cdot 10^{30} \text{ cm}^{-2} \text{ h}^{-1}$ | $5 \cdot 10^{30} \text{ cm}^{-2} \text{ h}^{-1}$ |

Fig. 6 Summary of characteristics of various storage rings.

TABLE 1

| | m_ρ (MeV) | Γ_ρ (MeV) | BR $\times 10^5$ | $\Gamma_{\rho \rightarrow e\bar{e}}$ (keV) |
|-------------|----------------|---------------------|------------------|--|
| Novosibirsk | 754 ± 9 | 105 ± 20 | 5.0 ± 1.0 | 7.13 ± 0.51 (from their fit) |
| Harvard | | 97 ± 20 | 5.8 ± 1.2 | |
| Orsay | 760 ± 4 | 112 ± 12 | 6.54 ± 0.72 | |
| DESY/MIT | | | 6.4 ± 1.5 | |
| Average | 759 ± 4.0 | 108 ± 8.5 | 6.04 ± 0.50 | 6.52 ± 0.75 (from average BR) |

The result of the $e^+ + e^- \rightarrow \rho \rightarrow \pi^+ + \pi^-$ spectrum from Orsay is also shown in Fig. 7, and the above table summarizes the results of the two colliding beam experiments together with earlier results from DESY-MIT and from Harvard groups.

Thus,

$$\frac{\gamma_\rho^2}{4\pi} = \frac{\alpha^2}{12} \frac{m_\rho}{\Gamma_{\rho \rightarrow e^+e^-}} = 0.52^{+0.07}_{-0.06}$$

for the coupling constant when the ρ meson is on the mass shell. Using

$$\frac{\gamma_\rho^2}{4\pi} = \frac{3\Gamma_0}{m_0} \left(1 - \frac{4m_\pi^2}{m_0^2} \right)^{-\frac{3}{2}},$$

from the π form factor we have:

$$\frac{\gamma_\rho^2}{4\pi} = 0.53 \pm 0.04$$

for the coupling constant when the photon is on the mass shell.

2.3.2 The branching ratio of $\phi \rightarrow k^+ k^-$

An experiment was performed at DESY by the DESY-MIT group¹⁶⁾ using a precision spectrometer and counter techniques. The experiment is very similar to the experiment this group has done on the ρ^0 meson, and it has the following major experimental facts:

1. Normalization and polarization: They have measured both the production of ϕ by photons on carbon (with 10^4 events) and the decay of $\phi \rightarrow e^+ e^-$ (with 40 events) with the same apparatus, thus reducing the major systematic errors in the normalization. Their system has a mass resolution of ± 5 MeV/c² for $\phi \rightarrow K^+ K^-$

events, and of ± 20 MeV/c² for $\phi \rightarrow e^+ e^-$ events. With 10^4 events they find that photoproduction of ϕ on complex nuclei is via diffraction mechanism. Thus the angular distributions for K pairs and for electron pairs are, respectively:

$$W_{KK} = \frac{3}{8\pi} \sin^2 \theta^*; \quad W_{ee} = \frac{3}{16\pi} (1 + \cos^2 \theta^*).$$

ORSAY- ρ -EXPERIMENT

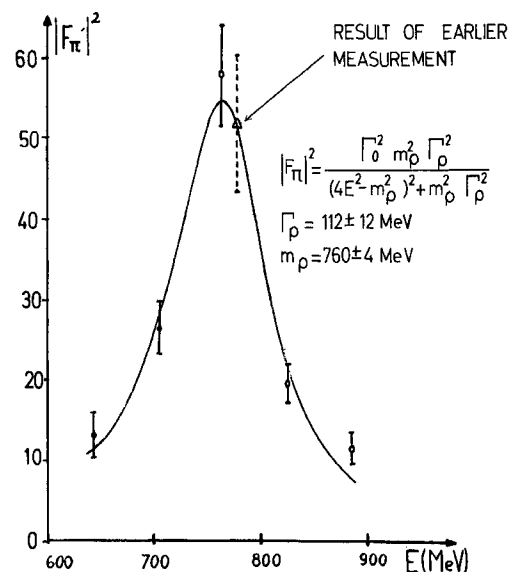
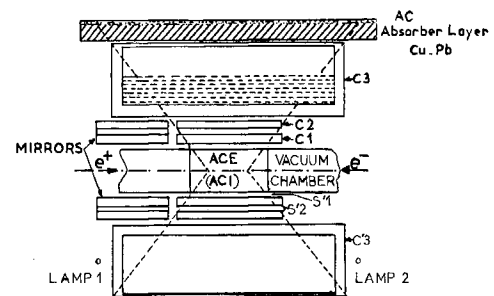
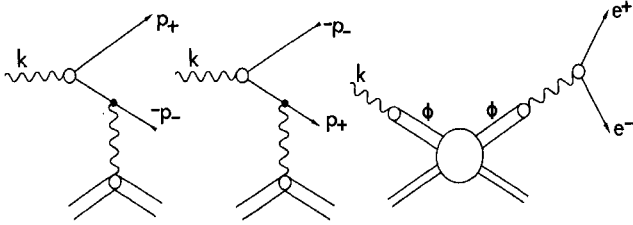


Fig. 7 Experimental set-up and results on $e^+ e^- \rightarrow \rho \rightarrow \pi^+ \pi^-$ from Orsay.

2. QED pair contamination in the yield: To first order both the Bethe-Heitler and ($\phi \rightarrow e^+e^-$) diagrams contribute to the reaction

$$\gamma + C \rightarrow C + e^+ + e^-$$



However, since the BH cross-section varies rapidly with angle ($\sim \theta^{-6}$), whilst the $\phi \rightarrow e^+e^-$ cross-section varies slowly with angle, the signal ($\phi \rightarrow e^+e^-$)/background (BH - e^+e^- pairs) $\sim \theta^3$.

To reduce BH background, the e^+e^- pair was measured at large angles of 22° to 30° . The BH background under the narrow ϕ peak is then $< 1/2$ of the total yield.

3. Since the ρ^0 has a large width, the $\rho \rightarrow e^+e^-$ yield contaminates the $\phi \rightarrow ee$ spectrum. However, since the ϕ has a narrow width, a good mass resolution on e^+e^- will enable one to pick out the peak with a small ρ background. Using the $\rho \rightarrow e^+e^-$ spectrum measured in the same apparatus and with the measured diffraction (pure imaginary amplitude) cross-section, they estimate an over-all 10% contamination of ρ plus (ρ, ϕ) interference under the ϕ peak.

Figure 8 shows the resulting $\phi \rightarrow K^+K^-$ and $\phi \rightarrow e^+e^-$ spectrum. Integrating the area under the spectra, one obtains directly

$$\Gamma(\phi \rightarrow e^+e^-)/\Gamma(\phi \rightarrow K^+K^-) = (5.7 \pm 1.7) \times 10^{-4}.$$

Using $\Gamma(\phi \rightarrow K^+K^-)/\Gamma(\phi \rightarrow \text{all}) = 0.473$ one gets

$$\text{BR} = (2.70 \pm 0.80) \times 10^{-4}.$$

A beautiful but difficult experiment on the ϕ branching ratio was reported by the Orsay colliding beam group¹⁷⁾. Since they have both electrons and positrons in one ring, two beams of equal energy of 510 MeV/c² collided and produced ϕ 's at rest; since each K meson has a mass of ≈ 500 MeV/c², there is very little Q-value in the ϕ decay and the charged K-pairs do not escape the wall of the vacuum chamber to be detected. This experiment is done by detecting the $\pi^+\pi^-$ pairs from the $\phi \rightarrow K_L^0 K_S^0; (K_S^0 \rightarrow 2\pi)$ decay and by

detecting the $\pi^+\pi^-\pi^0$'s from ϕ decay directly.

[Since ϕ is a vector meson (in pure C = -1 state) it does not decay into K_1K_1 or K_2K_2 pairs. It only has the $\phi \rightarrow K_1K_2$ mode.]

K_1K_2 decay: The K_1K_2 decays were identified by the two charged π 's of the charged decay mode of the K_1 . The angle θ between the two π mesons is close to 180° and is always larger than a minimum angle given by kinematics ($\theta = 150^\circ$ at $2E = m_\phi$). This was a very efficient criterion for the identification of the K_1 decays. The range of the π 's is rather short and provides another criterion. The result of this part of the experiment [based on 150 events, and using the branching ratio $B(\phi \rightarrow K_1K_2) = 0.389 \pm 0.031$] yields a BR = $(3.10 \pm 0.5) \times 10^{-4}$.

This is in good agreement with the earlier DESY - MIT results of $(2.7 \pm 0.8) \times 10^{-4}$.

$\pi^+\pi^-\pi^0$ decay: Again two charged π 's were detected. The corresponding angle θ is not peaked close to 180° and the range of these π 's is usually larger than in the K_S^0 case. Here the kinematics cannot be reconstituted. The efficiency of the detection system for

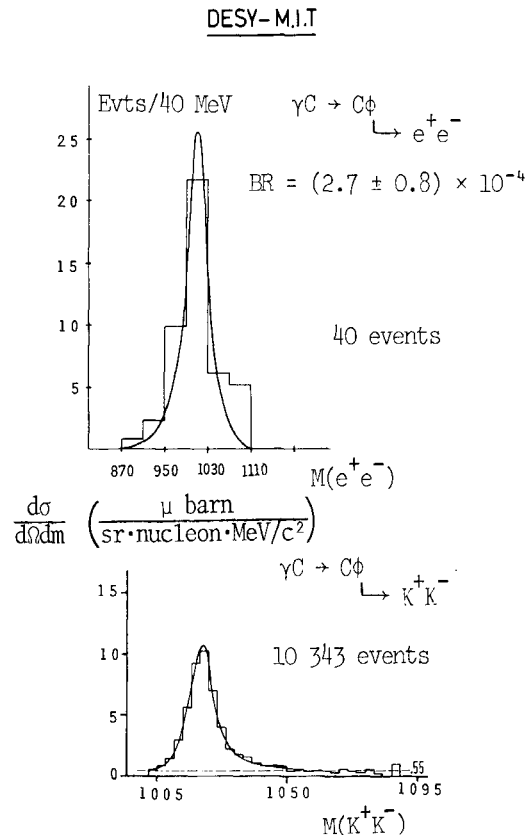


Fig. 8 Invariant mass spectra of $\phi \rightarrow e^+e^-$ and $\phi \rightarrow K^+K^-$ measured in the same apparatus, by the DESY-MIT group.

3π decays is weaker and has been computed by Monte Carlo method to be 4%. This, combined with the smaller branching ratio of the ϕ for 3π decay, leads to roughly three times less ϕ 's being detected through this mode. Using the value $B(\phi \rightarrow 3\pi) = 0.138 \pm 0.043$, this part of the measurement yields a $BR = (5.8 \pm 1.4) \times 10^{-4}$. This is in strong disagreement with the more precise result given above. The Orsay group has also measured the various branching ratios for ϕ decay and they find the values:

$$\begin{aligned} B(\phi \rightarrow K^+K^-)/B(\phi \rightarrow K_1K_2)/B(\phi \rightarrow 3\pi) &= \\ &= 0.48 \pm 0.024/0.312 \pm 0.016/0.208 \pm 0.04. \end{aligned}$$

This is somewhat different from the results obtained from the Rosenfeld table:

$$\begin{aligned} B(K^+K^-)/B(K_1K_2)/B(3\pi) &= \\ &= 0.473 \pm 0.032/0.389 \pm 0.031/0.138 \pm 0.043. \end{aligned}$$

From this they obtain, using the K_S^0 events:

$$\begin{aligned} BR(\phi \rightarrow e^+e^-) &= (3.9 \pm 0.62) \times 10^{-4}; \\ \Gamma_{\phi \rightarrow ee} &= (1.62 \pm 0.26) \text{ keV}. \end{aligned}$$

It is worth while pointing out that both the DESY-MIT group experiment and the Orsay storage ring experiment are very difficult ones. In the DESY experiment the counting rate is almost one count/day. Thus it was entirely possible to run three days without any counts. One hundred events represent a major effort to keep the detection system from changing. The Orsay experiment has the difficulties already outlined. Thus it is very gratifying to see that these two very different experiments yield the same result.

The first successful experiment on ϕ and ω decay, and thus on the direct determination of the $(\omega-\phi)$ mixing angle, was done at CERN by the Zichichi group¹⁸⁾ (Fig. 9) studying the reaction $\pi^-p \rightarrow nV^0; (V^0 \rightarrow e^+e^-)$. In order to study the decay mode $\phi \rightarrow e^+e^-$, a π^- beam of momentum 1.93 GeV/c was used. The mass of V^0 was determined to ± 15 MeV by measuring the velocity and direction of the neutron. In addition, the decay of $\phi \rightarrow e^+e^-$ was identified and measured by the opening angle and the energy of electron pairs as determined in two large shower detectors, each one having a rejection power against pions of the order of 6×10^{-4} .

A total of 9 ± 3 events was observed. Normalizing this yield to the production cross-section from bubble chamber data, they obtain a branching ratio $BR = (6.1 \pm 2.6) \times 10^{-4}$ and a corresponding $\Gamma(\phi \rightarrow e^+e^-) = 2.1 \pm 0.9$ keV (using $\Gamma_{\text{tot}} = 3.4 \pm 0.8$ keV).

The following table summarizes the results of measurements on $\phi \rightarrow \ell^+\ell^-$. Together with the new results from Orsay of $\Gamma_{\text{tot}} = 4.2 \pm 0.9$, these results yield, for the first time, an accurate value of $\gamma_\phi^2/4\pi$.

TABLE 2

| Groups | Γ_ϕ (MeV) | $BR \times 10^4$ | $\Gamma_{\phi \rightarrow ee}$ (keV) |
|----------------|---------------------|------------------|--|
| Bologna - CERN | | 6.1 ± 2.6 | |
| DESY/MIT | | 2.7 ± 0.8 | |
| Orsay | 4.2 ± 0.9 | 3.9 ± 0.62 | 1.62 ± 0.26 (from their best fit) |
| Average | 4.2 ± 0.9 | 3.55 ± 0.48 | |

From these we have:

$$\begin{aligned} \Gamma(\phi \rightarrow e^+e^-) &= 1.49 \pm 0.35 \text{ keV} \\ \gamma_\phi^2/4\pi &= 3.04_{-0.66}^{+1.07}. \end{aligned}$$

2.3.3 The branching ratio of $\omega \rightarrow \ell^+\ell^-$

An experiment, where for the first time the $\omega \rightarrow \ell^+\ell^-$ was resolved from $\rho \rightarrow \ell^+\ell^-$, has been done at CERN by the Zichichi group¹⁸⁾ using the same techniques as they employed for the ϕ (Fig. 9). The primary π^- momentum was in this case 1.67 GeV/c and the mass resolution ± 10 MeV. Taking the ω - ρ interference to be zero

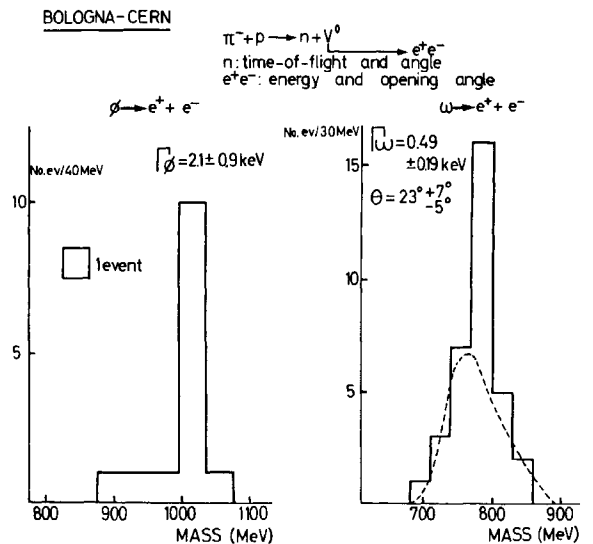


Fig. 9 Experimental results on $\omega \rightarrow e^+e^-$ and $\phi \rightarrow e^+e^-$ from the Bologna-CERN group.

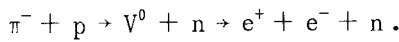
and using the known production angular distribution, they obtain a branching ratio, based on 11 events, of $BR = (0.40 \pm 0.15) \times 10^{-4}$ or $\Gamma_{\omega \rightarrow e^+e^-} = 0.49 \pm 0.19$ keV.

The Orsay group of Augustin et al.¹⁹⁾ has just finished a beautiful experiment on $e^+ + e^- \rightarrow \omega \rightarrow \pi^+ \pi^- \pi^0$ by detecting the $\pi^+ \pi^-$. The three-body events were identified, and separated from two-body events and background by selecting events giving two non-collinear tracks originating from the beam. The resulting spectrum, obtained with the same apparatus as in the ρ and ϕ experiments, is shown in Fig. 10. This experiment yields a branching ratio $= (0.85 \pm 0.16) \times 10^{-4}$, and a best fit $\Gamma_{\omega \rightarrow e^+e^-} = 1.04 \pm 0.19$ keV.

From the average of these two branching ratios, we obtain a $(BR)_{av} = (0.61 \pm 0.11) \times 10^{-4}$. This, together with the world data on the width of ω (both groups prefer this value) of 12.2 ± 1.3 MeV, gives:

$$\begin{aligned} (\Gamma_{\omega \rightarrow e^+e^-})_{av} &= 0.744 \pm 0.156 \text{ keV} \\ (\gamma_{\omega}^2/4\pi)_{av} &= 4.69_{-0.81}^{+1.24} \end{aligned}$$

The Dubna group of Baldin has also observed²⁰⁾ the e^+e^- decay mode of ρ , ω , and ϕ . The experiment was done by measuring the reaction

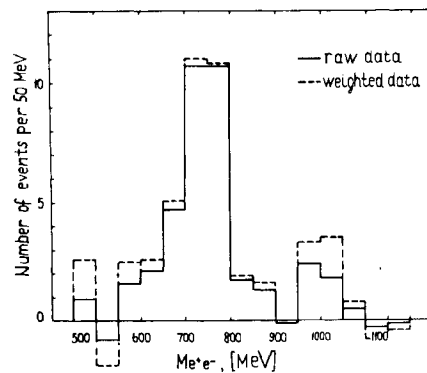
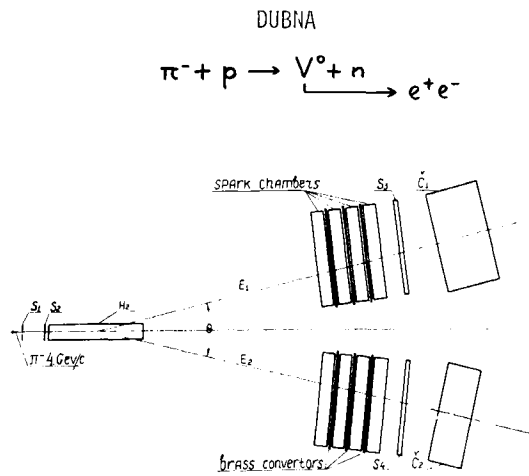


The conditions of the experiment allows one to detect, with high constant efficiency, the e^+e^- pairs in the mass range from 500 to 1200 MeV (Fig. 11). For each event, their system makes it possible to measure three

parameters, the energies E_1 and E_2 of electrons from V^0 decay, and the opening angle θ between them. The knowledge of the above three parameters allows one to calculate the effective mass of the event. Assuming a mixing angle of 38° (which, as we shall see, is a valid assumption consistent with existing data), this experiment yields:

$$\begin{aligned} B_{\rho} &= (5.3 \pm 1.1) \times 10^{-5} \\ B_{\omega} &= (6.5 \pm 1.3) \times 10^{-5} \\ \text{and } B_{\phi} &= (6.6_{-2.8}^{+4.4}) \times 10^{-4}. \end{aligned}$$

Binnie et al.²¹⁾ from the Rutherford Laboratory used the reaction $\pi^- + p \rightarrow \phi + n$ at 1.58 GeV/c to study both the production and the leptonic decay rates of ϕ . The K^+K^- mode was selected by scintillation counters and threshold water Čerenkov counter and spark



Based on SU(3):

$$\begin{aligned} B_{\rho} &= (5.3 \pm 1.1) \times 10^{-5} \\ B_{\omega} &= (6.5 \pm 1.3) \times 10^{-5} \\ B_{\phi} &= (6.6_{-2.8}^{+4.4}) \times 10^{-4} \end{aligned}$$

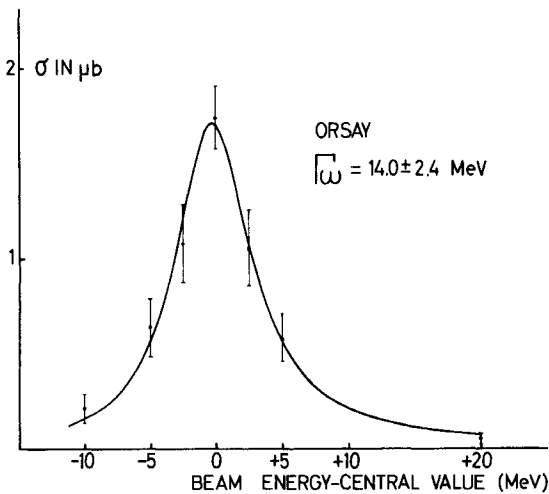


Fig. 10 Experimental results on mass spectra of $e^+e^- \rightarrow \omega \rightarrow \pi^+ \pi^- \pi^0$ from Orsay.

Fig. 11 Experimental set-up and results on leptonic decays of vector mesons from the Baldin group at Dubna.

chambers. The e^-e^+ decay of the ϕ was selected via thin-foil optical spark chambers, lead plates, and scintillation counters. This experiment yields a result of

$$\begin{aligned} \text{BR} &= (7.2 \pm 3.9) \times 10^{-4} \\ \text{or } \Gamma_{\phi \rightarrow e^+e^-} &= 2.4 \pm 1.5 \text{ keV} \\ \text{or } (\gamma_{\phi}^2/4\pi) &= 1.9_{-0.7}^{+2.9}. \end{aligned}$$

Binnie et al. also measured the branching ratio of $\omega \rightarrow e^+e^-$, based on three events. They give a ratio lying between 5×10^{-5} and 6×10^{-4} .

These results are in agreement with other previous measurements.

In summary

The large amount of accurate data on leptonic decays of vector mesons (ρ, ω, ϕ) from both production ex-

periments and colliding beam experiments are in good agreement with each other. The average results of the three independent experiments plotted on the Sakurai circle (based on Weinberg's first sum rule) are shown in Fig. 12. These results yield the values of the generalized mixing angle θ of:

$$\begin{aligned} \text{Bologna-CERN} & \theta = 23^\circ \quad \begin{matrix} + 7^\circ \\ - 5^\circ \end{matrix} \\ \text{Orsay} & \theta = 35.1^\circ \pm 3.3^\circ \\ \text{DESY-MIT} & \theta = 40^\circ \quad \begin{matrix} + 5^\circ \\ - 7^\circ \end{matrix} \quad \begin{matrix} \text{(using } \Gamma_{\omega \rightarrow ee} = \\ 1.04 \pm 0.19 \text{ keV} \\ \text{from Orsay).} \end{matrix} \\ \text{Average} & \theta = 31.6^\circ \quad \begin{matrix} + 3.9^\circ \\ - 4.9^\circ \end{matrix} \end{aligned}$$

The average value of θ is obtained from the average values of BR above.

The comparison of the average values of $V^0 \rightarrow \ell^+\ell^-$ with various theoretical models is shown in Table 3:

TABLE 3

| Decay | Average experimental results | | | | | | Theoretical models | | | | |
|-----------------------------|--------------------------------|-----------------------------|---|---------------------------|------------------------|--|--------------------|--------|------|--|-----------------------------------|
| | BR | Γ_{tot} (MeV) | $\Gamma_{V \rightarrow \ell\ell}$ (keV) | $\frac{\gamma_V^2}{4\pi}$ | γ_V^{-2} | Group | SU(3) | Sakur. | DMO | Quark D.W. | Mass mix. K.L.Z. |
| $\rho \rightarrow e^+e^-$ | $6.04 \pm 0.50 \times 10^{-5}$ | 108.0 ± 8.5 | 6.52 ± 0.75 | $0.52_{-0.06}^{+0.07}$ | 9 | DESY-MIT Novosib. Orsay Harv. | 9 | 9 | 9 | $\Gamma_{V \rightarrow ee}$ (keV) 5.7 | $\Gamma_{V \rightarrow ee}$ (keV) |
| $\phi \rightarrow e^+e^-$ | $3.55 \pm 0.48 \times 10^{-4}$ | 4.2 ± 0.9 | 1.49 ± 0.35 | $3.04_{-0.66}^{+1.07}$ | $1.54_{-0.40}^{+0.43}$ | Bol-CERN DESY-MIT Orsay | 2 | 1.33 | 1.34 | 0.95 | 1.2 |
| $\omega \rightarrow e^+e^-$ | $6.1 \pm 1.1 \times 10^{-4}$ | 12.2 ± 1.3 | 0.74 ± 0.16 | $4.69_{-0.81}^{+1.24}$ | $1.00_{-0.21}^{+0.21}$ | Bol-CERN Orsay | 1 | 0.65 | 1.21 | 0.61 | 0.6 |

In conclusion:

i) The data agree with the prediction of Weinberg's first sum rule, based on the current mixing model. It should be noted, however, that the Orsay result, without any finite width correction on Γ_{ρ} , is 1.8 standard deviations away from the predictions of Weinberg's first sum rule.

ii) The average values of the partial widths of $V^0 \rightarrow e^+e^-$ agree remarkably well with the quark-model calculations of Dar and Weisskopf.

iii) Both the Orsay data and the DESY/MIT data prefer the mixing angle $\theta = 39^\circ$ given by Das, Mathur and Okubo²²⁾, whereas the CERN data prefer the prediction of Oakes and Sakurai²³⁾, $\theta = 28.2^\circ$.

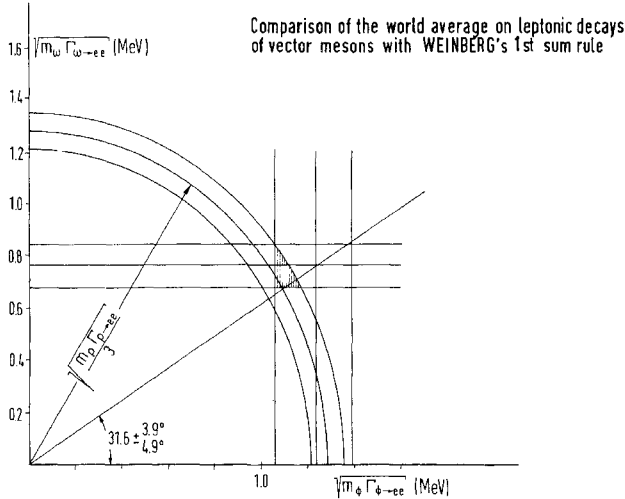


Fig. 12 Comparison of the world average on leptonic decays of vector mesons with Weinberg's first sum rule.

iv) Because of the large difference between the CERN results and the Orsay (and DESY/MIT) results, the average values of the data are not accurate enough to exclude the mass mixing models given by Kroll, Lee and Zumino²⁴). In fact, the average values of the data are surprisingly in agreement with the predictions of simple SU(3).

v) The total widths of vector mesons determined directly from their leptonic decays are $\Gamma_\rho = 108.0 \pm 8.5$ MeV, $\Gamma_\omega = 14.0 \pm 2.4$ MeV, and $\Gamma_\phi = 4.2 \pm 0.9$ MeV. These values are somewhat different from those obtained from the analysis of strong interaction experiments:

$$\Gamma_\rho = 90-150 \text{ MeV,}$$

$$\Gamma_\omega = 12.2 \pm 1.3 \text{ MeV,}$$

$$\text{and } \Gamma_\phi = 3.4 \pm 0.8 \text{ MeV.}$$

3. PHOTOPRODUCTION OF VECTOR MESONS

3.1 Motivation

Since photons and vector mesons have the same quantum numbers, it is very likely that at high energy and small momentum transfers the reaction $\gamma A \rightarrow V^0 A$ could have similar behaviour to that of $\pi A \rightarrow \pi A$, i.e. they should have the following characteristics:

$$i) \quad \frac{d\sigma}{dt} \sim |J_1(R\sqrt{-t})|^2 \approx \exp[a(A,t)t], \quad t \text{ small}$$

where $a(A,t)$ is a measure of nuclear density; its value depends sensitively on the t -range used and on A .

ii) As in the case of πp scattering, the total cross-section should be either slowly decreasing with increasing energy or be almost constant.

iii) For diffraction scattering, the produced vector mesons carry the same polarization as the initial photons. Thus the angular distribution of the decay K pairs in photoproduction of ϕ mesons should be $\sim \sin^2 \theta^*$, where θ^* is the angle, in the ϕ rest system, between the decay K meson and the recoil nucleus direction.

To study the detailed mechanism by which vector mesons are produced at high energy and low momentum transfer on complex nuclei, we compare the data with the predictions of the diffraction models²⁵) of Drell and Trefil, Ross and Stodolsky, Margolis, and Trefil, in which the forward production amplitude is expressed (in the laboratory system) as

$$f_A = 2\pi f_H \int_{-\infty}^{\infty} dz \int_0^{\infty} b db e^{i\Delta \cdot b} e^{i\Delta_m \cdot z} \rho(z,b) \times \exp\left[-\frac{\sigma}{2} \int_z^{\infty} \rho(z',b) dz'\right] \quad (21)$$

where the factor $\exp(i\Delta \cdot b)\rho(z,b)$ comes from the nuclear shape; $\exp(i\Delta_m \cdot z)$ comes from the difference in initial and final mass; $\exp[-\sigma/2 \int_z^{\infty} \rho(z',b) dz']$ from the attenuation of the vector meson by nuclear matter after its production, and where f_H is the production amplitude on hydrogen. $\sigma = \sigma_{VN}$ is the vector-meson-nucleon total cross-section. The model of Drell and Trefil, and Ross and Stodolsky assumes

$$\rho(r) = \begin{cases} = \text{const} & r \leq R \\ = 0 & r > R \end{cases}$$

Thus the nucleus is treated in an average way as an absorbing medium, rather than as a collection of individual nucleons. Clearly, the model is best for nuclei in which A is large.

The Margolis model, based on an approximate summation of the multiple scattering series of Glauber, uses for the nuclear density a Woods-Saxon distribution

$$\rho(r) = \rho_0 \{1 + \exp[(r-c)/a]\}^{-1}.$$

In the Margolis model, terms in $1/A$ and also the effect of each individual vector meson nucleon scattering term $(d\sigma/dt)(\gamma p \rightarrow Vp) = a \exp(bt)$ are dropped. Thus the model is best for production on heavy nuclei at small momentum transfers, but will not apply to $A \leq 12$, when $1/A$ terms are important.

The model of Trefil uses a density distribution

$$\rho(r) = \prod_{j=1}^A \exp[-(r_j/R)^2], \quad R = \begin{array}{l} \text{determined} \\ \text{by r.m.s.} \\ \text{nuclear radius.} \end{array}$$

This model keeps terms $\sim A^{-1}$ and b/R , and thus in principle should apply to all nuclei for both coherent and incoherent production.

For heavy nuclei at small momentum transfers there is very little difference between the three above-mentioned models. The difference between the models occurs at large t or on small A .

In all three models, the following important properties are to be noted:

A. To determine σ_{VN} , one compares the relative yields

$$\frac{d\sigma}{d\Omega dm} (A_i) \Big/ \frac{d\sigma}{d\Omega dm} (A_j)$$

for a set of nuclei (Be, C, Al, Cu, Ag, Ta, Pb) for a narrow mass band near the peak of the resonance, so that the relative background contribution is small. Comparison of relative yields is the best way to determine σ_{VN} . It corresponds to the classical way of measuring a total cross-section with different target thicknesses.

B. In principle, one can also determine σ_{VN} by matching the relative yields of

$$\frac{d\sigma}{dt} \Big|_{t=0} (\gamma A \rightarrow AV^0) \Big/ \frac{d\sigma}{dt} \Big|_{t=0} (\gamma p \rightarrow pV^0)$$

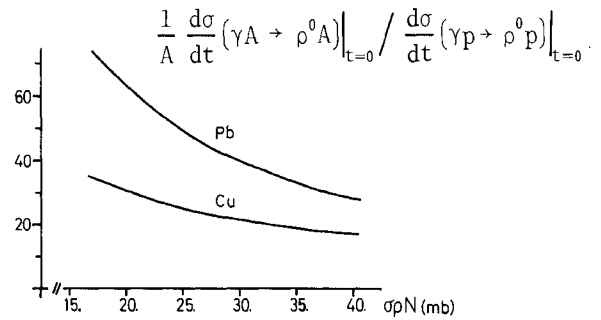
on each nucleus with

$$|f_A(R, t, \sigma_{VN}) / f_H|_{t=0}^2.$$

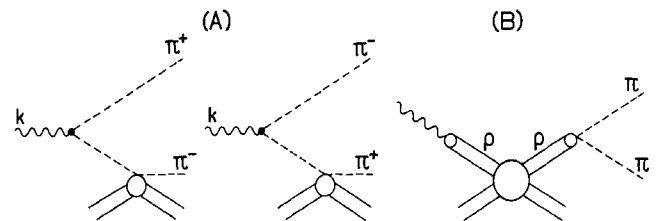
In practice, however, there are some difficulties associated with this method:

1. The function $|f_A(R, t, \sigma_{VN})|_{t=0}^2 \sim R^4$, therefore the $|f_A/f_H|^2$ and the corresponding value σ_{VN} for large

R depends critically on the nuclear radius parameters used. For example, as shown in the following figure taken from the calculation of Margolis and Kölblig²⁵⁾ on the dependence of $\sigma_{\rho N}$ on the ratio $|f_A/f_H|^2$, in the case of Pb an 8% change in nuclear radius would correspond to a change of $\sigma_{\rho N}$ from 30 mb to 40 mb.



2. For a wide resonance such as the ρ meson, the absolute normalization of the experimental data cannot be accurate to more than $\sim 25\%$. This is due to the fact that there is no reliable way of describing the shape of a wide resonance whose reported width varies between $\Gamma_\rho = 90$ and $\Gamma_\rho = 150$ MeV. The value Γ_ρ and thus the amount of pure ρ mesons in the observed $\pi^+\pi^-$ pairs depends sensitively upon the assumptions of Breit-Wigner form and background function. The two most commonly used methods are: the Söding mechanism²⁶⁾, whereby a photoproduced π pair is elastically scattered off the nucleus (diagram A). The interference between (A) and (B) below introduces a distortion in the resonance shape:



The Söding mechanism not only cannot be calculated exactly, but also it constitutes serious double counting, since the $\pi^+\pi^-$ in diagram (A) must be in a P-state in order to interfere with the pure ρ diagram (B). The method where one modifies the spectrum by a $(m_\rho/m_{\pi\pi})^4$ factor [Ross and Stodolsky²⁷⁾] and uses an empirical background to fit the data, is also somewhat arbitrary, since the resultant cross-section is somewhat dependent on the background function used.

Thus, depending on the method by which the data were analysed, the ratio of the integrated cross-section

$$\frac{\int_A (d\sigma/d\Omega dm) dm}{\int_H (d\sigma/d\Omega dm) dm} = \frac{(d\sigma/dt)(\gamma A \rightarrow A\rho^0)}{(d\sigma/dt)(\gamma p \rightarrow p\rho^0)}$$

can easily vary by 25% or more, as shown by the above figure. In the case of Cu, a 25% variation in the ratio corresponds to a change of $\sigma_{\rho N}$ from 30 mb to 40 mb.

C. With the knowledge of σ_{VN} , and with the assumption of pure imaginary scattering amplitude, one can now use the vector dominance model prediction [Eq. (8)] or its equivalent term:

$$\frac{d\sigma}{dt} \Big|_{t=0} (\gamma A \rightarrow AV^0) = \frac{1}{16} \frac{\alpha}{4\pi} \left(\frac{\gamma_V^2}{4\pi} \right)^{-1} \sigma_T^2(V^0A) \quad (22)$$

to extract the value $\gamma_\rho^2/4\pi$ and compare it with the values obtained from π -meson form factors, analysis of π^+ , π^- , π^0 photoproduction, etc., where the photon is also on the mass shell.

Since at finite energies the minimum momentum transfer $t = m_V^2/4k^2$ is far away from zero [typically on lead nucleus $d\sigma/dt \sim \exp(400t)$], the procedure of extrapolating $d\sigma/dt|_{t=0}$ from the measured $d\sigma/dt$ has all the difficulties (i.e. R^4 dependence, uncertainty in normalization, etc.) outlined above. These difficulties can be overcome²⁸⁾, however, if one notes that in the optical model one has

$$\sigma_T(V^0A) = 4\pi \int_0^\infty b db \left[1 - \exp\left(-\sigma_{VN} \int_0^\infty \rho(b,z') dz'\right) \right] \sim R^2, \quad (23)$$

and if one now calculates $(d\sigma/dt)^{1/2}$ from Eq. (21) with exactly the same set of density parameters R and $\rho(b,z)$ one has:

$$\begin{aligned} \left[\frac{d\sigma}{dt} (\gamma A \rightarrow V^0A) \right]^{1/2} &= 2\pi f_H \int_0^\infty b db \int_{-\infty}^\infty dz \times \\ &\times e^{i\Delta \cdot b} e^{i\Delta_m \cdot z} \rho(b,z) \exp\left(-\sigma_{VN}/2 \int_z^\infty \rho dz'\right) \\ &\stackrel{\Delta \rightarrow 0}{=} \frac{4\pi f_H}{\sigma_{VN}} \int_0^\infty b db \left(1 - \exp\left[-\sigma_{VN} \int_0^\infty \rho(b,z') dz'\right] \right) \sim R^2. \end{aligned} \quad (24)$$

Note that both $\sigma_T(V^0A)$ and $(d\sigma/dt)^{1/2}$ have the same functional dependence on R . Thus it follows from Eq. (22) that:

$$\begin{aligned} \frac{\gamma_\rho^2}{4\pi} &= \frac{1}{16} \frac{\alpha}{4\pi} \frac{\sigma_T^2(V^0A)}{\left. \frac{d\sigma}{dt} \right|_{t=0} (\gamma A \rightarrow V^0A)} \\ &= \frac{1}{16} \frac{\alpha}{4\pi} \frac{\sigma_{VN}^2}{\left. \frac{d\sigma}{dt} \right|_{t=0} (\gamma \rho \rightarrow V^0\rho)} \end{aligned} \quad (25)$$

independent of $R, \rho(b,z)$.

Therefore, the best way in which to obtain $\gamma_\rho^2/4\pi$ from photoproduction of vector mesons on nuclei is to determine σ_{VN} from relative yields for a set of nuclei in a narrow mass band near the peak of the resonance where the background is small and where no absolute normalization is necessary.

Using the σ_{VN} so obtained, one then calculates $\sigma_T(V^0A)$ from Eq. (23) and extrapolates $d\sigma/dt|_{t=0}$ from the measured total cross-section $d\sigma/d\Omega$ with $|f_A(R,t,\sigma_{VN})|^2$ -- with exactly the same values for R and $\rho(z)$. In this case it follows from the analysis of Eq. (25) that one has a unique $\gamma_\rho^2/4\pi$ independent of R and $\rho(z)$.

For example, with $d\sigma/dt|_{t=0}^{(H)} = 150 \mu\text{b}/\text{GeV}^2$ one has the following:

- i) if the relative measurements yield a $\sigma_{\rho N} \cong 30 \text{ mb}$, then it follows from Eq. (25) $\gamma_\rho^2/4\pi \cong 0.5$ for all A ;
- ii) if the relative measurements yield a $\sigma_{\rho N} \cong 40 \text{ mb}$, then $\gamma_\rho^2/4\pi \cong 1.0$ for all A .

3.2 Experimental results

3.2.1 Photoproduction of ρ mesons

1. On hydrogen: Large amounts of experimental data now exist on photoproduction of ρ on hydrogen, deuterium, and on complex nuclei.

The experiment of Ritson's group (SLAC, CIT, Santa Barbara, Northeastern Collaboration)²⁹⁾ used a bremsstrahlung photon beam and a hydrogen target, and observed the recoiling protons produced in the target with a 90° bent spectrometer. The data were obtained by the photon subtraction technique. The results from 4 to 18 GeV are shown in Fig. 13. They are consistent with $d\sigma/dt = d\sigma/dt|_{t=0} \times \exp(Bt + Ct^2)$ with $B = 8-10 \text{ GeV}/c^2$.

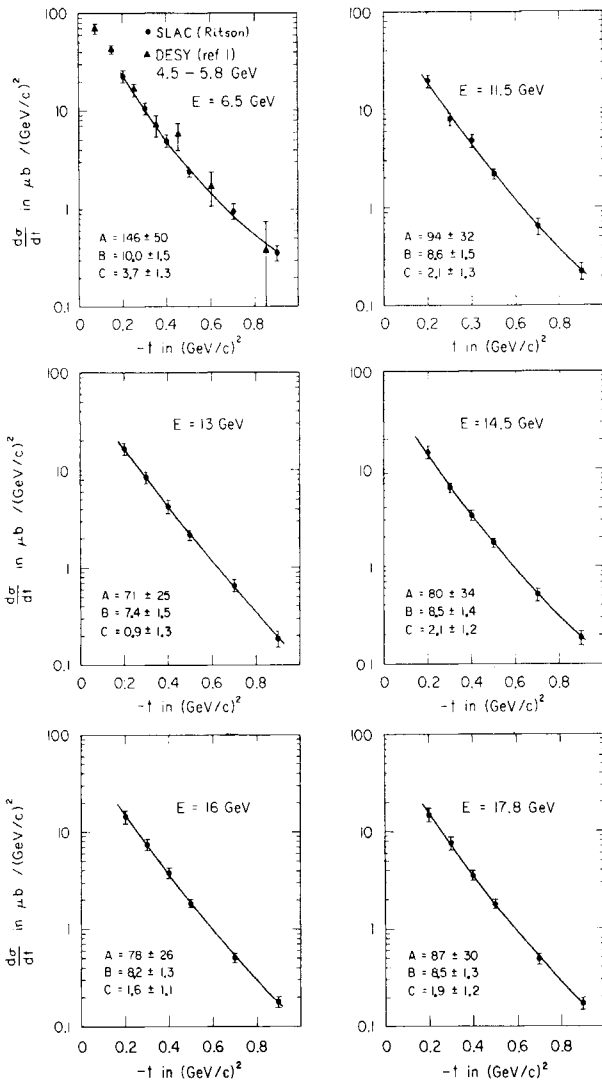


Fig. 13 Experimental results from the Ritson group at SLAC. $d\sigma/dt$ in $(\text{GeV}/c)^2$ versus t , for the reaction $\gamma + p \rightarrow p + \rho^0$ at incident photon energies from 6.5 GeV to 17.8 GeV. The lines drawn through the data points are the best fits to the expression $d\sigma/dt = A e^{Bt+Ct^2}$. The values of A, B, and C found at each energy are shown in the figure. Their units are $\mu\text{b}/(\text{GeV}/c)^2$, $(\text{GeV}/c)^{-2}$, and $(\text{GeV}/c)^{-4}$, respectively.

The experiment of Mozley's group³⁰⁾ at SLAC used a 2.2 metre streamer chamber to study the multibody photoproduction. A collimated bremsstrahlung beam of 16 GeV peak energy and 3 mm diameter was incident on a 3 atm hydrogen gas target extending through the chamber. The chamber was mounted on a large magnet with an 8 kG field and triggered with a fourfold coincidence array of scintillation counters.

The experiment of Silverman's group³¹⁾ at Cornell used a bremsstrahlung beam, scintillation counters, and spark chambers to measure the positive and negative charged particles which traverse the spectrometer. The entire magnet system was mounted on a platform which rotated vertically about the target, thus enabling them to vary the production angle.

Figure 14 summarizes the results of $d\sigma/dt|_{t=0}$ from the above groups together with the results³²⁾ from the DESY bubble chamber collaboration, the SLAC HBC group of Ballam, and the DESY counter group of Heinloth. As seen from the figure, the value $d\sigma/dt|_{t=0}$ decreases slowly with increasing energy, thus implying that σ_{pp} also decreases with increasing energy. Figure 15 shows the summary of published values of σ_{pp} from the various groups. These data show two interesting features:

- i) at lower energies (2-3 GeV) the value σ_{pp} depends, to $\approx 25\%$, on the assumption of the fits; and
- ii) within the errors, the data are consistent with a slowly decreasing σ_{pp} with increasing energy.

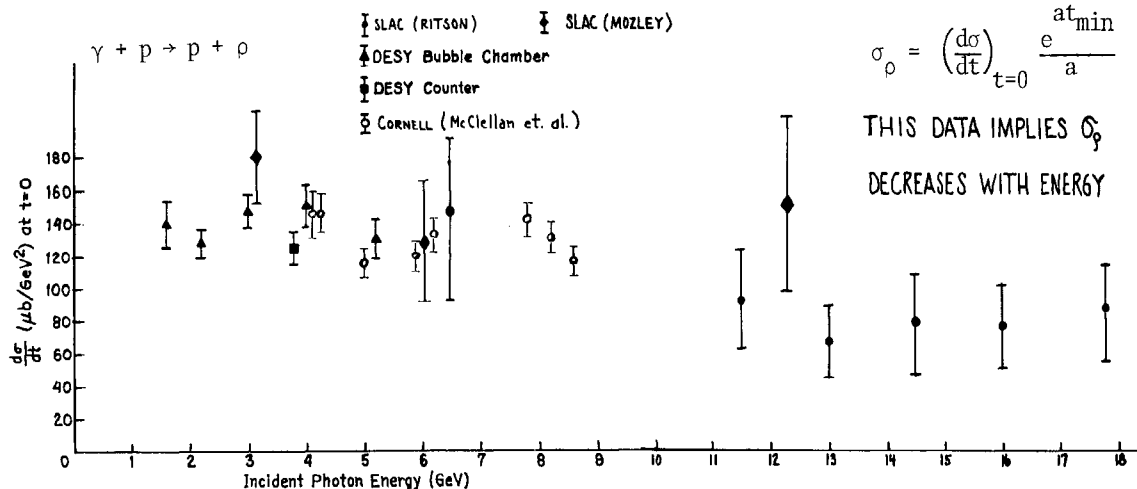


Fig. 14 Summary of $d\sigma/dt|_{t=0}$ ($\gamma p \rightarrow p\rho^0$). The decreasing of this value with increasing photon energy indicates that σ_{pp} decreases slowly with energy.

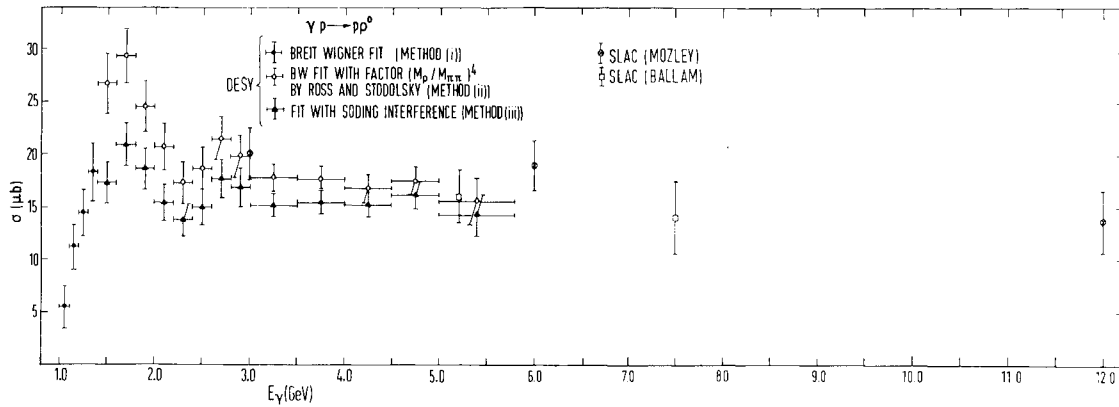


Fig. 15 Summary of total cross-section $\sigma_{tot}(\gamma p \rightarrow p\rho^0)$. Note that in the low-energy region, $E_\gamma \leq 4$ GeV, the value σ_{tot} depends sensitively on the method of analysis used.

The DESY group of Criegee and Timm³³⁾ has measured ρ production with polarized photons. Measurements with polarized photons provide a strong check on ρ production models. In a diffraction process (cross-sections σ_1 in Fig. 16) the decay pions tend to emerge in a plane containing the polarization (electric) vector of the photon, whilst in 0^- exchange processes they come out perpendicularly with cross-sections σ_2 . This group has determined the ratio $R = \sigma_2/\sigma_1$ by measuring the $\pi^+\pi^-$ pairs on hydrogen with photons of two different polarizations. For photon energies between 2.0 and 2.5 GeV, and squared momentum transfers between -0.07 and -0.40, they find $R = 0.17 \pm 0.07$. This ratio indicates that ρ^0 photoproduction on hydrogen is dominated by the diffraction process. Since non-resonant π pairs have not been subtracted from the data, R represents an upper limit for non-diffractive ρ^0 production.

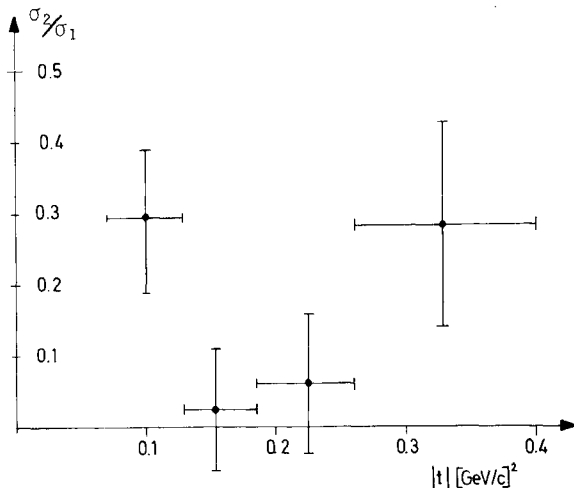


Fig. 16 Experimental results of the photoproduction of the ρ meson on protons with polarized photons, at an energy of 2.2 GeV. See text for further explanation.

2. On deuterium: Figure 17 shows the summary of the data on deuterium from the DESY bubble chamber collaboration³²⁾ and from Cornell³¹⁾. The Cornell experi-

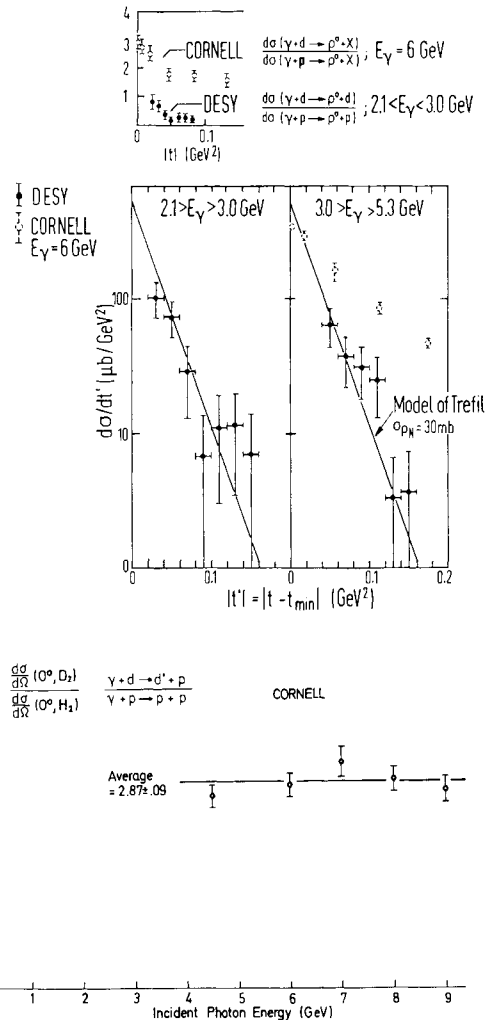


Fig. 17 Summary of photoproduction of ρ mesons on deuterium. The straight lines on the $d\sigma/dt$ plot are the predictions of the diffraction model of Trefil. See text for details.

ment only measures the $\pi^+\pi^-$ from ρ decay, the bubble chamber experiment observes all final states. The bubble chamber data agree with the coherent diffraction model calculation of Trefil with $\sigma_{\rho N} \approx 30$ mb. The Cornell data exhibit coherence at small t -values. In the large t -region, the D_2 data have the same t -dependence as hydrogen and the ratio of cross-sections $\sigma_d/\sigma_p \approx 1.9$. The Cornell group also measured deuterium to hydrogen ratios at $\theta = 0^\circ$, and as a function of E_γ . To an accuracy of about 5%, this ratio is independent of energy from 4 GeV to 9 GeV and averages to 2.87 ± 0.09 . This ratio is different from the expected value of ≈ 3.5 , based on coherent production and Glauber corrections. The Cornell result indicates that photoproduction of ρ on hydrogen cannot be completely diffractive.

3. On complex nuclei: As discussed before, measuring ρ production on complex nuclei enables one to compare the relative yields with equation (21) and thereby obtain $\sigma_{\rho N}$. With the value $\sigma_{\rho N}$, one can then proceed to determine the coupling constant $\gamma_\rho^2/4\pi$ and compare the value with the analysis of other photoproduction data when the photon is on the mass shell.

The experiment done at DESY by the DESY-MIT group³⁴⁾ used a double-arm spectrometer with a mass resolution of ± 10 MeV. The relative yields were measured at three different energies of 2.7, 3.5, and 4.5 GeV. To reduce the background contribution, comparison with Eq. (21) was made at the central peak mass region between 720 and 820 MeV. The results shown in Fig. 18 yield an average value of $\sigma_{\rho N} = 31.3 \pm 2.3$ mb for this energy region.

To obtain $\gamma_\rho^2/4\pi$, they integrated the forward cross-section $d\sigma/d\Omega dm$ over their spectrometer acceptances ($3.0 < p < 6.2$ GeV, $8^\circ < \theta_{\pi\pi} < 26^\circ$). They have also used an $(m_\rho/m_{\pi\pi})^4$ factor in their mass distribution to fit the spectrum. Their integrated cross-sections over their acceptances are: $d\sigma/d\Omega(C) = 5.0 \pm 0.4$ mb/(sr·nucleon), $d\sigma/d\Omega(Cu) = 11.2 \pm 1.1$ mb/(sr·nucleon), $d\sigma/d\Omega(Pb) = 10.0 \pm 1.0$ mb/(sr·nucleon). From their spectrometer acceptance windows they then calculate an average value of $|f_A(R = 1.35 A^{1/3}f, \sigma_{\rho N} = 31 \text{ mb}, t)|^2$ where each Monte Carlo event is weighted by the production mechanism of ρ . The values $\sigma_{tot}(\gamma A)$ are again calculated using Eq. (23) with the same $R = 1.35 A^{1/3}f$,

$\sigma_{\rho N} = 31$ mb. From this information, the values $\gamma_\rho^2/4\pi$ follow directly via:

$$\frac{\gamma_\rho^2}{4\pi} = \frac{\alpha}{4} \frac{k^2}{16\pi^2} \frac{\sigma_T^2(R = 1.35 A^{1/3}f, \sigma_{\rho N} = 31 \text{ mb})}{\left. \frac{d\sigma}{d\Omega}(A) \right/ |f_A(R = 1.35 A^{1/3}f, \sigma_{\rho N} = 31 \text{ mb}, t)|^2} \\ \approx 0.50 \pm 0.10 \text{ for C, Cu, Pb.}$$

These numbers, as discussed before, depend only on $\sigma_{\rho N}$ and the events/acceptance, and are independent of any extrapolation procedure used -- the R^4 factor cancels out in this case.

The experiment done at Cornell³¹⁾ used the spectrometer discussed previously. Their measured A -dependence of forward cross-sections for $E_\gamma = 6.0$ GeV is also shown in Fig. 18. The curves in the figure are the optical model calculations for various assumptions about $\sigma_{\rho N}$. They used in their analysis the nuclear density distributions $\rho(b,z)$ as given by Hofstadter for electron scattering. The value they obtained this way depends on A , being 30 mb for copper and 37 mb for lead. The authors attribute this discrepancy to the neutron size being larger than the proton size.

It is clear from the published data that the values of $\sigma_{\rho N}$ determined from DESY and Cornell do not contradict each other.

To deduct $\gamma_\rho^2/4\pi$, the Cornell group proceeded in a manner quite different from the DESY method. They extrapolated the value $d\sigma/dt|_{t=0}$ with the function $|f_A(t, \bar{R} = \text{electromagnetic radius}, \sigma_{\rho N} = 40 \text{ mb})|^2$. For $\sigma_T(\rho A)$ they used the published values of Bellettini et al. on proton-nucleus total cross-sections, i.e. they took $\sigma_T(\rho A) = \sigma(pA)$. In this way by extrapolating the ratio $\sigma^2(pA)/(d\sigma/dt, t=0)$ to $A \rightarrow \infty$ they obtained a value $\gamma_\rho^2/4\pi = 1.05 \pm 0.20$.

It is interesting to note that if one uses $\sigma_T(\rho A) = \sigma(nA)$ in the Cornell analysis [the Eq. (3) of the Cornell paper], i.e. if one takes the measured values from Longo et al. or from Pantuer et al.³⁵⁾ on neutron-nucleus total cross-section and thus avoids the difficult problem of subtracting the Coulomb interference term from proton-nucleus total cross-section, then the value of $\gamma_\rho^2/4\pi$ ($A \rightarrow \infty$) is much closer to the results obtained from six or more other ways under similar kinematic conditions when the photon is on the mass shell (Fig. 19).

The experiment of Leith's group³⁶⁾ is one of the first successful coincidence experiments done on the 20 GeV SLAC. They used a large acceptance wire spark chamber spectrometer and a 9 GeV monochromatic photon

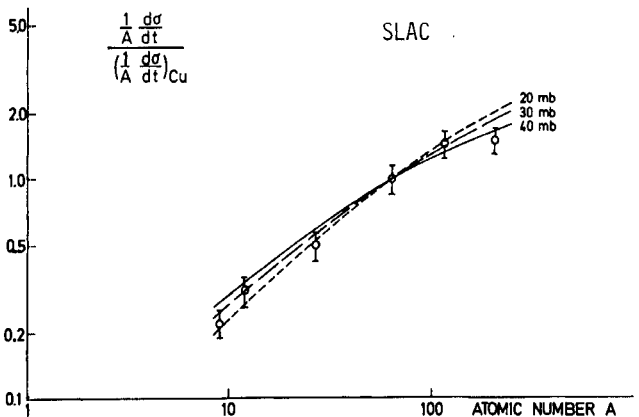
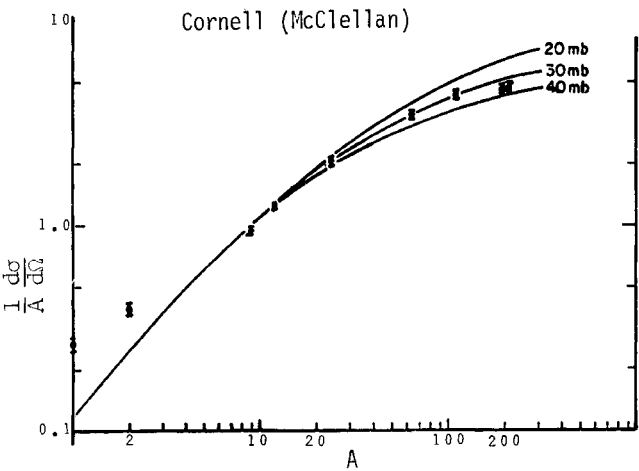
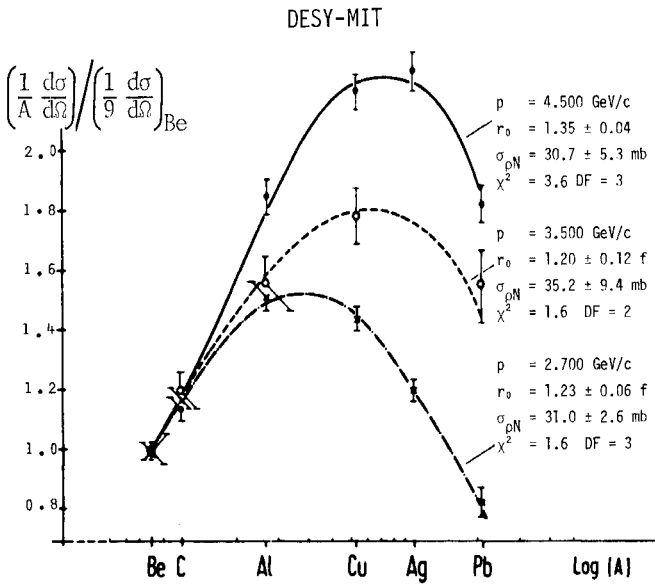


Fig. 18 Summary of relative yields of production of ρ mesons on complex nuclei from measurements at DESY at photon energies of 2.7, 3.5, and 4.5 GeV; from Cornell at 6 GeV; and from SLAC at 9 GeV. See text for explanation of the solid curves.

$$X(A) = \frac{\alpha}{4} \frac{k^2 \gamma^2}{(4\pi)^2} \frac{\sigma_T^2}{\frac{d\sigma}{d\Omega}(\gamma+A \rightarrow \rho+A)_{\text{on shell}}} \quad \frac{\gamma \rho^2}{4\pi} = \lim_{A \rightarrow \infty} X(A)$$

↓ DESY

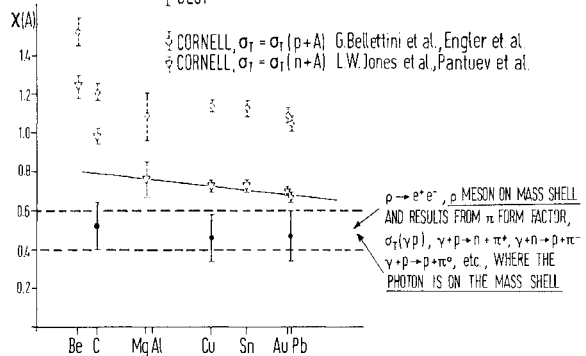


Fig. 19 Comparison of the coupling constant $\gamma_\rho^2/4\pi$ determined from the DESY analysis and from the Cornell analysis. The solid line is the result of the Cornell analysis if one replaces $\sigma_{\rho A}$ with the two results of $\sigma_{\rho N}$. The region between the dotted lines is determined from various other analyses of experiments where the photon is on the mass shell.

beam to study the photoproduction of ρ on hydrogen and complex nuclei (Fig. 20). The resolution of the monochromatic peak is $\approx \pm 1.5\%$. The spectrometer itself consists of a wide aperture, uniform field magnet, followed by a set of trigger counters and four wire spark chambers interfaced on-line with an IBM 1800 computer. Figure 18 shows the result of their preliminary analysis on the relative yields of ρ on complex nuclei. The data are consistent with $20 \leq \sigma_{\rho N} \leq 40$ mb. Using the assumption $\sigma_T(\rho A) = \sigma(\rho A)$, and not extrapolating to $A \rightarrow \infty$, they obtain an average value $\gamma_\rho^2/4\pi = 1.2 \pm 0.3$.

An experiment on electroproduction of ρ^0 was done at DESY by the Heinloth group³⁷⁾. The energy of the primary electron was 4.9 GeV, the energy of the virtual photon varied between 2.7 and 4.0 GeV. The momentum transfer was $|q^2| < 0.3$ GeV². The result agrees with a Breit-Wigner $\times (m_\rho/m_{\pi\pi})^4$ distribution function, and its t -dependence agrees well with the predictions of vector dominance.

The following table summarizes³⁸⁾ some of the results of various ways of determining the coupling constant $\gamma_\rho^2/4\pi$.

It is important to observe that the coupling constant $\gamma_\rho^2/4\pi = 0.5$ determined from direct measurements of leptonic decays of ρ when the ρ meson is on the mass shell is almost identical to that determined from various other measurements when the photon is on the mass shell.

TABLE 4

| Reactions | |
|---|---|
| <u>p meson on mass shell</u> | |
| $e^+ + e^- \rightarrow \rho^0$ | $\frac{\gamma_\rho^2}{4\pi}$ 0.52 \pm 0.07 - 0.06 |
| <u>Photon on mass shell</u> | |
| 1. $\sigma_T^2(\gamma p) / \frac{d\sigma}{dt} (\gamma p \rightarrow \rho^0 p)$ | $\frac{\gamma_\rho^2}{4\pi}$ 0.5 \pm 0.1 |
| 2. π meson form factor | 0.53 \pm 0.04 |
| 3. $\gamma p \rightarrow \pi^+ n, \gamma n \rightarrow \pi^- p$ from 3 to 8 GeV | 0.45 \pm 0.10 |
| 4. π^+/π^- ratio from deuterium | 0.45 \pm 0.10 |
| 5. $d\sigma/dt (\gamma A \rightarrow \rho^0 A)_{C,Cu,Pb}$ DESY | 0.5 \pm 0.1 |
| 6. $\Gamma(\omega \rightarrow \pi\gamma) / \Gamma(\omega \rightarrow 3\pi)$ | 0.65 \pm 0.10 |
| 7. $\frac{d\sigma}{dt} (\gamma p \rightarrow \pi^0 p) / \frac{d\sigma}{dt} (\pi N \rightarrow \rho_\perp N)$ | ~ 0.5 |
| 8. $\frac{d\sigma}{dt} (\gamma p \rightarrow \pi^+ n)$ versus $\frac{d\sigma}{dt} (\pi^- p \rightarrow \rho^0 n)^{38)}$ | 0.45 (for this comparison see Fig. 21) |
| 9. $d\sigma/dt (\gamma A \rightarrow \rho^0 A)$ Cornell | 1.05 \pm 0.20 |
| <u>Indirect measurements</u> | |
| 1. $\Gamma(\phi \rightarrow K^+ K^-)$ | $\gamma_\rho^2/4\pi$ equiv. = 0.45 \pm 0.10 |
| 2. $\Gamma(K^* \rightarrow K\pi)$ etc. | $\gamma_\rho^2/4\pi$ equiv. = 0.6 \pm 0.1 |

The idea that the coupling constant varies slowly with q^2 seems to be quite valid.

3.2.2 Photoproduction of ω mesons

For photon energies $2.1 < E_\gamma < 5.8$ GeV, the result of the DESY bubble chamber collaboration³²⁾ is shown in Fig. 22. The cross-section for $\gamma p \rightarrow p\omega$ can be described in the following form as a function of E_γ :

$$\sigma(\gamma p \rightarrow p\omega) = (18.4 \pm 5.8) \times E_\gamma^{-1.6} + (1.9 \pm 0.9) E_\gamma^{-0.08} \mu b.$$

This expression was chosen because it is the behaviour expected for the sum of two production mechanisms: i) one-meson exchange $\sim E_\gamma^{-1.6}$, ii) diffraction

production $\sim E_\gamma^{-0.08}$. Thus below 3 GeV, photoproduction of ω is dominated by one-meson exchange, whereas at higher energies it is dominated by the diffraction mechanism.

3.2.3 Photoproduction of ϕ mesons

1. On protons: Figure 23 shows the summary of the results from Ritson's group at SLAC²⁹⁾ from the DESY bubble chamber group³²⁾ at lower energies (2.5 to 5.8 GeV), and the result from the DESY-MIT group³⁴⁾ at $E_\gamma = 5.2$ GeV and $t \approx 0$.

The Ritson data and the bubble chamber data both yield a slope $d\sigma/dt \sim \exp(5t)$. The DESY-MIT data

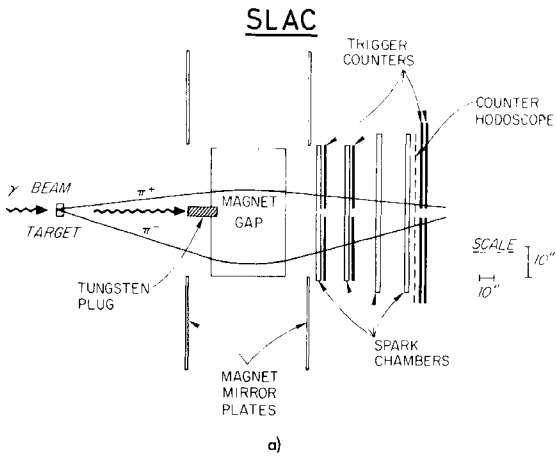


Fig. 20a Schematic drawing of the SLAC spectrometer.

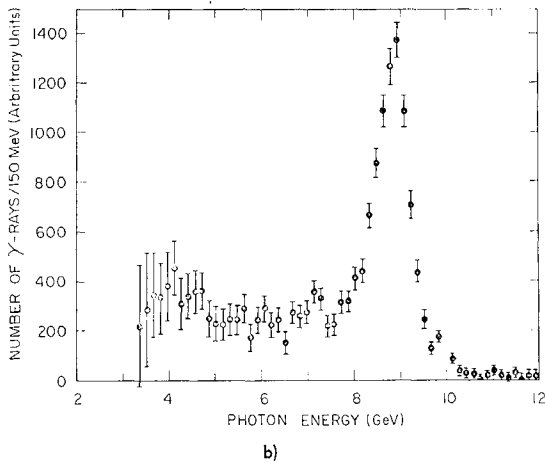


Fig. 20b Energy spectrum of the annihilation beam as measured in the pair spectrometer mode $\gamma + Al \rightarrow Al + e^+ + e^-$.

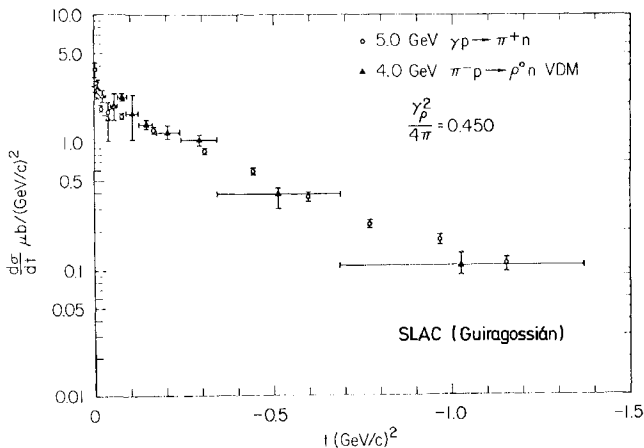


Fig. 21 Comparison of the vector dominance model by Derado and Guiragossian. The \blacktriangle are the predicted $\gamma p \rightarrow \pi^+ n$ cross-sections using the measured $\pi^- p \rightarrow \rho^0 n$ cross-sections and the vector dominance model. The \circ are the experimental results on $\gamma p \rightarrow \pi^+ n$ from Boyarski et al. at SLAC. The agreement is good.

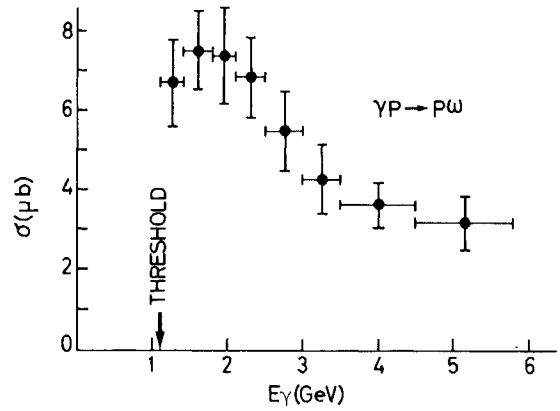


Fig. 22 Total cross-section for $\gamma + p \rightarrow p + \omega$ from the DESY bubble chamber group.

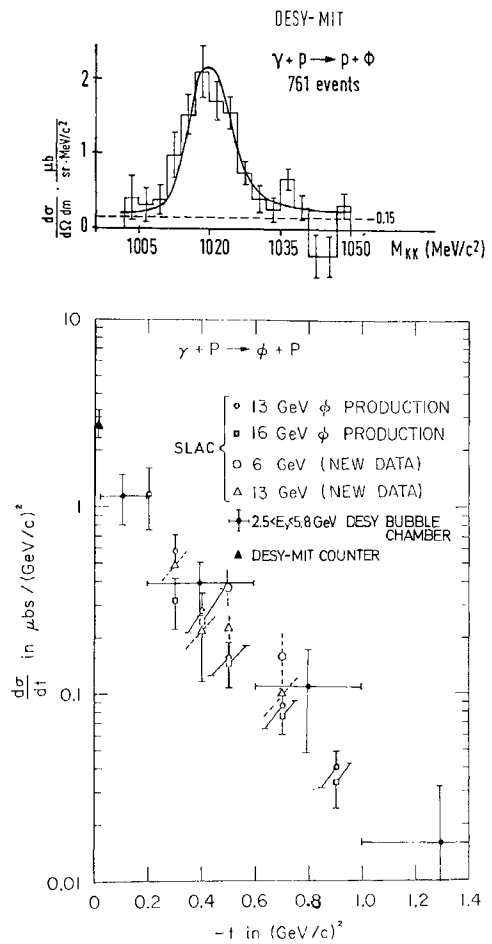


Fig. 23 Invariant mass spectra of the reaction $\gamma + p \rightarrow p + \phi$ from the DESY-MIT group, and summary of the data on $d\sigma/dt$ ($\mu\text{b}/\text{GeV}^2$) versus t from SLAC and DESY.

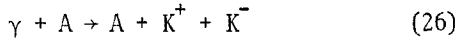
are consistent with this, but are also consistent with a higher slope, say $\exp(8t)$. The bubble chamber data can be summarized as $d\sigma/dt = (1.6 \pm 0.6) \exp [(3.5 \pm 0.9)t] \mu\text{b}/\text{GeV}^2$ with the integrated cross-sections: $\sigma_\phi(2.5 - 3.5 \text{ GeV}) = (0.41 \pm 0.14) \mu\text{b}$, $\sigma_\phi(3.5 - 5.8 \text{ GeV}) = (0.45 \pm 0.13) \mu\text{b}$.

In analysing the ϕ -production data on hydrogen, it is important to note that the competing reaction $\gamma p \rightarrow p + \phi + \pi^+ + \pi^-$ has a total cross-section:

$$\begin{aligned} \sigma_T(3.5 - 4.5) &= (0.2 \pm 0.1) \mu\text{b}, \\ \sigma_T(4.5 - 5.8) &= (0.6 \pm 0.2) \mu\text{b}. \end{aligned}$$

This makes the analysis of counter experiments with bremsstrahlung beams difficult.

2. On complex nuclei: The DESY-MIT group³⁴⁾ has just completed an experiment studying the reaction



at an incident photon energy of 5.2 GeV on targets of Be, C, Al, Cu, Ag, Ta, and Pb. They detected the K^+K^- pairs with four large-aperture Čerenkov counters, and with hodoscopes in the spectrometer to provide a mass resolution of ± 5 MeV. A total of 20,000 K^+K^- events was observed. The K^+K^- mass spectra from Be, C, Al, Cu, Ag, Pb are shown in Fig. 24. The mass resolution of the hodoscope system has not been unfolded. The errors in Figs. 24 and 25 are statistical only. An additional normalization uncertainty of $\pm 16\%$ is not included.

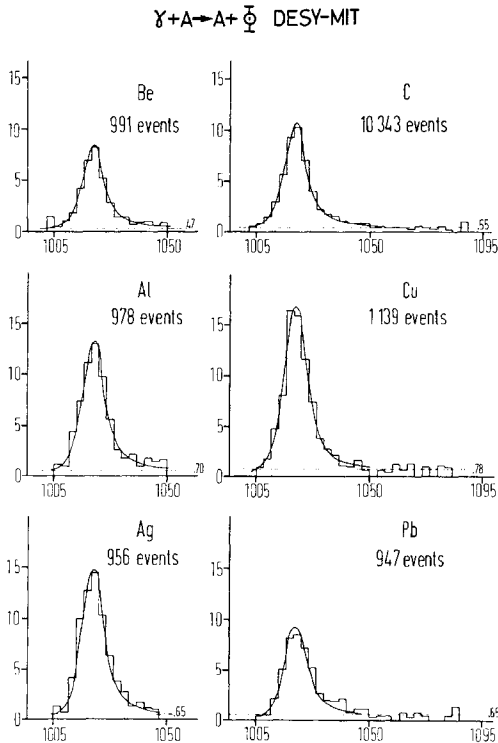


Fig. 24 Kaon pair invariant mass spectra $d\sigma/d\Omega dm$ ($\mu\text{b}/\text{sr} \cdot \text{nucleon} \cdot \text{MeV}/c^2$) at $\langle p \rangle = 5.2$ GeV/c for target nuclei of Be, C, Al, Cu, Ag, Pb. The dotted lines are the estimates of the non-resonant background contributions. The solid curves are the $\phi \rightarrow 2K$ mass distribution produced via a Monte Carlo program which generated ϕ mesons ($m_\phi = 1019.5$ MeV, $\Gamma_\phi = 3.4$ MeV) at the target.

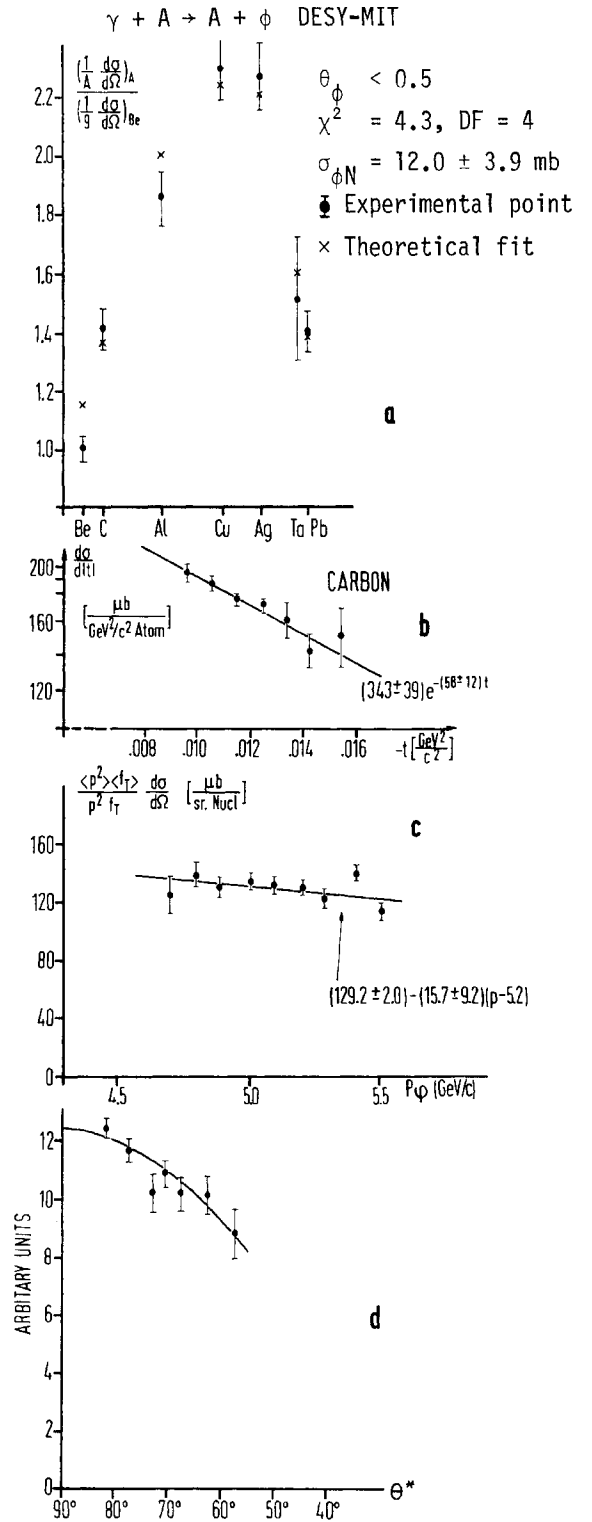


Fig. 25a Dependence of $d\sigma/dt$ upon A , the atomic number of the target. The results are shown for average ϕ momentum $p = 5.2$ GeV/c. The crosses are best fit points to the model of Drell-Trefil.

Fig. 25b The typical behaviour of $d\sigma/dt$ is shown as a function of t , the square of momentum transfer to the nucleus, for a carbon target. The solid curve is the best fit to $e^{\alpha t}$.

Fig. 25c The behaviour of $\frac{\langle p^2 \rangle \langle f_A^2 \rangle}{p^2 |f_A|^2} \cdot \frac{d\sigma}{d\Omega}$ as a function of p . To a good approximation, the cross-section $d\sigma/d\Omega$ is proportional to p^2 . (See text for details.)

Fig. 25d The angular distributions of the decay kaons in the ϕ^0 rest system. θ^* is the angle between the decay products and recoil target particle in the ϕ c.m.s. As seen, the data agree well with the $\sin^2 \theta^*$ distribution function.

As seen from Fig. 24, in the K^+K^- invariant mass region 1000 to 1085 MeV/c², reaction (26) is dominated by ϕ -meson production. Within the statistical accuracy, no other enhancements were observed.

To study the mechanism by which ϕ mesons are produced at high energy and low momentum transfer, they compare the data with the predictions of the diffraction models of Drell and Trefil, Ross and Stodolsky, Margolis, and Trefil, in which the forward production cross-section is expressed (in the laboratory system) as $d\sigma/d\Omega$ (total) = $d\sigma/d\Omega$ (coherent) + $d\sigma/d\Omega$ (incoherent): $d\sigma/d\Omega$ (coherent) = $C(A)p^2 |f_A(R, t, \sigma_{\phi N})|^2$, where p is the momentum of the ϕ meson, R is a set of parameters which describe the nuclear density distribution, t is the square of the momentum transfer to the nucleus, and $C(A)$ is a normalization constant. The coherent cross-section includes those reactions in which the nucleus remains in its ground state, whilst the incoherent cross-section includes reactions in which the nucleus is excited or fragmented. The function $f_A(R, t, \sigma_{\phi N})$ defined in Eq. (21) is chosen such that $|f_A(R, 0, \sigma_{\phi N})|^2 = 1$.

By measuring $d\sigma/d\Omega$ as a function of A , t , and p , one can compare the experimental data to the different theories of production, and determine the value of $\sigma_{\phi N}$.

The results of these comparisons are as follows (they restrict the analysis to the mass region $1016 < m < 1025$ MeV/c² as defined in Fig. 24):

a) A-dependence: The cross-section $d\sigma/d\Omega$ ($\theta_\phi < 0.5^\circ$) was measured on targets of Be, C, Al, Cu, Ag, Ta, and Pb, at $\langle p \rangle = 5.2$ GeV/c. The relative cross-sections

$$\frac{1/A \cdot d\sigma/d\Omega (A)}{1/9 \cdot d\sigma/d\Omega (\text{Be})},$$

normalized to Be, are shown in Fig. 25a. The A-dependence of the production cross-section yields information on the mean free path in nuclear matter. To obtain $\sigma_{\phi N}$, the data were first corrected for contributions from non-resonant background and incoherent production. The background ($\sim 5\%$) was subtracted by matching a Monte Carlo calculation of the non-resonant mass spectra to the data outside the peak. The incoherent contribution to $d\sigma/d\Omega$ was estimated, using the model of Trefil, by calculating the difference

between the cross-section summed over all nuclear states and the cross-section due to the ground state only. For the heavier elements, this agrees with the same calculation from the model of Margolis. The determination of $\sigma_{\phi N}$ was carried out using three different theoretical models. The measured coherent production cross-section was matched both to the Drell-Trefil model, using a step function density distribution to describe the nucleus, and to the Margolis model, using a Woods-Saxon density distribution. The data without incoherent subtraction were also matched to the model of Trefil.

The best value of $\sigma_{\phi N}$ is then

$$\sigma_{\phi N} = (12.0 \pm 3.9) \text{ mb}.$$

There is no significant difference in the value of $\sigma_{\phi N}$ obtained from different theories of nuclear photoproduction. The value of $\sigma_{\phi N}$ is to be compared with the quark-model prediction of Joos⁸⁾, $\sigma_{\phi N} = 11$ mb.

b) t-dependence: The typical behaviour of $d\sigma/dt$ as a function of four-momentum transfer squared, $t = (p-k)^2$ at a fixed central ϕ^0 laboratory momentum of 5.2 GeV/c, is shown in Fig. 25b for the C target. In the t -region of this experiment $0.009 < |t| < 0.016$ (GeV/c)², the data are fitted well by a form $d\sigma/dt \sim e^{at}$ with $a = (58 \pm 12)$ (GeV/c)⁻².

c) p-dependence: The behaviour of

$$\frac{\langle p^2 \rangle \langle f_A^2 \rangle}{p^2 |f_A|^2} \cdot \frac{d\sigma}{d\Omega}$$

as a function of p over a momentum range from 4.7 to 5.6 GeV/c is shown in Fig. 25c. The fit of this quantity to the data yields

$$\frac{\langle p^2 \rangle \langle f_A^2 \rangle}{p^2 |f_A|^2} \frac{d\sigma}{d\Omega} = (129.2 \pm 2.0) - (15.7 \pm 9.2) \times (p - 5.2).$$

This quantity is relatively independent of p , consistent with $d\sigma/d\Omega$ varying as p^2 in agreement with the predictions of the diffraction model. However, due to the limited p -range available, a small decrease in the total cross-section with increasing p cannot be excluded.

d) ϕ -polarization: As a consistency check of the diffraction production of ϕ mesons, they show in

Fig. 25d the angular distribution of the decay kaons in the ϕ^0 rest system. As seen, the data agree well with the distribution function

$$W_{KK}(\theta^*) = \frac{3}{8\pi} \sin^2 \theta^*$$

(θ^* is the angle between decay products and the recoil target particle measured in the K^+K^- c.m.s.). The data show that the ϕ mesons produced are transversely polarized, which is consistent with the other evidence that they are produced via diffraction off the whole nucleus.

To summarize, the dependence upon p , t , and A of the high-energy, small-angle ϕ^0 photoproduction cross-section is in agreement with the general features of the diffraction model, and the cross-section can be expressed in the simple form

$$\frac{d\sigma}{d\Omega} = C(A)p^2 |f_A(R, t, \sigma_{\phi N})|^2 \underset{t \rightarrow 0}{\approx} C(A)p^2 e^{at}.$$

The ϕ -nucleon cross-section obtained in this experiment agrees well with the quark-model predictions.

4.4 Total photon hadron cross-sections

In the vector dominance model one can relate photoproduction cross-sections of vector mesons with the vector meson nucleon cross-sections [Eq. (8)]. In particular, the total γp cross-section can be expressed as:

$$\sigma_{\text{tot}}(\gamma p) = \sqrt{4\pi\alpha} \left[\left(\frac{d\sigma}{dt} \Big|_{t=0} (\gamma p | p p) \right)^{\frac{1}{2}} + \left(\frac{d\sigma}{dt} \Big|_{t=0} (\gamma p | p \omega) \right)^{\frac{1}{2}} + \left(\frac{d\sigma}{dt} \Big|_{t=0} (\gamma p | p \phi) \right)^{\frac{1}{2}} \right] \frac{1}{\gamma_\rho^2/4\pi} \quad (27)$$

Since

$$\frac{d\sigma}{dt} \Big|_{t=0} (\gamma p | p p), \quad \frac{d\sigma}{dt} \Big|_{t=0} (\gamma p | p \omega), \quad \frac{d\sigma}{dt} \Big|_{t=0} (\gamma p | p \phi)$$

are all measured values, and since $\gamma_\rho^2/4\pi$, $\gamma_\omega^2/4\pi$, $\gamma_\phi^2/4\pi$ are determined from leptonic decays, measurement of $\sigma_{\text{tot}}(\gamma p)$ thus enables us to compare it directly with the prediction of the vector dominance

model. This measurement provides the most direct confirmation that the coupling constants $\gamma_\rho^2/4\pi$, etc., have almost the same values independently of whether the ρ or the photon is on the mass shell.

Two experiments³²⁾ were done on $\sigma_{\text{tot}}(\gamma p)$. The one from SLAC was done at 7.5 GeV. The method used was to expose the SLAC 40-inch HBC to high-energy positron-electron annihilation radiation (plus a background of wide-angle bremsstrahlung), and to subtract out the bremsstrahlung contribution by making an identical exposure using electron-induced radiation instead of that from positrons. Their result is $\sigma_{\text{tot}}(\gamma p) = (151 \pm 24) \mu\text{b}$.

The DESY experiment was done on the 85-cm HBC. Using a tagged photon beam, they have measured the cross-section from 0.5 GeV up to 5.0 GeV. Their result, together with the SLAC result, is shown in Fig. 26.

Also shown in Fig. 26 is the region predicted by the vector dominance model. As seen, the data agree well with the vector dominance model and provide an excellent consistency check on the interrelations of the various experimental numbers obtained so far.

4.5 Upper limits -- rare decays of vector mesons

Finally, the following upper limits on rare decays of vector mesons are obtained:

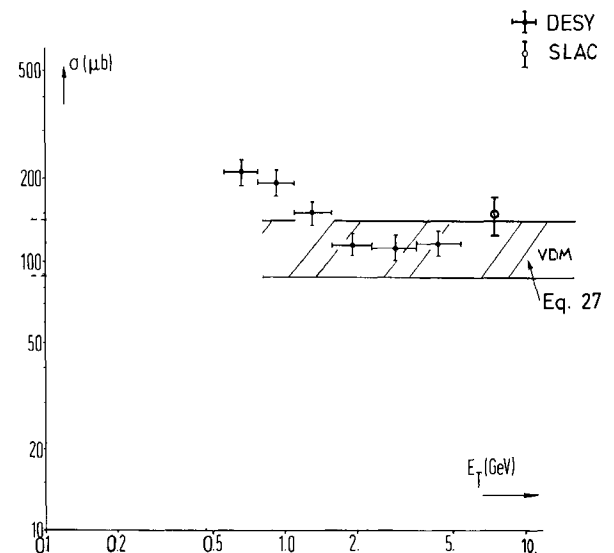


Fig. 26 Summary of experimental results on total hadronic cross-sections from DESY and from SLAC. The shaded region is the prediction of the vector dominance model (Eq. 27).

From Dubna³⁹): $R_1 = \frac{N(\omega \rightarrow \eta\gamma)}{N(\omega \rightarrow \pi^0\gamma)} = 0.22 \pm 0.11$

$$R_2 = \frac{N(\omega \rightarrow \pi^0\pi^0\gamma)}{N(\omega \rightarrow \pi^0\gamma)} = 0.25 \pm 0.15$$

From Bonn-Pisa⁴⁰): BR ($\phi \rightarrow \pi^0\gamma$) $\leq 1.2 \times 10^{-2}$.

merit special thanks for helping me to prepare this report.

I wish to thank also Drs. M. Binkley, A. Dar, T.M. Knasel, R. Marshall, J.J. Sakurai and J.S. Trefil for many interesting discussions, and Drs. P. Dalpiaz and T. Massam for their help with the final text.

Acknowledgements

Drs. U. Becker, William K. Bertram and M. Rohde

REFERENCES AND FOOTNOTES

1. W.C. Barber et al., paper 154.
2. U. Becker, et al., paper 958.
3. W.W. Ash et al., paper 34.
4. C. Bernardini et al., paper 707.
5. For complete references see: S.C.C. Ting, Proc. Int. Symp. on Photons and Electrons, SLAC, Stanford (1967), p. 452; and J.J. Sakurai, Vector mesons 1960-1968, University of Chicago Preprint EFI 68-59.
6. A. Dar and V.F. Weisskopf, Phys. Letters 26 B, 670 (1968).
7. M. Gell-Mann, D. Sharp and W.G. Wagner, Phys. Rev. Letters 8, 261 (1962).
8. H. Joos, Proc. Int. Conf. on Elementary Particles, Heidelberg (1967), p. 349.
9. R.J. Oakes, Nuovo Cimento 44 A, 440 (1966).
10. R. Gatto, Proc. Int. Symp. on Electron and Photon Interactions at High Energies, Hamburg (1965), p. 106.
11. J.K. de Pagter, J.I. Friedman, G. Glass, R.C. Chase, M. Gettner, E. von Goeler, R. Weinstein and A.M. Boyarski, Phys. Rev. Letters 16, 35 (1966).
12. J.G. Asbury, W.K. Bertram, U. Becker, P. Joos, M. Rohde, A.J.S. Smith, C.L. Jordan and S.C.C. Ting, Phys. Rev. Letters 19, 869 (1967).
13. A. Wehmann, E. Engels, L.N. Hand, C.M. Hoffman, P.G. Innocenti, R. Wilson, W.A. Blanpied, D.J. Drickey and D.G. Stairs, contribution to this Conference.
14. V.L. Auslander, G.I. Budker, J.N. Pestov, V.A. Sidorov, A.N. Skrinskii and A.G. Khabakhpashev, contribution to this Conference.
15. J.E. Augustin et al., paper 651.
16. U. Becker et al., papers 951, 952, 953.
17. J.E. Augustin et al., paper 649.
18. D. Bollini, A. Buhler-Broglin, P. Dalpiaz, T. Massam, F. Navach, F.L. Navarra, M.A. Schneegans and A. Zichichi, papers 198 and 199. For $\phi \rightarrow e^+e^-$, Nuovo Cimento 56 A, 1173 (1968); for $\omega \rightarrow e^+e^-$ and mixing angle ($\omega\text{-}\phi$), Nuovo Cimento 57 A, 404 (1968).
19. J.E. Augustin et al., paper 650.
20. R.A. Astvatururov et al., paper 768.
21. D.M. Binnie, A. Duane, A.R. Farugui, P.J. Horsey, W.G. Jones, M.E. Kay, D.C. Mason, P.J. Nicholson, I.U. Rahman, J. Walters and J.G. Wilson, Phys. Letters 27 B, 106 (1968).
22. T. Das, V.S. Mathur and S. Okubo, Phys. Rev. Letters 19, 470 (1967).
23. R.J. Oakes and J.J. Sakurai, Phys. Rev. Letters 19, 1266 (1967).
24. N.M. Kroll, T.D. Lee and B. Zumino, Phys. Rev. 157, 1376 (1967).

25. S.D. Drell and J.S. Trefil, Phys. Rev. Letters 16, 552 and 832 (E) (1966).
M. Ross and L. Stodolsky, Phys. Rev. 149, 1172 (1966).
B. Margolis, Phys. Letters 26 B, 524 (1968); Nucl. Phys. B4, 433 (1968).
K.S. Kölbig and B. Margolis, CERN preprint TH 894 (1968).
J.S. Trefil, MIT (CTP-15, to be published).
26. P. Söding, Phys. Letters 19, 702 (1965).
27. M. Ross and L. Stodolsky, Phys. Rev. 149, 1172 (1966).
28. U. Becker and J.S. Trefil, contribution to this Conference.
29. W.G. Jones et al., paper 679.
30. M. Davier et al., paper 565.
31. G. McClellan et al., paper 33.
32. Aachen-Berlin-Bonn-Hamburg-Heidelberg-München Collaboration, paper 47.
J. Ballam, G.B. Chadwick, Z.G.T. Guiragossian, P. Klein, A. Levy, M. Menke, E. Pickup, T.H. Tan and G. Wolf, contribution to this Conference.
H. Blechschmidt, DESY Report (1967).
33. L. Criegee et al., paper 623.
34. J.G. Asbury, U. Becker, W.K. Bertram, P. Joos, M. Rohde, A.J.S. Smith, C.L. Jordan and S.C.C. Ting, contribution to this Conference and Phys. Rev. Letters 19, 869 (1967).
35. M.J. Longo et al., Proc. Topical Conf. on High-Energy Collisions of Hadrons, CERN (1968), CERN 68-7, Vol. 1, p. 523.
V.S. Pantuer and M.N. Khachatryan, Zh. Eksper. Teor. Fiz. 42, 909 (1962) [English transl.: JETP 15, 626 (1962)].
36. F. Bulos et al., paper 333.
37. H. Blechschmidt et al., paper 7.
38. For example, J.J. Sakurai, contribution to this Conference.
I. Derado and Z.G.T. Guiragossian, paper 797.
A. Dar, V.F. Weisskopf, C.A. Levinson, H.J. Lipkin, Phys. Rev. Letters 20, 1261 (1968).
R. Diebold and J.A. Poirer, Phys. Rev. Letters 20, 1532 (1968).
39. I.V. Chuvilo et al., paper 70.
40. P. Braccini, L. Foà, K. Luebelsmeyer, D. Schmitz, contribution to this Conference.

DISCUSSION

SILVERMAN: I would like to thank Professor Ting for the very comprehensive review, particularly of the $\gamma\rho^2$ situation, all of which I agree with except for one small point which I would like to come back to. It is clear that when in the world roughly 10 or 20 measurements all agree on what $\gamma\rho^2$ is, and one experiment disagrees, he has a little bit of explaining to do, and so I would like to say one or two words. Firstly, I would like to point out that, at least in principle, all of the measurements of $\gamma\rho^2$ having to do with leptonic decay are different measurements than the ones having to do with photoproduction; that is to say, the leptonic decay measures $\gamma\rho^2$ at the ρ mass, and the photoproduction measures $\gamma\rho^2$ at the photon mass, and therefore in principle they could be

different. Now if you say that there is no real reason to say those values of $\gamma\rho^2$ are the same, then our number is not in disagreement with the other 20 measurements, but in fact is in disagreement with the DESY measurement and in rather good agreement with the SLAC measurement. Well, that is one point as far as the world compilation of $\gamma\rho^2$ is concerned.

Now there is only one other point--a brief one--I would like to make, which I hope I can make clear, and that was in the reanalysis of our data which Professor Ting did which showed that if he used 30 mb instead of 40 mb on the t -dependence of copper, the cross-section at $t = 0$ would come out a factor of two higher. I would like to comment on that, but I want to be sure you remember that the curve I am talking

about is the t -dependence on copper, where there was one fitted curve that was the solid curve, one that we had fitted, and another that Professor Ting had fitted using 30 mb. First let me say, as Professor Ting so ably pointed out in his talk, that the t -dependence is very insensitive to $\sigma_{\rho N}$. If you will recall, he said that if you took 10 mb for $\sigma_{\rho N}$ and 30 mb in the case of carbon, that would have changed the coefficient in the exponential e^{bt} from, I believe it was, 44 to 47; and I agree with that, it is very insensitive. Therefore the factor of 2 that was obtained by Professor Ting was not really the change from 30 to 40 mb; it was due to a normalization, to the shift of the whole curve up and down, that caused mostly the factor of 2 in my opinion. Now let me say what the normalization is. Our curve was an attempt to make an absolute fit to our data, both at the coherent and in the incoherent region; in the incoherent region, using the results of Margolis, and in the coherent region, using a Drell-Trefil modified-type theory, but similar to what everybody has been using. Now, that solid curve was the best fit including the incoherent region. That is not where our $t = 0$ cross-section comes from. Our $t = 0$ cross-section comes from making measurements at the smallest t that is possible, and then making the extrapolation from there. Therefore, if you look at that curve which was intended to include also the incoherent region as part of the fit, you will mistake what you think we took for the $t = 0$ cross-section. That process I described last Friday. We measure the cross-section at 6 milliradians approximately, and then, extrapolating that, to $t = 0$ using the optical model. Now, one final word: the use of the optical model--the radius. The sensitivity to the radius of how the extrapolation goes has been talked about quite a lot, and I agree with that. I would like to tell you what radius we used. We used, in fact, the electron scattering radius parameters given by Hofstadter. As Professor Ting pointed out, in the low t -region these lead to a result of the form e^{bt} ($e^{\alpha t}$ in his case); b is sensitive to the radius, α I have compared with values which were used by Leith and others at Stanford and they are in quite close agreement. I have compared them with the values obtained by proton scattering on nuclei by Bellettini et

al., and they are in quite close agreement, and unless I misunderstand the ϕ paper from DESY where they also say they use the mean square radius from the electron scattering, there should be quite close agreement with those measurements also. Therefore I agree that our value of $\gamma\rho^2$ is different. I do not agree that one can so easily (we may have made a mistake), but not so easily as Professor Ting showed, change the cross-section on any of our measurements by a factor of two.

TING: It is the duty of the rapporteur to point out the important facts and conclusions of the papers submitted to this Conference. Based on the published papers, there are then the following facts which differ slightly from the remarks made by Professor Silverman. These are:

i) As shown in the table at the conclusion of the section on the photoproduction of the ρ meson, there are many other ways to determine the coupling constant $\gamma_\rho^2/4\pi$ where the photon is on the mass shell. A few examples are: (1) $\sigma_\tau^2(\gamma p)/[d\sigma/dt(\gamma p \rightarrow p\rho)]$; (2) $(\gamma + p \rightarrow \pi^+ n) + (\gamma + n \rightarrow \pi^- + p)$; (3) the π -meson form factor; (4) π^+/π^- ratio from deuterium; (5) $(\gamma p \rightarrow \pi^0 p)/(\pi + N \rightarrow \rho_\perp + N)$; (6) $(\gamma + p \rightarrow \pi^+ n)$ versus $(\pi^- p \rightarrow \rho^0 n)$, etc., all of which yield a value of $|\gamma_\rho^2/4\pi| = 0.5$ in agreement with the DESY value on $\gamma + A \rightarrow A + \rho^0$. These numbers are equal to the value $0.52^{+0.07}_{-0.06}$ determined when the ρ meson is on the mass shell.

ii) Based on the calculations made by K.S. Kölbig and B. Margolis [(Nucl. Phys. B6, 93 (1968) and submitted to this Conference] a figure was plotted in the introduction section on the photoproduction of vector mesons. As shown, a change of $[d\sigma/dt(\gamma + Cu \rightarrow Cu + \rho^0)]/[d\sigma/dt(\gamma + p \rightarrow p + \rho^0)]$ by 25% will change the corresponding $\sigma_{\rho N}$ from 30 to 40 mb. A change of the Cu normalization by a factor of two alone will change the $\sigma_{\rho N}$ from 30 to ≥ 100 mb.

iii) As stated before, for a wide resonance like the ρ , due to the difficulties associated with (1) the exact form of the Breit-Wigner used, (2) the ways the background is subtracted, and (3) the hydrogen cross-section which, as measured by different groups in the same energy region (3 to 6 GeV), varies from 120 to

170 $\mu\text{b}/\text{GeV}$, it is not easy to obtain the ratio $[\text{d}\sigma/\text{d}t(\text{Cu})]/[\text{d}\sigma/\text{d}t(\text{H}_2)]$ to better than the 25% level.

iv) Since in the energy region $E_\gamma \leq 6 \text{ GeV}$ the obtainable $t_{\min} = m_\rho^2/4k^2 \neq 0$, and since on heavy nuclei the models based on diffractive scattering off the whole nucleus are sensitive to the nuclear parameters used, the matching of the models with the experimental points to determine $\sigma_{\rho N}$ thus depend critically on the radius parameter. For example, a change of the radius parameter by 8% in Pb will correspond to a change of $\sigma_{\rho N}$ from 30 to 40 mb.

v) In the photoproduction of pairs at large angles, since the background of e^+e^- pairs decreases like θ^{-8} , all the measured pairs are $\pi^+\pi^-$ pairs. The cross-section $\text{d}\sigma/\text{d}t\text{d}\Omega(\pi^+\pi^-)$ is not difficult to obtain. However, to determine how many of the measured $\pi^+\pi^-$ pairs are from the ρ decay is difficult since there is no unique way to do this. Thus the extrapolated value of $\gamma_\rho^2/4\pi$ is very much method dependent. One way to minimize the errors in extrapolation is to use a consistent set of parameters to extrapolate $\sigma_T(\rho A)$ and $\text{d}\sigma/\text{d}t|_{t=0}$, for then $(\gamma_\rho^2/4\pi)$ will be independent of any nuclear density functions. See [Eq. (25)] and $\gamma_\rho^2/4\pi = (1/16)(\alpha/4\pi)(\sigma_{\rho N}^2)/(\text{d}\sigma/\text{d}t)_H$; therefore with $\text{d}\sigma/\text{d}t_H = 150 \mu\text{b}/\text{GeV}^2$ if $\sigma_{\rho N} = 30 \text{ mb}$ one has $\gamma_\rho^2/4\pi = 0.5$. If $\sigma_{\rho N} = 40 \text{ mb}$ one has $\gamma_\rho^2/4\pi \approx 1.0$.

BECKER: Concerning the nice ρ^0 photoproduction experiment done at Cornell, I still have a few questions left:

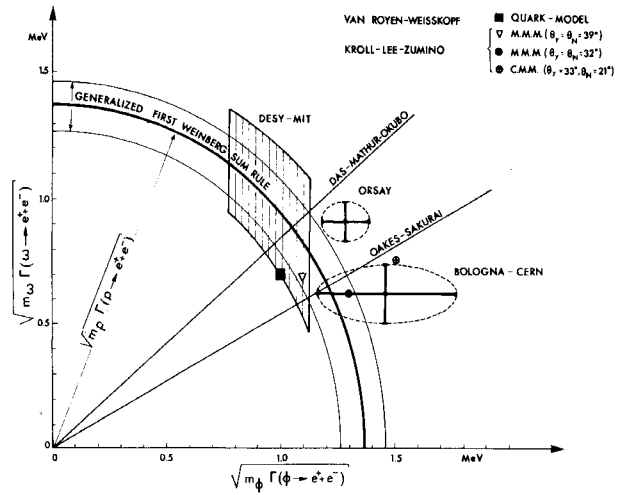
- i) One of them is about the A-fit on the slide, which turned out to be a smooth line. On the other hand, it was said the density distributions as given by Hofstadter were used. Thus you get one discrete value per nucleus A, and not a smooth curve.
- ii) Another question is whether the incoherent contribution, that means all contributions besides those of the coherent production from the nucleus remaining in the ground state, were removed before doing the A fit, since that might be very sensitive on the carbon normalization and if this comes lower all other points come closer to the 20 mb line.
- iii) The third question was whether in the determination of $(\gamma_\rho^2/4\pi)$ finally now the older Bellettini et

al. measurement on $\sigma_T(p+A)$ or the newer $\sigma_T(n+A)$ from neutron nucleus scattering data of Longo et al. are to be used. What is the answer to that? And a related point: Concerning the assertion that on large nuclei the total cross-sections $\sigma(KA) = \sigma(\pi A) = \sigma(pA) = \sigma(nA)$ approach the geometrical limit, I want to point out that these values, calculated by optical model on Pb using a Woods-Saxon potential and particle-proton cross-sections, the obtained ratios: $\sigma^2(K^+\text{Pb}) : \sigma^2(\pi\text{Pb}) : \sigma^2(\rho\text{Pb}) : \sigma^2(p\text{Pb}) = 1 : 1.7 : 1.7 : 2.05$ indicate that in the value $\gamma_\rho^2/4\pi \sim \sigma_T^2$ even at Pb one may be still far off the geometrical limit.

DAR: I would like to make two remarks. First, there is an additional independent determination of the ρ^0 -photon coupling at $q^2 = 0$. Namely the ratio $\Gamma(\omega \rightarrow \pi^0\gamma)/\Gamma(\omega \rightarrow 3\pi)$ provides an additional determination of the ρ^0 -photon coupling at $q^2 = 0$. The measured ratio yields a value for this coupling constant which is in agreement with the value obtained at DESY from ρ^0 photoproduction. My second remark is that the radii used by Prof. Silverman for extrapolating his photoproduction cross-sections to $q^2 = 0$ are the electromagnetic radii which are 15% smaller for heavy nuclei than the density radii deduced from p-nucleus and n-nucleus elastic scattering at high energy. Since the value of the cross-sections at forward direction behave like R^4 , a small change in the radius can produce a large change in the forward cross-section, and consequently can yield significantly different values of the ρ^0 -photon coupling. The analysis of DESY experiments used the radii which are similar to the proton-nucleus radii deduced from the Bellettini 19.3 GeV data.

ZICHICHI: I would like to make a comment. The comment concerns the ω - ϕ mixing angle and the first Weinberg sum rule. These two things have been presented on the same footing--in fact, for instance, the DESY data have been used to produce a value for θ . I think it is correct to say that we are faced with two really distinct problems: one is the ω - ϕ mixing; the second one is the first Weinberg sum rule. If the first Weinberg sum rule would collapse, we could attribute this collapse to many things: for instance, to the way in which the integrals of the

spectral functions are evaluated, i.e. through pole dominance, and no-one would worry if this would turn out not to be true. On the contrary, if θ would have been found to be off, this result would have generated the collapse of the great SU(3) castle. Now, as you have insisted on the difference between the ω width measured at CERN and the one measured at Orsay, I would like to make it clear that the ω - ρ interference in our experiment has been carefully analysed. We have made a fit to strong interaction data, and using a particular model which fits these data we find that the angle changes by $\pm 3^\circ$ for complete constructive interference (+) and complete destructive interference (-). So my conclusion, which agrees perfectly with that of the Rapporteur, is that the results originally obtained by the Bologna-CERN group on the ω - ϕ mixing angle are confirmed by the Orsay data, as can be seen in the following figure.



The lowest data are those of the Bologna-CERN experiment. The next one is that of Orsay. Then we see the DESY-MIT data.